Université catholique de Louvain

École Polytechnique de Louvain

ICTEAM Electrical Engineering

Luxembourg Institute of Science and Technology

Materials Research and Technology department

Cycled-growth and transport modelling of ZnO nanowires network towards low-temperature gas sensing

PAR

Nohora CAICEDO

THÈSE PRÉSENTÉE EN VUE DE L'OBTENSION DU GRADE DE DOCTEUR EN PHYSIQUE

Composition du Jury

1 Damien LENOBLE	LIST, Luxembourg
2 Renaud LETURCQ	LIST, Luxembourg
3 Denis FLANDRE	UCL, Belgium
4 Jean-Pierre RASKIN	UCL, Belgium
5 Laurent FRANCIS	UCL, Belgium
6 Romain GWOZIECKI	CEA, Grenoble

Septembre 2017

Acknowledgements

Je souhaite avant tout remercier monsieur Damien Lenoble, chef d'unité du département de nanomatériaux au LIST. Je tiens à lui exprimer ma plus profonde gratitude pour avoir été mon directeur de thèse au cours de ces quatre dernières années. Je retiendrai sa patience, sa gentillesse et ses qualités humaines qui sont très difficiles à trouver au jour d'aujourd'hui. Merci, Damien.

Je tiens également à faire part de mon immense gratitude à Renaud Leturcq, que je ne pourrai jamais assez remercier. Merci d'avoir pris le relais de l'encadrement de ma thèse, qui, grâce à toi, a pu déboucher sur de très bons résultats. Je remercie ton exigence, ton perfectionnisme, ta disponibilité et les nombreuses discussions que nous avons eues. Grâce à mon expérience au LIST et avec ta supervision, j'ai pu développer de nombreuses compétences qui m'ont permis de m'améliorer en tant que scientifique. Merci, Renaud.

Je remercie aussi chacun de mes directeurs ou co-directeurs de thèse à l'UCL. Merci à Denis Flandre à Jean-Pierre Raskin. Mes visites sur Louvain-La-Neuve ont toujours été un plaisir tant grâce à qu'à leur gentillesse et leur disponibilité. Je les remercie pour leur implication dans mon travail de thèse, leur regard constructif sur mes travaux et aussi pour les différentes discussions que nous avons pu avoir.

Je remercie les membres du jury: monsieur Romain Gwoziecki (CEA) et monsieur Laurent Francis (UCL) qui m'a fait l'honneur de présider mon jury, pour avoir accepté d'évaluer mes travaux, leurs différents commentaires et questions qui m'ont permis de parfaire mon travail.

L'aboutissement de ce travail de thèse est le résultat des apports de plusieurs personnes qui ont contribué de façon directe ou indirecte, et envers qui je suis très reconnaissant. Bien qu'il n'y ait que mon nom sur ce manuscrit, je tiens à remercier à toutes les personnes qui ont contribué à mon projet NANOSENSE. Je remercie Jean-Sébastien Thomann pour ses connaissances très solides en chimie inorganique et qui m'a beaucoup aidé à la compréhension de ce domaine. Je suis extrêmement reconnaissante envers Didier Arl qui, en plus de m'avoir fait part de son savoir-faire sur le FIB et scientifique plus généralement, m'a apporté beaucoup au niveau personnel grâce ses grandes qualités humaines. Didier, merci pour tous les conseils, tu m'as beaucoup aidé ces 4 dernières années. Stéphanie Girod, merci pour ta disponibilité et ta rapidité lors de la fabrication de contacts, tu m'as fait gagner beaucoup de temps la dernière année, merci.

My most sincere thanks to all my collegues with whom I have shared every day in the laboratory. Noureddine, Cesar, Petru, Guillaume, Bianca Rita, Kevin, Siva, Manuel and Jerome. I would like to thank all the people in the MRT department, especially those with whom I have been able to work, whether to carry out analyzes, to be trained on equipment, or simply to exchange on all types of subjects. Without forgetting MRT-Support, Asmaa and Samir. It was a pleasure to have met you all!

Un grand merci, à présent, aux docteurs de mon bureau, la F 1.14, la version CRP-Gabriel Lippmann avec qui j'ai passé des beaux jours et des moments inoubliables : Rodolphe, Vincent, Moustapha et.... même Jonathan, que je remercie beaucoup. And the new LIST-version of F1.14 : Alex, Sunil, David, Serena, Divya, Hameeda, Rishab, Sabrina and Joao. Good luck with your PhD thesis defences ! Thanks you so much for making the stage of my life so unforgettable.

Nunca podre dejar de agradecerle a mis amigos mas especiales en Luxemburgo que han estado desde el inicio hasta el final conmigo. A Marta, Cristina, Eric, Candela, JuanLu, Miquel, Alberto y Maria. Como siempre lo dije, la única razón por la cual pude pasar estos cuatro años en

Luxemburgo fue gracias a ustedes ! Gracias chicos por el apoyo, consejos, chistes, viajes, historias, risas, en fin.... tantos momentos inolvidables. Los quiero!

Je souhaite remercier ma belle famille française Patrick, Maryse et Coline, je ne suis plus seule, et c'est grâce à vous !. Je vous remercie pour tout votre soutien, amour et conseils.

De la misma manera quiero agradecer el apoyo incondicional a mi familia, especialmente mis padres y mi hermano, Armando, Mireya y Cristhian, sin duda alguna la formación, amor, fe y ejemplo me ha hecho la mujer que soy hoy en día. Soy lo que soy y estoy donde estoy gracias a ustedes !. Les Amo.

A mi esposo, Nicolas, gracias por tu apoyo y amor incondicional en los momentos mas difícil de este recorrido. Este doctorado es un merito compartido. Te amo.

Contents

List of Figures

List of Tables

Part I.

Introduction

Context

The recent evolution of industrial processes increasingly involves the use and manufacture of highly dangerous substances, particularly toxic and combustible gases. Worldwide incidents involving asphyxiation, explosions, and loss of life are a constant reminder of this problem. The recent emergence of concern over environmental pollution and efficiency in a variety of combustion processes has already led to the development of a wide variety of devices and methods, and a large number of instruments are now available commercially. Techniques such as gas chromatography and infrared absorption are widely used for accurate analysis and detection of these gases. However, installation of these conventional instruments is costly, requires a sampling system and complicated maintenance. During the past three decades, rapid growth has been seen in the sensor technology. Most of the advances in gas sensors have been sustained by development based on rather empirical methods, and consequently a full understanding of the gas sensing mechanisms is lacking in the published literature. Moreover, these sensors are often subject to deterioration with time (low shelf-life) and also to interference by other coexisting gases (low selectivity). From a practical standpoint, a gas sensor is useful only if it can detect the desired active component in the presence of non-interfering background constituents meaning that the sensor must be selective and work according to the acceptable and controllable levels of sensitivity and detectability. Many investigations are being done in order to mass-produce sensitive, selective, reliable, and inexpensive sensors, capable of detecting even low concentrations of gases such as CO, CO_2, O_2, H_2, NO, etc. [15, 40, 58]. Among other industries, space applications require a tight control of contamination. As a particular case, molecular contamination inducing uncontrolled deposited materials leads to deterioration on the performance, lifetime and reliability of spacecraft hardware. As stated by the project partners CNES and ESA, in-orbit experiments do not provide any information on the molecular nature of the contaminants. Therefore, there is a strong requirement to integrate into satellites and spacecrafts a real-time, qualitative and quantitative analysis technique. A miniaturized chemical

sensor may distinguish a contaminant from another, allowing accurate monitoring of a deposited contaminant, controlling molecular contamination and permitting the in-orbit spacecraft integration. The latter is the ultimate goal of the framework program agreed upon between the LIST, CNES and ESA. Within this framework program, this PhD thesis focuses research and study on the fabrication and on the physics of the elaborated sensing devices based on horizontal nanowires network. At the beginning of this project, no activity had been realized at LIST concerning gas sensors, thus this work firstly involved developing a full fabrication process of a ZnO gas sensor using LIST technological Platform. In collaboration with UCL and using their WELCOME Platform, we perform characterization of the fabricated devices and improvements the comprehension of electrical transport mechanism in order to contribute to the fundamental understanding of the sensing behavior.

Research up to date

Metal oxide-based materials are known for their reduction-oxidation reactions on their surface mainly due to the ability of transition metal cations to change their oxidation state. These redox reactions on the surface lead to changes on the electrical resistance of the material, allowing electrical measurements as a sensing response of the reactions at the surface by changing the electro-physical properties of polycrystalline metal oxides [130, 24]. Currently, several systems based on metal oxides structures have already demonstrated sufficiently high sensitivity. However, their selectivity remains a serious challenge, thus, they require a high power consumption due to the working temperatures (above 150 °C) and most of them are not compatible with in-space operations, which adds additional challenges to the sensor technology, for example the miniaturization, reliability and long-term operation.

Objectives

In this thesis, we investigate an original metal oxide based gas-sensing device that integrates nanostructured ZnO nanowires-based network, allowing a low-power consumption and the integration into sensors' arrays. These devices are foreseen to improve the sensor's characteristics as sensitivity and selectivity for Semi-Volatile Organic Compounds (SVOC) for the real-time, qualitative and quantitative control of contamination. Moreover, and from a conceptual point-of-view, this system may allow a local Joule heating in order to tailor the surface reaction, thus creating a heater-free device. The fabrication of this sensor requires the growth of ZnO nanowires using standard nanotechnology techniques (liquid-phase synthesis). However, research on metal-oxide nanowires as sensors is still in its early stages.

Innovation/originality

Different sensing devices (such as electric nose, biosensors ...) have been recently developed to determine the chemical origin of the contamination [199, 191]. Considering that molecular contamination in spatial and terrestrial environments mostly comes from organic compounds, the combined analysis of microsensors array makes identification of organic contamination feasible [9, 164]. These micro sensors have been mainly based on the Micro Electro-Mechanical Systems (MEMS) technologies which may cause severe reliability issues when considering space environments. Semiconductor metal oxide-based gas sensors offer multiple benefits such as compact size, low cost, long life, and compatibility with standard circuits technology. The originality of our study is the size-controlled network-based ZnO nanowires that improves sensitivity, the response time, the power consumption related to their physical and chemical properties [31]. One of the perspectives of this work is to develop a ZnO nanowires-based network functionalized by a surface grafting aiming to increase the specific interaction with phthalate molecules in order to provide a selective sensor. In our thesis, the device struc-

ture responses are investigated for O_2 and CO_2 gases used as gas models.

Methodology/PhD Structure

In the first chapter of this thesis a review of the current technological state of metal-oxide based gas sensors devices is presented. The existing ZnO-based gas sensing devices and potential approaches to improve sensitivity and selectivity towards SVOC are discussed. To achieve the technological goal which is the fabrication of a ZnO nanowire network-based sensing device, a review of the current technological state of the existing ZnO nanowire synthesis and devices is presented as well. This literature overview will allow the definition of our technological strategy and the fabrication techniques, as well as the optimization procedures which will be described in Chapter 2. Chapter 3 introduces the sensitive layer fabrication using liquid-phase synthesis of ZnO nanowires. Outcomes, drawbacks and optimization of the synthesis of ZnO nanowires are thoroughly investigated. The obtained results overcome the standard limitations of liquid-phase growth of ZnO nanowires such as controlling the structure and the aspect ratio, in which we obtained the highest reported value (20, instead of 13) found for homogeneous synthesis [31]. The electrical transport mechanism on the ZnO nanowire network is fully studied in Chapter 4. The first part of this chapter reviews previous conduction models adapted to ZnO polycrystalline thin film and proposes a non-linear conduction model adapted to ZnO nanowires-network devices. The second part presents a validation of this model by analyzing the thin film resistance contribution and the temperature dependence of the device behavior. The controlled ZnO nanowires will allow us to propose an accurate conduction model for an uniform network-based thin film. To this date, few reports have been published on the electrical transport mechanism of network-based devices but, to our knowledge, no reports have been published on ZnO nanowires network. Finally, Chapter 5 shows the sensing activities of ZnO nanowire networks towards an oxidant and reducing gas which involves different sensing mechanisms. Latter on this chapter, the proposed conduction model is correlated to

the sensor electronic performance allowing the determination of its physical parameters which have never been discussed in previous reports.

1. State-of-the-art of Metal Oxide-based gas sensors

In this chapter a general review of the current technological state of gas sensor devices is presented, especially, focused on the conductometric sensing mechanism, such as metal oxide-based sensing devices. Metal oxide sensing mechanism and potential approaches to improve sensitivity and selectivity towards SVOC are discussed. Among metal-oxide gas sensors, ZnO is one of the most promising semiconductors due to its properties and applications such as the sensing field, this chapter will be mainly centered in gas sensing devices based on ZnO materials. In particular, we focus on ZnO nanowires, since they have shown upgrades as sensors due to a large surface-to-volume ratio, independence of a heating system, etc. Several configurations of gas sensor devices using ZnO nanowires such as normal resistive sensors, conductometric sensors and FET sensors will be also mentioned.

1.1. Gas sensors: general overview

Gas sensors development began with the need to detect the environment pollutants such as toxic gases that can be harmful to organic life, such as humans or animals. Gas sensors comprise a transducer and an active layer for converting the chemical information into another form of electronic signal like frequency change, current change or voltage change, optical signal, etc. The main purpose of any gas sensors is to provide reliable real-time information about the chemical composition of the environment. An ideal device designed for gas sensing should operate

continuously and reversibly, without being deteriorated. The sensitivity and selectivity to a target gas, which is present in the surrounding environment, are the most important requirements in gas sensing. The device should produce a measurable output signal proportional to gas concentration. Simple fabrication, fast response and recovery time, long life time, humidity insensitivity, high resistance to contamination and poisoning, and low noise are also useful features for the gas sensor market. However, no such ideal gas sensor could be found in the market today, in spite of great advances achieved over the past decades [95].
In our specific case, the sensor is required to use for environmental monitoring of dioctylphthalate (DOP), it must then be selective to this specific molecule and should be very sensitive in order to obtain accurate measurements besides of all the already mentioned properties which defined a good sensor for gas sensing market. For instance, conductometric metal oxide-based gas sensors have low selectivity and high sensitivity to air humidity [95]. However, in comparison with other type of sensors, these sensors have excellent sensitivity, very short response time, low cost, low noise, small size, and very good suitability for portable instruments. Those advantages compensate for their disadvantages and open many possibilities for further applications.

1.2. Conductometric gas sensors

Conductometric gas sensors consist in two electrodes contacting a conducting material which are used for measuring the electrical resistance of the device. The resistance of this material will change in the presence of gas due to a chemical reaction at the surface of the material. These devices are often called Chemiresistors. An added advantage of conductometric gas sensor is its long life expectancy. Several different materials have been reported to have conductometric gas sensor properties: conductive polymers, nanomaterials (such as graphene, carbon nanotubes and nanoparticles) and metal oxide semiconductors (studied in detail in the latter section).

1.2.1. Conductive Polymers

Conductive polymers such as polyaniline and polypyrrole are of great interest for sensing applications [104, 103]. Their sensing mechanism consists in a change of the polymer conductivity by an interaction produced by the targeted gas and polymer chain [80, 29]. A strong limitation of conductive polymers for sensing is the lack of selectivity due to the wide range of gas molecules that can interact with the polymer. Therefore, a chemical functionalization is required to react and give an accurate change in conductivity. Another solution would be the use of Molecularly Imprinted Polymers (MIP) that molds the target molecule and leaves cavities matching the its exact size and shape [11, 80]. Molecularly imprinting the conductive polymers increase the sensitivity by selecting the target's size and shape as well as the interaction with the conductive polymer itself [11]. However, MIP have shown strong limitations to work at high temperatures (above 100 ^{o}C).

1.2.2. Nanomaterials

Graphene

Graphene is a two-dimensional crystalline material, an allotropic form of carbon consisting of a single layer of graphite. The working principle of graphene-based devices is similar to other conductometric gas sensors, changes are produced in their electrical conductivity, due to gas molecules adsorbed on graphene's surface and acting as donors or acceptors [150]. The following characteristics of graphene increase the sensitivity and detect individual dopants. Graphene is a two-dimensional material which exposes its entire surface to adsorbates, maximizing their effect, it is highly conductive reducing the noise even in the limit of no charge carriers [150, 2] and; it has few crystal defects [2, 150, 162]. These features contribute to maximize the signal-to-noise ratio in order to detect changes in a local concentration by less than one electron charge at room temperature. Recent studies have been performed on graphene chemiresistor sensors showing excellent sensitivity [44].

Carbon nanotubes

Carbon nanotubes are allotropes of carbon with a cylindrical nanostructure. Nanotubes are categorized as single-walled nanotubes and multi-walled nanotubes. Carbon nanotubes have a large surface-to-volume ratio, low detection limits, high electron mobility, and quick response times. These properties make carbon nanotubes very attractive and suitable chemical nanosensors. They can respond to the presence of many different gases and their sensitivity goes up to ppb-level detection [93, 42, 168]. However, carbon nanotubes sensors have not shown to be very selective [21, 94].

Nanoparticles

Many different nanoparticles of varying size, structure and composition have been used as chemiresistor sensors [59, 82]. The most commonly used are thin films composed of metal nanoparticles embedded into an organic matrix [190, 146, 5, 176, 55]. Various metals have been employed, such as Au, Pt, Pd, Ag, and alloys of these metals. In these devices, metal nanoparticles provide electronic conductivity enabling a simple electrical signal transduction. The organic molecules matrix provide a selective binding site for the adsorption of the targeted molecules which is limited to thermal stability. Some of the advantages are the small size leading to higher gas interaction with the surface, thus, increasing the sensitivity. Their small size also allows faster response times, low cost and low power consumption.

Metal oxide-based gas sensors

Metal oxide-based materials are widely known for their application in gas sensors[95]. Some of their properties such as the variety of materials with different electrophysical, optical, and chemical characteristics, their high thermal and temporal stability, and their ability to work in

harsh environments, make metal oxides the best suitable materials for chemical sensing. Other advantages are their simplicity of device structure, low fabrication cost, compatibility with standard microelectronic technology and adaptability to a wide variety of reducing or oxidizing gases (such as CO, CO_2, H_2, H_2O, NH_3, SO_x, NO_x, etc.) [140]. On the other hand, one of the strongest limitations is their low selectivity. There are several methods to overcome this limitation, one of them, is the use of thermal cycling of the sensor element [151] which consists in varying the temperature in a cyclic manner due to its dependency of gases rate reaction. The other more common approach is using additional surface catalysts and promoters. However, these approaches do not fully solve the problem of low selectivity completely.

		Advantages	Disadvantages
	Conducive Polymers (MIP)	Selectivity High sensivity	Low operating temperatures
Nanomaterials	**Nanoparticles**	High sensivity Fast response and recovery Low power consumption	Poor thermal stability
	Carbon Nanotubes	High sensivity Fast response and recovery Low detection limits	Poor selectivity
	Graphene	High sensivity Fast response and recovery Low detection limits	Poor selectivity
	MOX	High sensivity Fast response and recovery Low cost Good thermal stability Compatibility with microelectronics	Sensitivity to humidity Low selectivity High power consumption

Table 1.1.: Summary table of the state of the art of conductometric gas sensors.

Considering the limitations and advantages of all conductometric gas sensors exposed in the table 1.1, we focused our work on metal oxide-based gas sensors which offer a good compromise in terms of cost, manufacturability, sensitivity, and thus have been chosen for this PhD. thesis.

1.3. Metal oxide-based gas sensors

1.3.1. Working principle and sensing mechanism

The most accepted mechanism for metal oxide-based materials is based on the reduction-oxidation reactions due to the ability of transition metal cations to change their oxidation state. These redox reactions are due to adsorption and/or reactions on the surface leading to changes of the potential energy, conductivity and resistance of the material, allowing electrical measurements as a sensing response [130, 24]. The working principle of the sensor consists in the reaction with the targeted gas with the surface resistance of the oxide, which is due to the adsorption of the gaseous species. For n-type semiconductors (ZnO, SnO_2, TiO_2, etc.), electrons are attracted towards the oxygen which is adsorbed on the sensitive surface reducing the electron current flow. The reaction to oxygen gas results in the adsorption of oxygen on the surface which leads to a higher resistance. In presence of a reducing gas, the oxygen from the surface reacts with the gas molecules, releasing electrons on the surface that are free to move in the oxide layer allowing a current to flow. On the other hand, p-type semiconductors (Cr_2O_3,NiO, etc) reaction to reducing gases results in electron donation to the surface which decreases the conductivity, therefore, increases the resistance.
In most cases, the metal oxide sensor needs to be heated at high temperatures (about 400 $^\circ$C) to produce the electrons flow through the grains of the material and the activation of redox reactions on the surface. The explanation for this is that the oxygen is absorbed in presence of air. Thus, the electrons could easily flow through the potential barrier of reduced height, and the sensor resistance decreases. The chemical reaction on the metal oxide surface strongly depends on the reactivity of surface materials and the working temperature of the sensor.
The most accepted sensing mechanism for metal-oxide based gas sensors is related with the oxygen chemisorption [91, 16, 72]. Oxygen chemisorption involves the formation of O^{2-}, O^-,O_2^- species at the surface. O^- is the most reactive species among O_2^- and O^{2-} which is not stable, making O^- the dominant species beyond 150 $^\circ$C [16, 20]. This reaction is

shown as follows:

$$O_2^- + e^- \quad \rightarrow \quad 2O_{abs}^- \tag{1.1}$$

The oxygen chemisorption introduces a depleted space region which is created by the adsorbed charges by the surface potential. The appearance of a reducing gas leads to a reaction with the adsorbed oxygen, resulting in a decrease resistance, thus, increasing the conductivity [16]. The reducing gas present in the ambient produces a counter reaction:

$$R + O_{ads}^- \quad \rightarrow \quad RO_{des} + e^- \tag{1.2}$$

Equation 1.2 shows how the reducing gas removes the chemisorbed oxygen, frees up an electronic carrier, and increases the conductivity of the semiconducting gas sensor. At low temperatures, the concentration of chemisorbed oxygen (O^-) on the surface of the metal-oxide material is usually low. Therefore, low activation of processes on the surface, exposure of the sensitive layer to the target gases results in low sensor response. With an increase of the temperature, the conductance response of the sensor is increased as well, due to the high concentration of chemisorbed oxygen and the interaction of the adsorbed gases with oxygen which is increased. Nevertheless, the desorption rate of adsorbed gases is also increased at higher operating temperatures meaning that at certain operating temperature, the latter processes starts to dominat the sensor response, and therefore, the sensor response to gases decreases [28, 3, 75].

1.3.2. Structure/composition of sensors

To differentiate the functions of metal oxide-based gas sensors, the device components are simplified as a receptor which interacts with the

reactive gases and a transducer which transduces the effect of interaction into signals to be measured [200]. The receptor function is given by the sensitive conducting surface, while the transducer function largely depends on its microstructure. Nevertheless, these functions are strongly dependent on factors such as the grain size, sensitive layer, target gas, etc.), which in a first approximation, tailor the sensitivity and the selectivity of the responses [190, 91].
Figure 1.1 shows a typical structure of a conductometric sensor. It consists of three elements, a sensitive conducting layer [45], heater, and contact electrodes. These electrodes are often interdigitated and embedded in the sensitive layer. To make the measurement, a DC voltage is applied to the device, and the current flowing through the electrodes is monitored as the response. This can be measured as a change in the current, which is correlated to the concentration of the chemical species. An integrated heater is required to reach the optimal temperature of the sensitive layer to work.

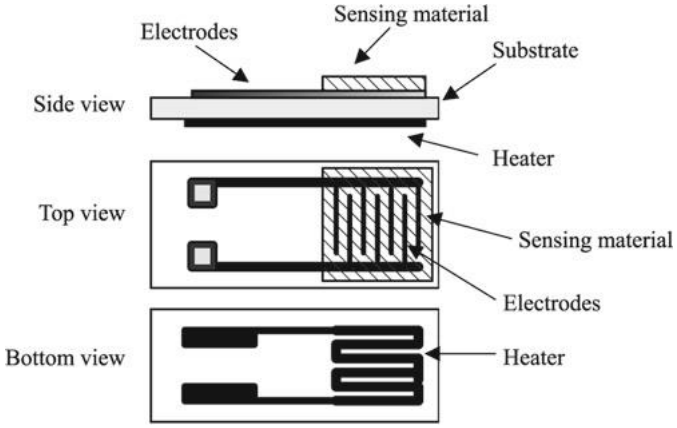

Figure 1.1.: Schematic diagram of typical conductometric metal oxide-based gas. [100]

In order to reduce the power consumption, metal oxide-based gas sensors can be embedded onto a SOI microplates that consists in a membrane composed of micro heaters that elevates the operating temperature, through Joule heating, of the sensitive layer. These sensors

offer low power consumption (˜20mW at 400 ° C), high sensitivity, low cost, low noise, reproducibility and reliability through device integration. These SOI-membrane-based sensing devices are particulary attractive for gas monitoring [165].

1.3.3. Morphology effect

Several factors and processes may influence gas sensitivity and selectivity properties of metal oxide-based gas sensors. The porosity, grain size, active surface area, area of intergrain contacts, thickness, and conductivity of the MOXs also typically influence the operating characteristics of the gas sensors [200, 96, 99]. The sensitive layer which undergoes redox reaction could be compact or porous. For compact layers, the gas mainly interacts with the top surface of the sensitive layer inducing a partly depleted layer while the conduction path of carriers takes place in the bulk region (see figure 1.2). Formally two resistances are formed in parallel and this explains the limited sensitivity of such thin-films morphology [16, 149].

In the case of porous layers, the gas may diffuse into the sensitive layer down to the substrate. The gas interaction can therefore take place at the surface of individual grains, at grain-grain boundaries and at the interface between grains and electrodes and grains and substrates (see figure 1.3). A fully-depleted regime may thus be reached depending on the grain size and the doping of the oxide materials. Many results have shown the gas sensitivity improvement with decreasing crystallite size (of the order of 5-10 nm) for different oxides such as SnO_2 [96, 99, 27], WO_3 [84, 66], and In_2O_3 [95, 99, 98, 97, 71]. The explanation is due to the volume of the layer which is accessible to the gases and therefore the active surface is much greater than the geometric area, thus increasing the sensor response [16]. Therefore, several studies have shown that polycrystalline materials with small size grains are the most suitable option for gas sensor sensitivity [99, 161] and responses [98] improvement.

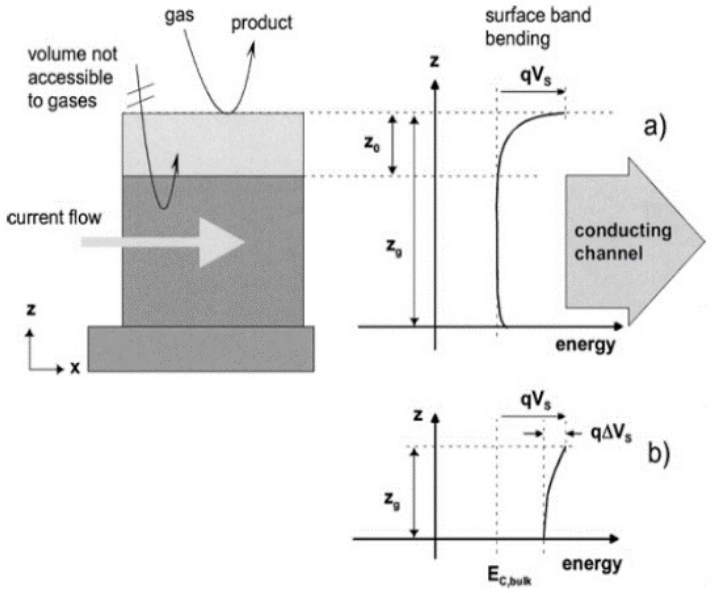

Figure 1.2.: Schematic representation of a compact sensing layer with geometry and energy band representations; Zo is the thickness of the depleted surface layer; Zg is the layer thickness and qVs the band bending. a) Represents a partly depleted compact layer, b) represents a completely depleted layer.[200]

1.4. ZnO based gas sensors

ZnO is a II-VI compound with a wide range of useful properties [89]. The abundancy of Zn and O in earth besides its stability [138], makes it very attractive. Zinc oxide characteristics and properties make it one of the most promising functional materials having enormous applications in electronics and optoelectronics devices [76, 182, 184, 183], such as ultraviolet (UV) lasers [67, 81], light-emitting diodes [136], field emission devices [211], high performance nanosensors [179, 186, 205], solar cells [107, 110, 187, 188], piezoelectric nanogenerators [178, 185, 203], and nanopiezotronics [180, 181, 182].

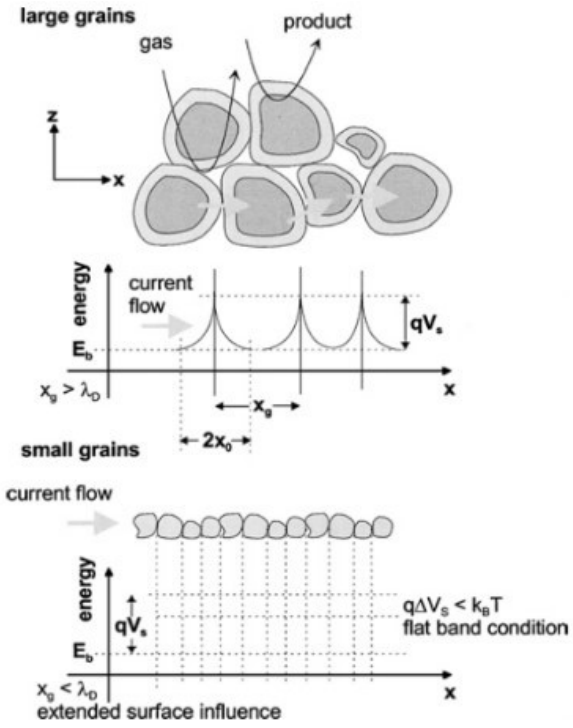

Figure 1.3.: Schematic representation of a porous sensing layer with geometry and energy band. λ_D Debye length, x_g grain size, qVs the band bending. [200]

1.4.1. Properties ZnO

Crystal structures

The crystal structures shared by ZnO are wurtzite, zinc blende, and rocksalt (figure 1.4); but at room temperature, the most stable phase, is wurtzite. The zinc-blende ZnO structure can be stabilized only by epitaxial growth on cubic substrates, and the rocksalt structure may be obtained at relatively high pressures. Wurtzite hexagonal structure is thus, the most found structure of ZnO, especially in liquid phase synthesis, for this reason, our work will be focused only on this structure. In the hexagonal unit cell of ZnO, each Zn atom is surrounded by four oxygen atoms at the corners of a tetrahedron, and vice versa. This tetrahedral coordination is typical of sp3 covalent bonding, but these materials also have a substantial ionic character. ZnO ionicity resides

at the borderline between covalent and ionic semiconductor. The lattice parameters of ZnO reported by the literature are 3.25 Å for a-axis and 5.21 Å for c-axis [49, 63, 85]. Nevertheless, the lattice parameters of semiconductors usually depend on the following factors: free electron concentration, defects, dopants, external strains or temperature.

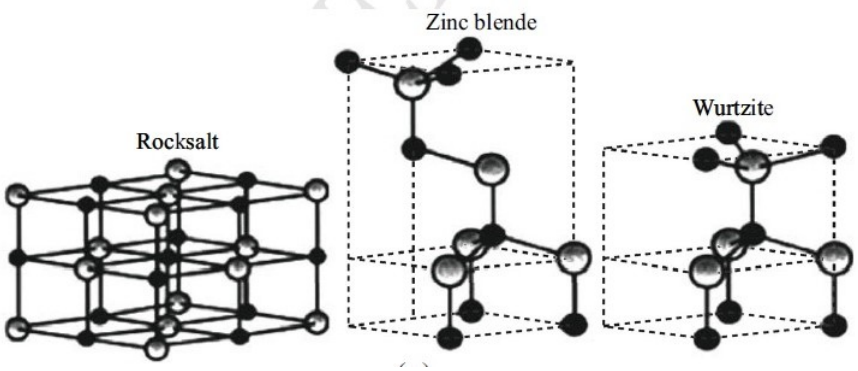

Figure 1.4.: ZnO crystalline structures: (a) rocksalt cubic (face center cubic), (b) zincblende cubic (center cubic) and (c) hegagonal wurtzite. The black balls represent oxygen and the gray ones, zinc. [157].

Electronic band structure

ZnO has a direct and wide bandgap of 3.44 eV at low temperatures and 3.37 eV at room temperature [124, 144], which in principle enables optoelectronic applications in the blue and UV regions of the spectrum. The large free-exciton ZnO binding energy (60 meV) [145], indicates that efficient excitonic emission in ZnO can persist at room temperature and even higher. For comparison, materials as GaN (25 meV) have low exciton binding energy and they are not suitable for working at high temperatures. The large exciton binding energy makes ZnO a promising material for optical devices that are based on excitonic effects.

Optical properties

In most cases, the strong photoluminescence (PL) of ZnO nanowires has two emission bands. The first one is located in the UV range and is associated with the direct transition of excitons, which corresponds to the photo-generated recombination of electrons with holes in the valence band or in traps near the valence band. This process produces UV light of about 370 nm, in line with the ZnO band gap value of 3.37 eV at room temperature. The other PL component is in the visible range, generated by the electron–hole recombination at a deep level, caused by oxygen vacancies, oxygen interstitials, antisite oxygen, zinc vacancies, zinc interstitials, and surface states. Two popular mechanisms for this visible emission are still under debate: one is recombination of electrons from the conduction band (CB) with holes in deep traps, and the other is recombination of holes from the VB with a deeply trapped electron [81, 132, 137, 204]. Nevertheless, these models agree that the ZnO visible emission intensity depends on the crystalline defect concentration.

Electrical properties

ZnO is attracting much attention for the its wide application range in electronics and optoelectronics field due to the direct and large bandgap. These advantages include high-temperature and high-power operation, lower noise generation, higher breakdown voltages, and ability to sustain large electric fields. The high n-type conductivity of wurzite undoped ZnO at room temperature is due to lattice defects (for instance oxygen vacancies or zinc interstitials). These defects introduce shallow donor levels in the electronic band gap of ZnO. Their existence and concentration on ZnO structures is highly dependent on the synthesis process. Even if the electrical properties of ZnO have been highly investigated, the origins of the intrinsic doping mechanisms in ZnO remain unclear. Also, the low symmetry of the wurtzite crystal structure combined with a large electromechanical coupling in ZnO gives rise to strong piezoelectric and pyroelectric properties. This material is often used as sensors, transducers and actuators.

1.4.2. ZnO Growth

The synthesis methods of ZnO could be divided in two groups, liquid and gas phase synthesis. ZnO thin films gas phase synthesis includes Physical Vapor Deposition (PVD) in which zinc precursors are vaporized at high temperatures ($<$ 900 °C) and oxidized (in oxygen or air) to form ZnO [92], and; Chemical Vapor Deposition (CVD), involving a chemical reaction between two vaporized precursors. Liquid phase synthesis was selected as ZnO nanowire growth technique for its low cost and simple preparation.

Liquid Phase Synthesis

Liquid phase synthesis comprises several synthesis techniques for the growth of ZnO in solution in a closed reactor, allowing a rise in pressure and hence growth at low temperatures. These methods can be applied for the development of nano or micro structures in solution, or on the surface of a sample. The advantages of this technique are its low cost and the low temperatures used (usually below the boiling point of the water), and the control of the size of the formed structures. Alternative to the conventional hydrothermal synthesis there is electroplating, microwave or ultrasonic synthesis. In an electrodeposition process, a zinc precursor is oxidized on the surface of a working electrode under the effect of a potential difference. This oxidation allows the ZnO to precipitate in insoluble form at the surface of the electrode. Any electrical conductive substrate on which ZnO is desired to be grown can be used as a working electrode. In Microwave synthesis, heat is supplied by microwave heating. The microwaves allow a better homogeneity of the heat in the solution as well as a direct heating of the reagents unlike a hot plate whose heat diffuses through the glassware. The growth rate in the case of microwave synthesis is much faster than in the case of a conventional hydrothermal process reducing time reaction to less than 30 min [141]. Ultrasonication is a new method for activating chemical,

organic or inorganic reactions. Although the ultrasonication mechanism is not yet fully understood, it is believed that the application of an ultrasonic wave in an aqueous medium causes a cavitation effect in the liquid [25]. The advantage of a chemical reaction initiated by ultrasound is the same as for microwave synthesis, the ultra-fast kinetics of the reactions.

1.4.3. ZnO Nanowires-based sensors

ZnO is one of the most promising semiconductors due to its properties and potential applications in several fields. In particular, ZnO thin films semiconductors have been widely studied in the field of gas sensors [148]. Since ZnO is a n-type semiconductor, it is more conductive and shows improved sensing behavior at temperatures above 150 °C. A local heater is usually required to raise the temperature of the sensing material to improve its reactivity. One-dimensional (1D) ZnO nanostructures such as nano needles, nanowires, nanobelts, nanotubes, etc, [202, 127, 62, 163, 102, 12] attract more and more interest due to its potential technological applications in nanoelectronics and molecular electronics [54, 207]. ZnO nanowires, have shown improvements in the sensing field due to their very large surface-to-volume ratio, independency of a heating system, dimensions comparable to the extension of surface charge region, superior stability owing to their high crystallinity, simple preparation methods and functionalization of their surfaces. They exhibit greater sensitivity due to their larger surface to volume ratio and the capability to work at room temperature. These advantages make them more interesting and suitable as sensing structures [177, 34, 143]. These structures have been synthesized by a wide range of techniques, such as wet chemical methods [106, 175], physical vapor deposition [81, 132, 204], metal–organic chemical vapor deposition [137, 134, 206], molecular beam epitaxy [76], pulsed laser deposition [78, 160], sputtering [36], flux methods [194], electrospinning [115, 116, 158], and even top-down approaches by etching. Number of configurations of gas sensor devices could be implemented using ZnO nanowires such as normal resistive sensors, conductometric sensors and

FET sensors. Various arrangements of the nanowires could also be investigated in these configurations.

Resistive or conductometric sensors

In resistive or conductometric gas sensors, the fundamental working principle of ZnO nanowire based gas sensors is based on resistance change in the nanowire channel due to chemical interaction of the target gas with nanowire surface. When the target gas molecules adsorb onto the nanowire surface, the change in the surface states causes a change in the resistance. This type of sensor requires two electrodes to measure current through the sensor and a heating system to achieve the required temperature of the ZnO nanowire to promote chemical interaction between the target gas and the device [43]. The output signal can be measured by ohmmeter or DC circuits [34, 142].

Single nanowire gas sensors:

A first approach to the fabrication of single nanowire-based sensors is to dilute ZnO nanowires into solvents in order to promote very small concentration, and to spin coat the solution on a substrate followed by deposition of electrodes. Another approach is to drop cast the nanowires on pre-deposited electrodes and, if alignment is required, to use dielectrophoresis. Once the nanowires are located using an optical microscope, measurements are carried out. However, this approach is not suitable for large scale fabrication, and the sensors lack reproducibility due to variation in aspect ratio and defects state [142].

Multiple nanowire gas sensors:

The multiple nanowire sensors are fabricated similar to single nanowire sensors but by using highly concentrated solution of nanowires. Nevertheless, the variation in concentration and density of nanowires located between the two electrodes is still an issue with reproducibility [142].

Nanowire thin film sensors

The most common approach for nanowire-based gas sensors fabri-

cation is to create a thin film of nanowires as a sensitive layer. The nanowire network can be random or aligned. Electrodes can be deposited on top of nanowire network or vice versa. Although this approach seems very similar to the others, the sensing mechanism averages the response of individual nanowires leading to improved repeatability and reproducibility [142]. Our work is based on ZnO nanowires network thin film gas sensors which are deposited on electrodes to maximize sensitivity.

Field effect transistors as sensors:

Field effect transistor (FET) gas sensors using a ZnO nanowire as a channel have been reported and demonstrated a superior performance [33, 34]. Fan et al. have demonstrated the dependency between the gate voltage and the sensitivity in oxygen detection reaching a maximum value of 64% at the voltage just above threshold [57]. They also found a dependency on sensitivity under NO_2 and NH_3 conditions [126]. Li et al. have also seen similar results towards high sensitivity of the ZnO nanowire FETs towards oxygen by changing in the drain current along with the threshold voltage [111]. Nanowire FETs show more sensitivity than resistive gas sensors due to the enhancement of conductivity through the gate voltage [34]. Multiple nanowire channel FETs have also been investigated recently in order to achieve the uniformity in the gas sensing properties. These gas sensors show very good sensing response but one of their major challenges is to reproduce the positioning of nanowire between source and drain [88].

1.5. Conclusions

A general review of gas sensors, in particular, due to the sensing mechanism, conductometric gas sensors devices are presented. Metal oxide -based gas sensors seem to be the most promising materials to improve both sensitivity and selectivity to hazardous gases. Among metal oxides, ZnO is selected to be our working material due to its promising properties (piezoelectricity), applications and its simple and low cost synthesis. Several configurations of gas sensor devices using ZnO structures such as normal resistive sensors, conductometric sensors and FET

Material	**Structure**	**T** ($^\circ$C)	R_g/R_o	$[O_2]$(%)	**Ref.**
ZnO	Nanoparticles	250	2	5	[53]
ZnO	Nanorods	50	0.74	97	[38]
ZnO	Nanorods	RT	1	0.0015	[4]
Mn-ZnO	Nanorods	RT	3	0.0015	[4]
ZnO	Nanowires	RT	0.1	0.0021	[198]

Table 1.2.: Summary table of reported ZnO- based gas sensors performances to oxygen gas. RT abbreviation for Room Temperature. T, R_g/R_o **and** $[O_2]$ correspond to the temperature, response and oxygen gas concentration, respectively.

sensors are discussed. ZnO-based gas sensors performances up-to-date to oxygen gas are listed in table 1.2. Our study is centered in gas sensing devices based on ZnO nanowires since they have large surface-to-volume ratio, independency of a heating system, dimensions comparable to the extension of surface charge region, superior stability owing to their high crystallinity, require simple preparation methods and functionalization of their surfaces is feasible.

2. Microfabrication and characterization of gas sensors

The present chapter gives an overview on the fabrication techniques, experimental setups and processes used along this thesis to achieve the creation of a ZnO nanowires network-based sensing device. The first part of this chapter presents the sensing device fabrication and its optimization. The second section describes all characterization techniques performed on ZnO nanowires.

2.1. Device fabrication

The fabrication of ZnO nanowire network based sensing devices involves synthesis of the sensing device, contacts fabrication to collect electrical signal, for this purpose, a mask is first designed, then an optical lithography is performed followed by a metal deposition. Once contacts are fabricated, nanowires are deposited on top of these contacts, a well-dispersed ZnO nanowire-based thin film is obtained using drop casting method. In order to improve the electric behavior of ZnO nanowires, annealings under different atmospheres are studied.

2.1.1. ZnO Nanowires synthesis and characterization techniques

ZnO nanowires were obtained by liquid phase synthesis and all chemicals were analytical grade reagents and used as reactants without further purification. Zinc chloride ($ZnCl_2$) and hexamethylenetetramine ($C_6H_{12}N_4 - HMTA$) (from Sigma Aldrich) were used as precursors.

The amounts of $ZnCl_2$ and $HMTA$ are equimolar in all our experiments corresponding to 10 mM. The precursors are prepared as separate solutions of 1 M concentration using MilliQ water (18.2 MΩ cm) as a solvent. The reaction solution was prepared by mixing 1 mL of these concentrated solutions of zinc chloride and $HMTA$ with 100 mL of water in separate containers making the reaction solution at 10 mM. Subsequently, precursors are completely dissolved in water and stored in a 250 mL round glass vessel which fits into a Radleys Tech Carrousel. The solution is heated at 85 °C and kept under magnetic stirring under argon conditions for 100 min. The magnetic stirring has always been controlled and kept constant at 350 rpm during the synthesis in order to avoid agglomerates. The resulting solution is washed with water three times using centrifugation of 4000 rpm during 5 min. The nanowire product is kept and stocked in ethanol solution of 25 mL. In order to perform the step-by-step growth, we have cycled the synthesis process by adding, every 100 min, 1 mL of $HMTA$ at 10 mM and 1 mL of $ZnCl_2$ at 10 mM without any purification step. The same procedure was repeated with the addition of an aqueous solution of polyethlylene glycol (PEG, molecular weight (Mw) = 6000, Sigma Aldrich) in order to investigate the role of this capping agent.
The Radleys Carousel equipment was used to synthetize ZnO nanowires (figure 2.1). It is located onto a stirring hotplate and will simultaneously heat and stir up to 6 different reactions from room temperature up to 180 °C. The temperature is rapidly and efficiently controlled by the hotplate's digital control and for more precision a Pt1000 temperature sensor is also used. It also contains an integral water-cooled reflux head which provides efficient cooling to all tubes; minimizing solvent evaporation and loss. Water circulates inside the reflux head creating a cooling zone within the upper part of each tube, where vapors cool and condense back into the reaction. The Carousel Radleys 6 accepts wide range of flask sizes including: 5ml, 10 ml, 25 ml, 50 ml, 100 ml, 170 ml and 250 ml sizes.

Figure 2.1.: Radleys Carousel Radleys setup.

2.1.2. Contacts fabrication

Substrate and cleaning

Silicon substrate wafers are supplied by the Siegert Wafer. The size is 4 inches of diameter silicon disks, well-oriented with (100) plane, their resistivity is between 10 and 20 mOhm.cm and with a p-type (boron) doping. Their thickness is about 750 um. The working face where the device is fabricated is mirror polished to avoid defects or disturbances during the growth process. SiO_2 layer of 270 nm is fabricated by thermal oxidation. These substrates are rinsed with distilled water, acetone and left under ethanol with sonications during 5 min before being dried with nitrogen.

Mask Design

After cleaning the SiO_2/Si substrate, the contact fabrication was started. Two types of contacts are then designed, one corresponds to squared-shape contacts with different geometries in order to allow the study of electrical transport through the nanowire network; the other type,

corresponds to the contacts designed for the final device for sensing application. The contacts were fabricated with titanium (5 nm thick) as adhesion layer for gold (50 nm thick) pads.
For the first analysis, an optical mask was designed using KLayout software. The contact geometry is varying as follows: contact gap (L) of 2 μm, 5 μm, 10 μm and 20 μm; and, contact width (W) of 10 μm, 50 μm, 100 μm, 200 μm, 300 μm. The contacts consisted of two larger 300µm-wide square pads for probe contacts connected with smaller pads in which different geometries are compared (figure 2.2).

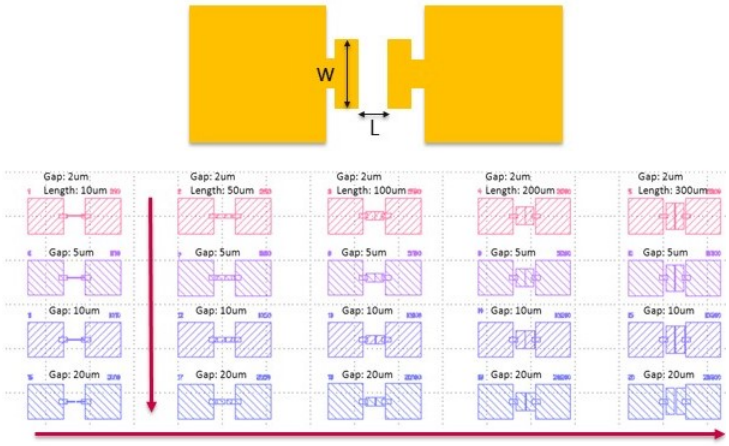

Figure 2.2.: Optical mask design on KLayout for square-shaped contacts using different geometries such as contact width (w) and the gap between the electrodes (L).

The final device contacts are designed in a way that the larger contribution from the ZnO junctions is obtained. In this manner, the interdigitated electrodes are fabricated with a total length of 1050 um and a gap of 20 um. These contacts are conceived in a way they could be integrated to the final device, they are then connected to two larger pads of 3 mm where the electrical probing will be made (figure 2.3).

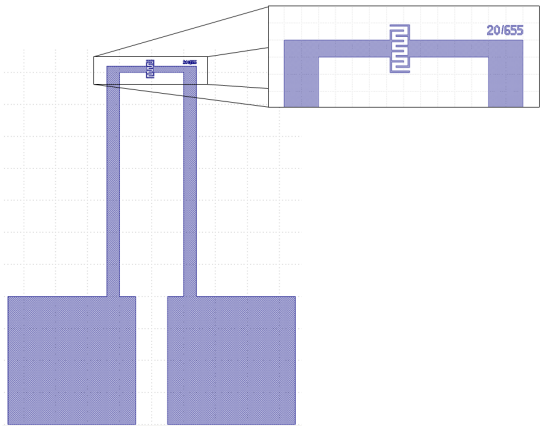

Figure 2.3.: Optical mask design on KLayout for final device single interdigitated contact.

Optical lithography

The optical lithography consists in depositing a positive photoresist onto the SiO_2/Si and using the designed mask, the substrate is then exposed to UV where the chemical properties of the exposed part of the resist will be changed, making it soluble in a solution (developer) and removed, after development the sample is prepared for metal deposition. Optical lithography is realized by exposing to UV light (15 W) using a double-sided emitter from MEGA Electronics (figure 2.4). Exposure time could vary from 0 to 500 s. Light vacuum is required and included while exposing the samples to UV. The photoresist stack is made by a bilayer of lor3A and S1813 with HDMS adhesion promoter exposed during 30 s on UV and developed using MF319 developer during 60 s.

Metal deposition

A custom-made evaporator by electron gun from Meca 2000 is used for metal deposition during contact fabrication (figure 2.5). Five available sources are available for deposition: Titanium (Ti), Gold (Au), Chromium (Cr), Aluminium (Al) and Platinum (Pt). In order to guarantee purity during deposition, ultra high vacuum is required and achieved

Figure 2.4.: UV exposure unit with double sided vacuum.

of around 5×10^{-9}. The machine is composed by a deposition chamber where the metal is deposited under high purity conditions; and an introduction chamber where the sample is introduced. The contacts for all devices are fabricated using Ti (5 nm) as an adhesive layer for gold (50 nm) on SiO_2 substrate. Once the deposition is realized, lift-off is then performed in acetone under sonication, the metallic layer in contact with the resist will be removed and only the ones in contact with the substrate will remain, leading to the contacts of the device.

Figure 2.5.: Custom built Meca 2000 evaporator reactor using an electron beam as a heating sorce.

2.1.3. ZnO Nanowires deposition

Spin coating

Spin coating is a procedure used to deposit uniform thin films based on ZnO nanowires network to a flat substrate. Once the synthetized nanowires are cleaned and rinsed, they are kept in ethanol solution. This solution is placed under sonication to enable a well-dispersed solution. This solution (1 droplet of 100 μL) is then used as an applied coating on the center of the substrate, the substrate remains fixed to the support using primary vacuum and rotated at low speeds. The deposited coating is spread using the centrifugal force. The excess of solution spins off the edges of the substrate, until the desired thickness is achieved. A spin coater is used to study the uniformity and the thin film network by changing rotation speeds and the amount of solution added during 180 s.

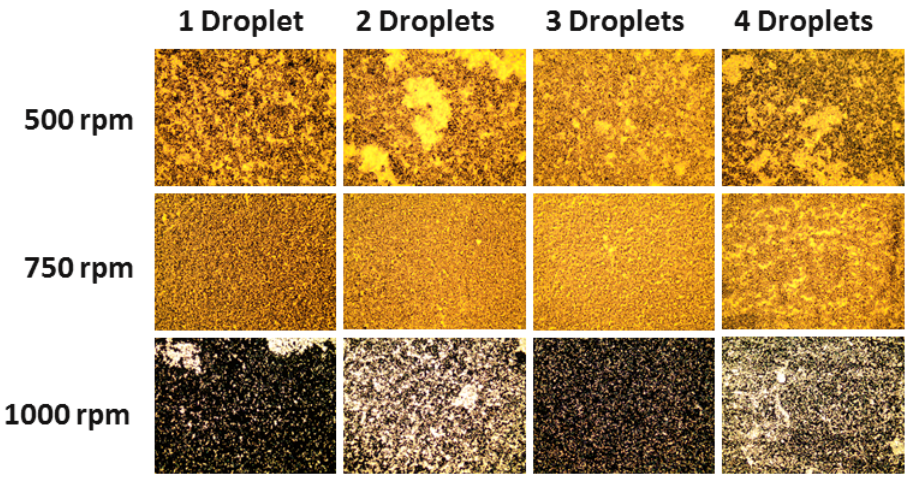

Figure 2.6.: Spin coating study of ZnO nanowires onto a flat Si/SiO_2 substrate at different rotation speeds for different amounts of nanowires solution during 180 s.

The study shown in figure 2.6 indicates the lowest quantity of the deposited solution is not enough to achieve an uniform nanowire network thin film where all nanowires are interconnected. At high and low speed such as 1000 rpm and 500 rpm respectively, the deposited nanowires are

either rotated too fast inhibiting the network formation and therefore difficulty to obtain the desired thin film or too slow allowing agglomeration between the nanowires leading to non-uniform thin films. Therefore, 750 rpm rotation speed seems to be the most suitable for an uniform nanowire network thin film, three droplets from the nanowires solution showed the best behavior for a well connected ZnO nanowire-based uniform network.

Drop Casting

Spin coating technique was used to characterize the uniformity of the well-dispersed ZnO nanowires on a flat substrate. In this particular case, the coating of nanowires on a substrate that contains pre-fabricated electrodes results in non-uniform coatings with agglomerations at the contact edges due to the non-existance of a flat surface. Therefore, drop casting is then considered as an option in to obtain the same quality of uniforms thin films based on networks as is demonstrated while using spin coating. The stocked ZnO nanowires corresponding to 1 cycle solution (length: 3 μm, diameter: 250 nm) is placed under ultrasonification during 5 min at RT. Later, a droplet of 50 uL is taken from the solution and deposited on the substrate containing the pre-fabricated contacts and left until is completely dry. As observed with spin coating deposition technique, one droplet is not enough to interconnect the nanowires, using three droplets show the best uniform thin film reproducing the obtained results by spin coating. This procedure was selected for the further device fabrication, the deposition of three droplets from the cleaned and rinsed solution where ZnO nanowires are stocked (figure 2.7).

2.1.4. Annealings

In order to improve I-V characteristics the deposited nanowires onto the substrate Ti/Au contacts, the annealing of the deposited nanowires was

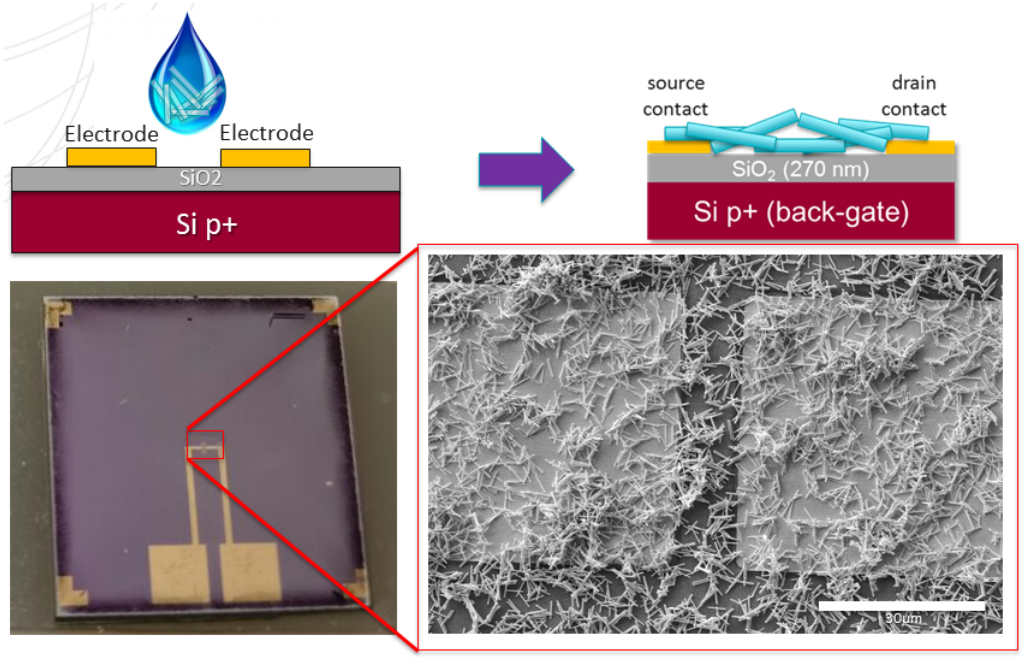

Figure 2.7.: Drop Casting of ZnO nanowires onto contact-fabricated substrate. Top-left panel: depsoition principle of 3 droplets of 50 μL are deposited onto the substrate. Top-right panel: cross-section scheme of the deposited ZnO nanowire network. Bottom panel: top-view of ZnO nanowires deposited onto the final sensing device and its SEM image using a scale 30 μm.

studied under different atmospheres at different temperatures (from 100 °C to 400 °C) to improve electrical transport and remove the remaining organic residues on the surface. Three main atmospheres are then investigated: air, argon and H_2N_2 (which is a mixture of 5% of hydrogen and 95% of nitrogen). The samples were annealed at different temperatures for one hour at environmental conditions (air) and under a constant flow of argon using a temperature-controlled stage of Bruker D8 HR X-ray diffractometer. Samples annealed under a reducing gas (H_2N_2) were prepared with Annealsys RTCVD AS-MASTER 2000 (figure 2.8) using different concentrations of hydrogen. The AS-Master rapid thermal processor allows processes from annealing to Rapid Thermal Chemical Vapor Deposition. Annealing processes can go up to 1450 °C providing

a suitable high controlled- process under ultra clean environment. The extended temperature range, the vacuum performance (atmosphere to 10^{-6} Torr) and gas mixing capability make reproducible processes.

Figure 2.8.: Annealsys AS-Master 2000 Rapid Thermal Chemical Vapor Deposition.

2.2. Characterization techniques

2.2.1. Scanning electron microscopy (SEM)

Scanning electron microscopy (SEM) is a high-resolution imaging technique based on the principle of interaction between the electrons and the material on the sample to be analyzed. It allows the imaging of

structures of nanometric size down to 10 nm. The morphology of the samples was examined by SEM-FIB (Focused Ion Beam) HeliosNanolab 650 from FEI (figure 2.9). The images were recorded with an acceleration voltage of 5 kV and a current intensity of 25 mA. Samples of ZnO could be imaged as such without the need to cover them with a conductive metal layer.

Figure 2.9.: FEI Helios NanoLab 650 SEM-FIB System.

2.2.2. X-ray diffraction (XRD)

The crystal structure of our metal oxides has been studied by X-ray diffraction (XRD). X-ray diffraction gives access to information on the crystal mesh parameters or the possible texturing of the film in a preferential orientation. The diffractometer used is a D8 diffractometer from the Bruker supplier equipped with a copper X-ray source with an emission wavelength of = 0.1542 nm (figure 2.10). The diffractograms are

recorded in $\theta - 2\theta$ mode, analyzing from 20° to 60°. The samples are carefully placed on the analysis zone by orienting them to avoid the substrate diffraction planes (in our case, silicon substrates). The determination of parameters of the ZnO wurtzite structure was obtained from diffractograms recorded according to:

$$d_{hkl} = \frac{1}{\sqrt{\frac{4}{3a^2}(h^2 + k^2 + hk) + \frac{l^2}{c^2}}} \tag{2.1}$$

where a, b and c are the mesh parameters of the wurtzite structure and h, k and l are the Miller indices of the planes.

Figure 2.10.: D8 Avanced Powder Diffractometer from Bruker.

2.2.3. Photoluminescence (PL)

The photoluminescence (PL) spectra of the adsorbed ZnO rods were measured at room temperature and carried out using an Infinite UV-Visible spectrometer M1000 Pro from TECAN (figure 2.11). This spectrometer is equipped with a monochromator allowing the selection of different excitation wavelengths, from the ultraviolet to infrared. Since the ZnO bandgap is 3.37 eV, or around 380 nm, the excitation source is fixed at 300 nm. The spectral range of detection extends from 300 nm to 800 nm, in order to detect the luminescence due to the excitonic

recombination (towards 380 nm) of the ZnO, as well as that due to the recombination of the different levels of transitions induced by defects in the material around 500-600 nm.

Figure 2.11.: Infinite M1000 PRO plate monochromator reades from TECAN.

2.2.4. Electrical characterization Cryo

I-V characteristics of the ZnO nanowires were measured using a Field-Upgradeable Cryogenic Probe Station CPX Model from Lake Shore Cryotronics, Inc (figure 2.12). The CPX operates over a temperature range of 4.2 K to 400 K. The probe station provides efficient temperature operation and control with a continuous refrigeration system using nitrogen or helium. A control heater on the sample stage along with the radiation shield heaters provide the probe station with fast thermal response. A Keithley 4200 source measure unit was used to measure resistivity of the nanowires-based network. The barrier height and ideality factor for the deposited film were extracted from the I-V curves.
Sensor response and recovery under presence of different gases behavior were also studied using this equipment which allows to control chamber pressure (kept constant at 1 atm) and gas flow inside the chamber. This chamber posses a high volume to be filled by the gas, the filling time process usually takes from 15-20 min for a flow of 1000 sccm.

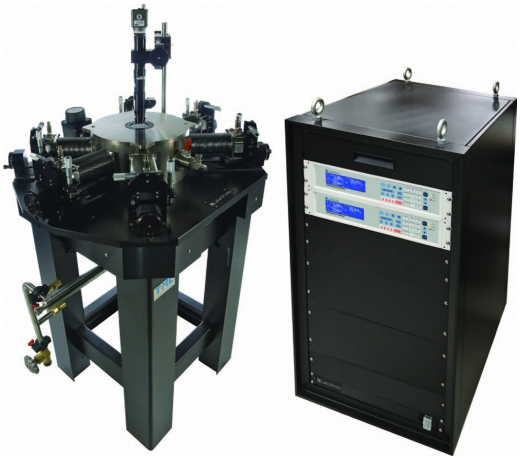

Figure 2.12.: Field-Upgradeable Cryogenic Probe Station CPX Model from Lake Shore Cryotronics, Inc.

2.3. Conclusions

This chapter presented the ZnO nanowire network-based device fabrication and characterization techniques used in this work. ZnO nanowires network-based thin films were synthesized by liquid phase synthesis technique to be used as a sensitive layer for the final sensing device. Uniform ZnO nanowire network-based thin film were created by drop casting the nanowires several times into the pre-fabricated contacts avoiding agglomerates in the network.

3. Development and characterization of ZnO nanowires by liquid-phase synthesis

Among other techniques, growth in liquid phase has been demonstrated as a very powerful and versatile technique to grow one-dimensional ZnO nanostructures over the mentioned gas phase techniques due to its low cost, flexibility, facility and environmentally benign processes with total reaction yield [189, 197]. It does not require high vacuum, sophisticated equipment and high temperature. Moreover, the shape of the ZnO nanostructures can be tuned by changing the experimental conditions including different precursors [68].

Our work is based on an aqueous chemical technique for synthesizing ZnO nanowires at low temperatures (∼85 °C) using homogeneous nucleation. The homogeneous nucleation is induced only by the addition of the precursors and heating which makes it spontaneous. This chapter introduces fabrication of ZnO nanowires by liquid-phase synthesis and growth mechanism. The main goal of this chapter is to overcome the standard limitations of liquid-phase growth of ZnO nanowires such as controlling the structure and improving typical published aspect ratios of 13 when using homogeneous nucleation. This last two factors will lead to propose an accurate conduction model for a ZnO nanowire network-based thin film. The last part of this chapter is dedicated to the influence of annealings under different atmospheres and their effects on ZnO nanowires.

3.1. Growth mechanism

The liquid phase synthesis process of ZnO refers to the structures crystallization in a solution or on a catalytic surface [17]. This technique has many advantages due to its low cost, synthesis temperature below 100 °C [122], controlled shape and size of the structures [68] and the presence of important crystalline defects such as oxygen vacancies [18]. The homogeneous growth could be achieved by the mixing of Zn^{2+} precursors (zinc acetate dehydrate [23] or zinc chloride [79], zinc formate, zinc sulphate or zinc nitrate [68]) and water under basic conditions (by using NaOH, HMTA or hydrazine Hydrate). Alkaline solutions are essential for ZnO nanostructures formation to enable the hydrolysis of divalent metal ions which do not occur in acidic solutions [47, 106, 112]. ZnO is crystallized by the hydrolysis of Zn^{2+} precursors in a basic solution which is formed by using a strong or weak alkalis. The alkaline medium allows the dehydration of some intermediates originated during the reaction of ZnO (for a given pH and temperature) [17, 196]. The most commonly used alkali compounds are KOH and NaOH. The main reactions involved in the synthesis of ZnO, Zn^{2+} salts in an alkaline medium are presented below [47, 48]. The growth mechanism may change from a precursor to another; but in all cases after stabilization at room temperature, $Zn[(OH)^{2-}]_4$ will be obtained and after increasing the temperature up to a 100 °C the nucleation of ZnO will be initiated following the reaction[90]:

$$Zn^{2+} + 2OH^- \leftrightarrow Zn(OH)_2 \tag{3.1}$$

$$Zn(OH)_2 + 2OH^- \leftrightarrow [Zn(OH)_4]^{2-} \tag{3.2}$$

$$[Zn(OH)_4]^{2-} \leftrightarrow ZnO_2^{2-} + 2H_2O \tag{3.3}$$

$$ZnO_2^{2-} + H_2O \leftrightarrow ZnO + 2OH^- \tag{3.4}$$

$$ZnO + OH^- \leftrightarrow ZnOOH^- \tag{3.5}$$

$Zn^{2+}$and OH^- ions combine with each other, and then they get dehydradated by proton transfer, forming chains as Zn^{2+}–O– $\cdots$ Zn^{2+}, and leading to the form of $[Zn_x(OH)_y]^{(2x-y)+}$ forming aggregates, as shown in equations 3.1 and 3.2. The product before obtaining ZnO is $Zn(OH)_4^{2-}$, which is not necessarily the case, depending on parameters such as concentration of precursors and pH value, other products could be obtained as $Zn(OH)^+$,$Zn(OH)_2$, or $Zn(OH)^{3-}$. In equation 3.3, the H_2O molecules formed by dehydration migrate into the solution. The aggregates usually contain fewer than 50 ions, and when they reach around 150 ions, by heating the solution, the wurtzite type ZnO domains are then nucleated. In the above equations, the O^{2-} species in ZnO are obtained from the base instead of the solvent H_2O. Therefore, growth of ZnO does not necessarily require the solvent to be H_2O [207]. It could also be with methanol [35], ethanol [117], and butanol [32], or even ionic liquids [7]. Probably one of the most commonly used as alkaline medium existing in literature for liquid-phase synthesis of ZnO nanowires is hexamethylenetetramine (HMTA)[174]. In the case of HMTA, H_2O molecules in the solution provide O^{2-} ions. HMTA is a nonionic cyclic tertiary amine. Even though the exact function of HMTA during the ZnO nanowire growth is still unclear, it has been suggested that it acts like a Lewis base that coordinates with Zn^{2+} ions [6].
An one-dimensional ZnO nanostructure grows along the c-axis on the polar surfaces such as ± [0001], with alternating Zn^{2+} and O^{2-} terminated ends [106]. When ZnO nuclei is formed, owing to the high energy of the polar facets, the incoming precursor molecules tend to adsorb on the polar surfaces. And, after the complete adsorption of one layer of precursor molecules, this polar facet switches charges with the other one with inverted polarity. For instance, a Zn^{2+} terminated surface changes into an O^{2-} terminated surface, or vice versa. Such a process is repeated over the reaction time, leading to a fast growth along the ±[0001] directions. The growth mediated by HMTA in aqueous solutions facilitates

the anisotropic growth in the [0001] direction, enhancing the inherent fast growth along c-direction on the polar surfaces of wurtzite ZnO, due to the attachment of HMTA molecules to the non-polar side facets [17]. HMTA also acts as a weak base and pH buffer [68], hydrolyzing in water and producing $HCHO$ and NH_3 gradually, as shown in equations 3.6 and 3.7. This is a crucial step in the reaction, if the HMTA hydrolyzes quickly, it will generate a large amount of OH^- groups in a very short period, not allowing the reaction with Zn^{2+} ions in solution, letting to its precipitation, and inhibiting the oriented growth of ZnO nanowires [13].

$$HMTA + 6H_2O \leftrightarrow 4NH_3 + 6HCHO \tag{3.6}$$

$$NH_3 + H_2O \leftrightarrow NH_4^+ + OH^- \tag{3.7}$$

NH_3 (as described in equations 3.8,3.9), one of the products of HMTA with water, plays two essential roles in the synthesis. First, it generates a basic environment which is needed for $Zn(OH)_2$ formation. Second, it coordinates with Zn^{2+} and thus stabilizes the aqueous Zn^{2+}. The latter reaction allows the creation of $[Zn(NH_3)_4]^{2+}$ species which control the kinetic speed of hydrolization and by heating the synthesis of non-agregated ZnO nanowires. $Zn(OH)_2$ dehydrates into ZnO when heated in an oven [174], in a microwave [167], under ultrasonication [83]), or even under sunlight [155]. Thus, the reaction of ZnO nanowires formation follows the order described below:

$$Zn^{2+} + 4NH_3 \leftrightarrow [Zn(NH_3)_4]^{2+} \tag{3.8}$$

$$[Zn(NH_3)_4]^{2+} + H_2O \leftrightarrow Zn(OH)_2 + 4NH_4^+ \tag{3.9}$$

$$Zn(OH)_2 \xrightarrow{\Delta} ZnO + H_2O \tag{3.10}$$

Parameters	Range
Precursor concentration	0.01 - 0.1 M ($ZnCl_2, HMTA$)
pH	6.6 - 9.1
Growth reaction time	80 - 120 min

Table 3.1.: Experimental plan summarizing the parameters tested during the synthesis of ZnO structures.

3.2. Growth parameters

In the case of thermodynamic reactions in ZnO, the preferential growth is along the c-axis direction to minimize the total surface energy resulting in rod-like structures. However, most reactions related to ZnO in solution are strongly influenced by other parameters such as Zn^{2+} counterion, temperature, pH, solvent, growth time, etc. [68, 197]. It is well known that increasing or decreasing the concentration of the chemical reactants will eventually influence the resultant products and especially their morphology. The reactions under alkali solutions could take place at room temperature by adjusting the ratio of Zn^{2+} and OH^{-}, giving rise to ZnO nanowires [8]. Growth time and temperature also control the ZnO nanowire morphology and aspect ratio [155, 195]. The rate of HMTA hydrolysis decreases with increasing pH and vice versa [68]. The growth of polar inorganic nanocrystals is sensitive to the solvents, and their morphologies could be tuned and controlled by the crystal and solvent interfacial interactions [35]. In such cases, the morphology of ZnO is largely directed by the polarity and saturated vapor pressure of the solvents [207]. The following table 3.1 summarizes all parameters that were tested during the ZnO synthesis in order to achieve ZnO nanowires growth.

3.2.1. Precursor concentration

The counter-ions have a strong effect on the resulting morphology of ZnO nanowires [68] but are independent in the growth process. Acetate, formate, and chloride mainly result in the formation of rods; ni-

trate and perchlorate mainly produce wires; and and sulfate yields flat hexagonal platelets. The growth mechanism may change from a precursor to another; but in all cases, after stabilization at room temperature, $Zn[0001][(OH)^{2-}]_4$ is obtained, and after increasing the temperature above 70 °C (equation 3.10), the nucleation of ZnO is initiated [197]. Here, we have chosen zinc chloride as it gives well-defined rods with a hexagonal shape typical for the wurtzite crystal structure of ZnO, and we have chosen HMTA due to its promotion of the [0001] growth direction [133].

Panigrahy et al. describe how the concentrations of HMTA and $ZnCl_2$ affect the growth of ZnO [133]. They have obtained needle-like, flower-like and disc-like structures. A needle-like structure is obtained with zinc chloride and HMTA concentrations of 0.01 M in a 1: 1 ratio, a flower-like structure with zinc chloride and HMTA concentrations of 0.1 M in a 1: 1 ratio and a disc-like structure with zinc chloride and HMTA concentrations of 0.1 M and 0.05 M, respectively, in a 2 : 1 ratio. This implies that a good control over the chemical reactants is crucial to gain direct control over the dimensions of the final ZnO nanorods. Here, we have performed a similar analysis (figure 3.1) and have chosen a concentration of 10 mM in order to obtain a rod-like nano-structure with a hexagonal crosssection and a homogeneous diameter with a pH which remains constant at 6.6.

Figure 3.1.: SEM images of ZnO nanostructures (prepared by liquid phase synthesis using zinc chloride and hexamethylene tetramine as precursor in the water) deposited by varying the concentration of the reactant (a) nanorods, (b) flower-like, and (c) nanodiscs- like structures.

3.2.2. Influence of pH

The pH value in a chemical synthesis has an important influence on the final product. Previous studies have already revealed the influence of pH on the ZnO obtained structures [8, 10, 68, 46]. HMTA hydrolyzes faster to produce the OH^- and ammonia. The created ammonia hydrolyzes into NH_4^+ and hydroxide increasing OH^- concentration in the solution. This will increase the final pH of the solution.
Amin et al. have studied the influence of pH on the ZnO final structure. Rod-like structures can only be grown at pH of 6.6. When the pH is increased to 8 nanotetrapod are obtained, due to the increase of hydroxide concentration leading to the anisotropic growth directions. If the pH reaches 9.1 the growth rate increases due to the increases of OH^- concentration resulting in a flower-like structure. However, for pH smaller than 4.6 no growth was observed, indicating the pH value was lowered by HCl [10]. In order to have a better control of the nanowire structure during the synthesis, the initial and the final pH values are measured and kept at 6.6 before and after the ZnO growth.

3.2.3. Growth reaction time

Verges et al. found a change of ZnO nanostructures from needles to rod-like morphology as a result of an increase of the growth time for solutions containing $ZnCl_2$ and HMTA [175]. Panigraphy et al. also found that the morphology and the final lengths of the nanorods are very dependent of the growth time [133]. The influence of the growth time on our ZnO nanowires is also shown above in figure 3.2. Figure 3.2a and b shows the SEM images of the ZnO nanoneedles and nanowires in equimolar concentration (10mM) of HMTA and $ZnCl_2$ at constant temperature of 85 °C and pH value of 6.6 for 80 and 100 min, respectively. After 100 min the precursors are consumed, and the structure is maintained. However, when the reaction time is only 80 min, the structure has a needle-like shape showing a pointed end transformed to a flat one as the nucleation is incomplete before 100 min. Our results show ZnO rods with an aspect ratio of 13 for one cycle. These results are consistent

with previous results reporting nanowires of 1.5 µm length and 80–110 nm diameter with a Cu seed layer, giving aspect ratios of about 16 for one single cycle obtained under similar conditions [133].

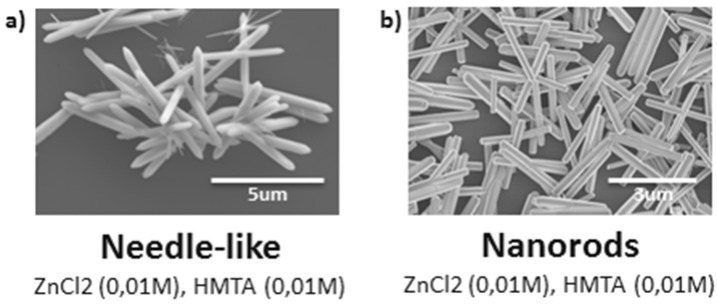

Figure 3.2.: SEM images of ZnO nanostructures synthetized using same concentrations of the reactants and varying the growth reation time. (a) nanoneedles grown after 80 min and (b) nanorods grown after 100 min.

3.2.4. Conclusion and choice of the best parameters

Table 3.2 summarizes the influence of parameters in liquid-phase synthesis and by adjusting these parameters, we can control the growth and impact on the morphology of ZnO structures. In order to obtain ZnO nanowires, the equimolar precursor concentration is fixed at 10mM, pH at 6.6 and the growth reaction time at 100 min.

Precursor concentration ($ZnCl_2$, HMTA)	**pH Influence**	**Growth reaction time**
Nanowires (10 mM, 10 mM)	Nanowires (6.6)	Nanoneedles (80 min)
Nanodiscs (10 mM, 50 mM)	Nanotetrapods (8)	Nanowires (100 min)
Nanoflowers (100 mM, 100 mM)	Nanoflowers (9.1)	Nanowires (120 min)

Table 3.2.: Summary table of the influence of precursor concentration, pH and growth time on the morphology of ZnO nanostructures grown by liquid-phase synthesis.

3.3. Shape controlling agent (PEG)

It is well-known that ZnO exhibits a wurzite crystal structure which is a polar molecule with $\pm[0001]$ polar surfaces and non-polar $[1\bar{1}00]$ and $[2\bar{1}\bar{1}0]$ faces. The non-polar surfaces are electrically neutral having a low surface energy and the polar surfaces have a high surface energy, which is the main factor for the differentiation of the growth rate along both the polar and non-polar directions [69]. Some surfactants or polymers can passivate specific ZnO facets by chemical or physical adsorption, thus adjusting the growth velocity and direction among preferential facets. In this way, nucleation and growth control of ZnO crystals are feasible by adding surfactants or polymers in the solution [8, 39, 51, 76, 105, 131, 135]. ZnO nanowires aspect ratio could be tailored by using polymers such as polyethylene glycol (PEG), able to control the shape and the size of these nanostructures, acting as a selective template which tunes nucleation and growth along a specific direction of ZnO nuclei [133].
The general formula of PEG is HO–$(CH_2$–CH_2–O–$)_n$–OH. The use of compounds of this type is particularly advantageous, since it forms a bond to the growth unit of the ZnO nuclei. In the presence of PEG, the Zn^{2+} ion from zinc chloride is easily adsorbed by the oxygen on the C–O–C chain. This interaction forms PEG coils into solvated $Zn(II) - PEG$ chains, in which the zinc concentration is higher in the polymer matrix as compared to the true solution. Thus, these coils neutralize with hydroxide ions to producing the $PEG - Zn(OH)_2$ complex. By introducing heating, the $PEG - Zn(OH)_2$ complex dehydrates to form ZnO nuclei. Due to the natural tendency of ZnO for polar crystal growth along [0001] direction, the oriented ZnO nuclei attach to form rod-like structures. The long-chain polymer PEG acts as a mediator for ZnO nanowires to grow and attain a definite shape by attaching itself to the non-polar facets. Hence, the presence of PEG gives an advantage for the growth of thin ZnO nanowires on the active sites of the $PEG-Zn(OH)_2$ complex [133]. The predicted reaction can be explained as:

$$HO\text{–}CH_2CH\text{–}\underset{\underset{Zn^{2+}}{|}}{O}\text{–}CH_2CH\text{–}\underset{\underset{Zn^{2+}}{|}}{O}\text{–}CH_2CH\text{–}\underset{\underset{Zn^{2+}}{|}}{O}\text{–}\ldots\text{–}\underset{\underset{Zn^{2+}}{|}}{O}\text{–}CH_2CH\text{–}OH \tag{3.11}$$

$$HO\text{–}CH_2CH\text{–}\underset{\underset{Zn(OH)_2}{|}}{O}\text{–}CH_2CH\text{–}\underset{\underset{Zn(OH)_2}{|}}{O}\text{–}\ldots\text{–}\underset{\underset{Zn(OH)_2}{|}}{O}\text{–}CH_2CH\text{–}OH \tag{3.12}$$

Panigraphy et al have already described the shape control of ZnO nanowires using PEG, capable of tailoring the aspect ratio of nanowires without changing their morphology; however, the impact of PEG's concentration has not been reported [133]. We propose an optimal PEG's concentration to control ZnO nanowires length after studying PEG's concentration impact on ZnO nucleation and hence, viscosity impact on ZnO hydrothermal synthesis which has never been yet discussed [31].
The optimal concentration of PEG obtained to achieve the highest aspect ratio of ZnO nanowires was determined by compairing different ZnO nanowires synthesis with different concentrations. The aspect ratio is obtained by statistically analyzing SEM images. This statistic consists in taking pictures of the sample in different places and counting at least 100 nanowires and measuring their length and diameter each time. Once the data are completed, statistics are made using histograms which show length and diameter distributions revealing an estimation of the median value. The histograms are considered as Gaussian- symmetric indicating a median value from the distribution of data. In some cases, a non-symmetric distribution could better fit the data. However, an assymetry of the distribution would mostly influence its third moment (skewness), and not the first (mean) and second (variance) moments, which are the ones used to be compared later. Figure 3.3a denotes the presence of ZnO nanowires of an average length of 2800 nm and average diameter of 450 nm which leads to an aspect ratio of 6. Figure 3.3b indicates an average length of 850 nm and diameter of 50 nm, thus aspect ratio of 17. Figure 3.3c points out nanowires of 850 nm length and

60 nm of diameter, so aspect ratio of 14. Figure 3.3d, 2800 nm length and 300 nm diameter, aspect ratio of 9 and figure 3.3e, wires of 1700 nm length and 200 nm diameter leading to aspect ratio of 8.5. Lengths and diameter should not be compared, in this particular case, due to concentration is not the same and nucleation conditions changes.

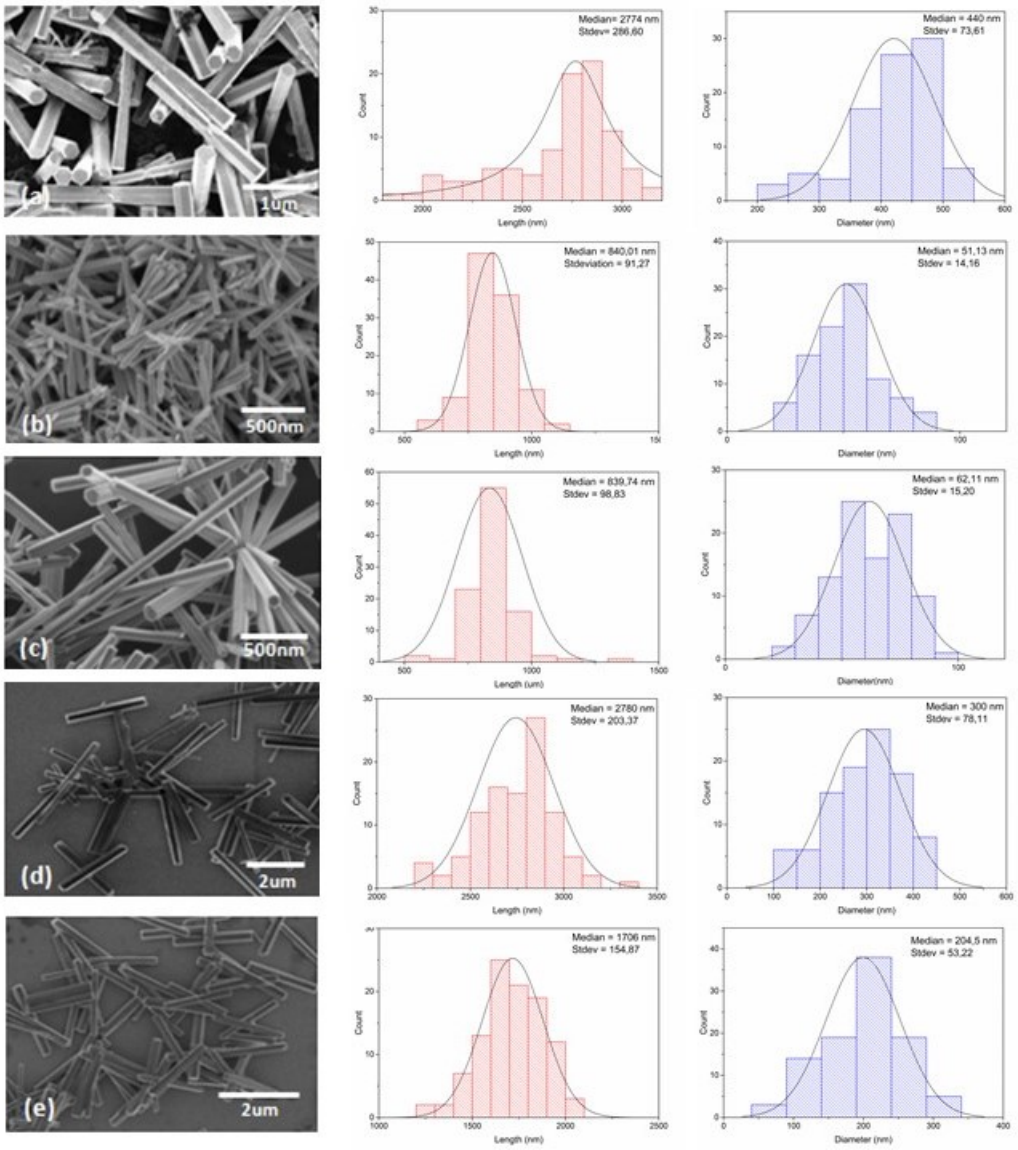

Figure 3.3.: PEG polymer effect on ZnO nanowires sizes. ZnO nanowires obtained (a) without, (b) 2% PEG, (c) 5% PEG, (d) 10% PEG and (e) 15% PEG. The nanowires length and diameter were extracted by measuring 100 nanowires on a single sample of 1x1 cm^2.

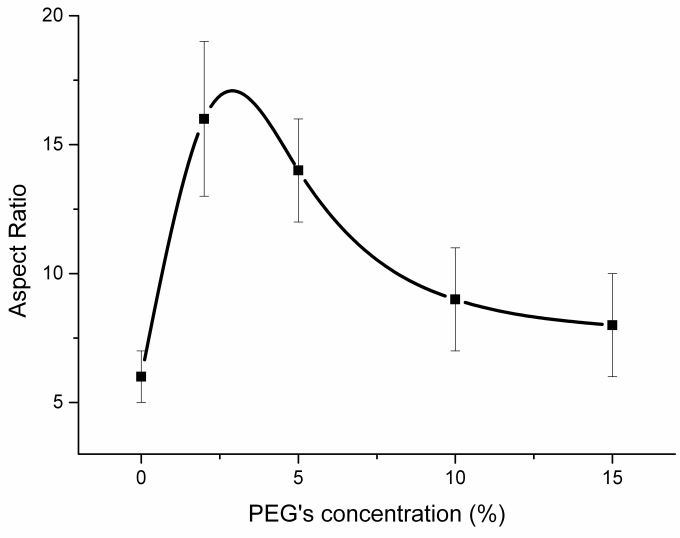

Figure 3.4.: Aspect ratio of the ZnO nanowires grown with PEG as a function of PEG concentration. Error bars correspond to the obtained values of standard deviation given by the figure 3.3.

Figure 3.4 shows that the aspect ratio increases as a function of PEG concentration which reaches a maximum of 16 at 2–3% and then decreases for larger PEG concentrations. Tamman (1925) suggested that this behaviour was caused by the sharp increase of the viscosity which restricts molecular movement and inhibits the formation of crystal structures. These viscous effects were incorporated by Turnbull and Fisher (1949) into the rate equation by taking into account the viscous free energy:

$$J = Aexp[-(16\pi\gamma^3 \upsilon^2)/(3k^3T^3(lnS)^2) + \Delta Gvisc/kT] \tag{3.13}$$

Where$S$ is the supersaturation $ratio = c/c*$ (c concentration of monomers and c* concentration of monomers at saturation equilibrium respectively), γ the surface energy, υ the molecular volume, k is the Boltzmann constant ($1.3805 * 10 - 23JK^{-1}$), T the Temperature of the system and $\Delta Gvisc$ the free energy related with the viscosity. There is an optimum

temperature for nucleation of a given system and any reduction to this value decreases the tendency to nucleate. Under normal conditions, the temperature range over which massive nucleation occurs may be quite restricted. Therefore, if a system has set to high viscous state, to induce nucleation the temperature would have to be increased to a value in the optimum region. According to this statement, the viscosity is an element playing an important role for nucleation, in this specific case, ZnO nucleation followed by ZnO wurzite nanowires formation [166].
So, as the nucleation is strongly dependent on the viscosity which is related with the PEG's concentration of the solution, this will strongly affect nucleation rate in the solution. The stirring parameters is always kept constant in each case. When the solution becomes more viscous, needs more stirring to generate rods in the same conditions resulting in the synthesis of different lengths and diameters generated by the solution itself. So, in this case, a variable that doesn't change and is reliable in each case may be the aspect ratio.
The rate of nucleation curve predicts an exponential growth once a critical supersaturation is reached. Once the supersaturation is achieved, the viscosity which restricts the molecular movements inhibits de formation of crystal structures, in this case ZnO nanowires along the c-direction. The results conclude that the aspect ratio increases as a function of PEG concentration up to about around 2-3 %, and then decreases, concluding that the optimal PEG's concentration should be around 2%PEG of the solution for shape-controlling and passivation of facet to be maximized. We finally conclude that the optimal PEG concentration to attain longer and thinner nanowires should be around 2% PEG, which is chosen for further experiments with our cycle growth method.

3.4. Cycle process for nanowire growth

Recent experiments have shown the possibility of imitating the gas phase growth in liquid by "washing" the solution and renewing the precursors, either using cycles [70] or, in a continuous way, using microfluidic channels [105]. These methods allow the formation of heterostructures in liquid phase [51]. They however require heterogeneous nucleation on a

substrate (similarly to gas phase growth) to be able to remove the solution but then lose the 3D aspect for mass production. Moreover, they have, up to now, been demonstrated on specific materials, mainly CdS, CdSe, ZnS and ZnSe [51, 105, 131], while reports on ZnO nanowires have shown unsuccessful solution phase synthesis involving cycles for aspect ratio improvement, resulting in increasing the width as well as the length of nanowires [68, 70]. Previous experiments using wet chemical methods have succeeded in increasing the ZnO nanowire length by adding a seed layer and by immersing the obtained nanowires in a second fresh solution bath. Unfortunately, this process is limited when repeated several times because the diameter starts to increase and the nanowires fuse together [70].

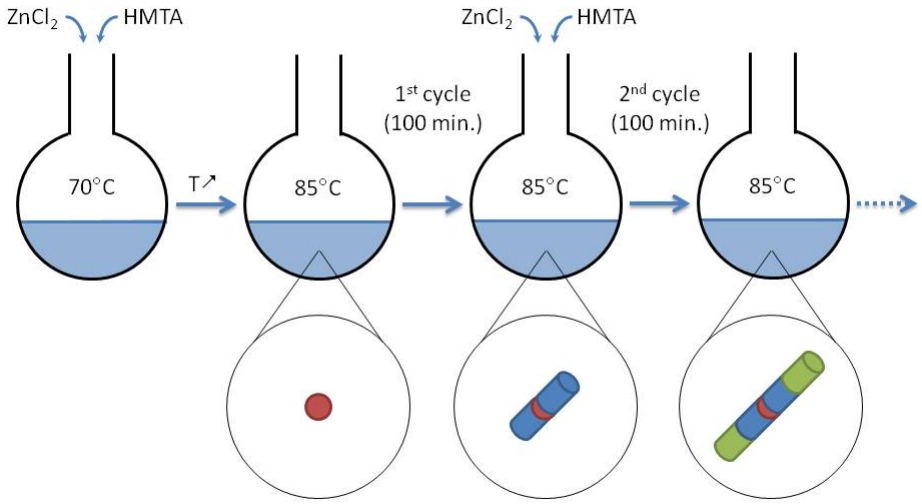

Figure 3.5.: Scheme of the experimental protocol for the cycle growth of ZnO nanowires.

A new concept of ZnO growth is introduced in figure 3.5. The principle of the method consists in adding a small amount of the precursors step by step employing the seeds created through this first growth phase which serve as nucleation sites for the further growth of nanocrystals, resulting in longer nanowires without using a ZnO seed layer as a cat-

alyst. The SEM images for the nanowires grown with n cycles (n = 1 to 4) are shown in figure 3.6 a1–a4 and the histograms in b1–b4 and c1–c4. We note that, from the third cycle, a second distribution of the lengths appears at half the value of the first. This second distribution is explained by the mechanical breaking of the nanowires due to the mechanical stirring applied during growth. The mechanical breaking occurs at the middle point, i.e. the two distributions are centred on two values that are equal, which is justified by the homogeneous nucleation, the growth occurring in both directions. The middle point is thus the seed (ZnO nuclei formed when the solution is heated above 70 °C) where the first nucleation occurs, resulting in the weaker point of the nanostructures. Figure 3.7 shows the average length and diameter as a function of the number of cycles for the unbroken nanowires (i.e. the highest length value), with the corresponding aspect ratio and the surface over volume ratio. In contrast to previous reports on ZnO nanowires [68, 70], we clearly see an increase in the nanowire length without any significant increase in the diameter up to 3 cycles. The diameter of nanowires starts to increase from the fourth cycle, and the corresponding aspect ratio starts to decrease.

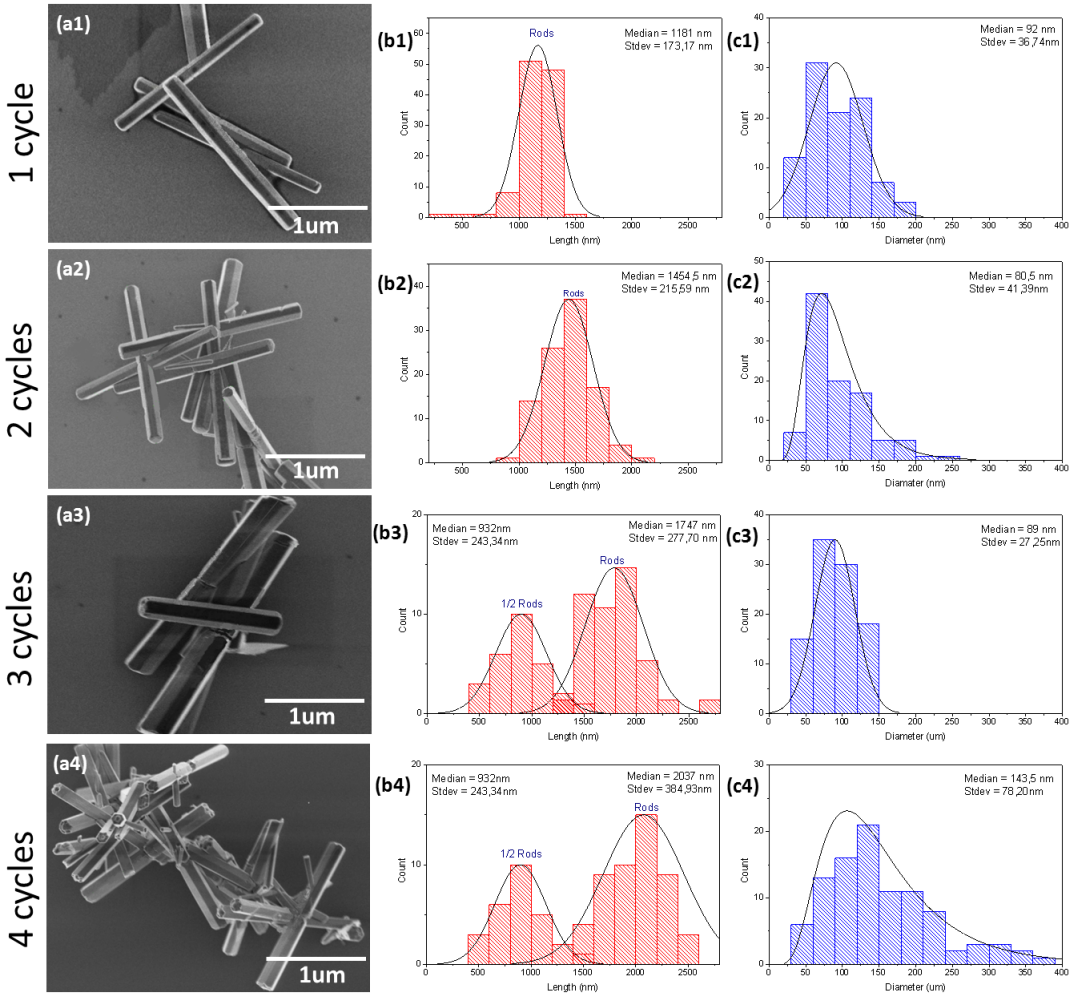

Figure 3.6.: Morphology of the ZnO nanowires grown with cycles. (a1–a4) SEM images of the nanowires deposited on a SiO_2 substrate for n cycles. Histograms of the (b1–b4) lengths and (c1–c4) diameters of nanowires grown with n cycles. The nanowires length and diameter were extracted by measuring 100 nanowires on a single sample of 1x1 cm^2.

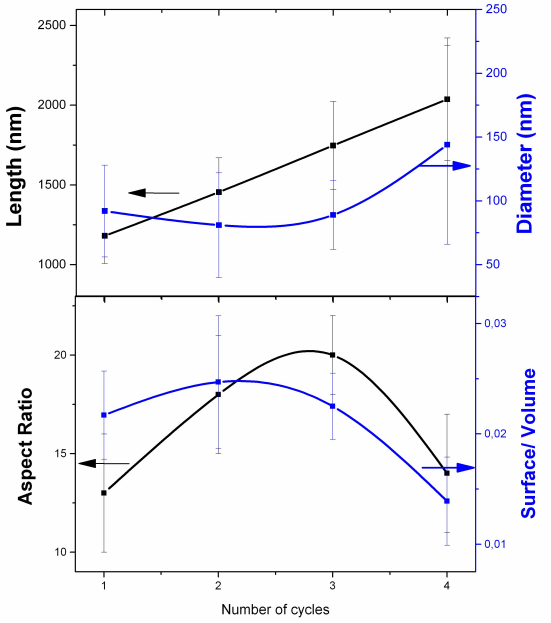

Figure 3.7.: Mean length and diameter (upper panel) and mean aspect ratio (lower panel) and surface-to-volume ratio of the ZnO nanowires as a function of the number of cycles. Error bars correspond to the obtained values of standard deviation given in figure 3.6. Length values extracted from the obtained distribution corresponding to an entire nanowire.

In order to compare the efficiency of a cycle during the synthesis, reference samples are synthesized by applying a single cycle but with the concentration of precursors corresponding to two and four times our reference concentration. The obtained results are shown in figure 3.8. As already reported, the increase in the precursor concentration degrades the aspect ratio and even change the morphology from nanowires to nanodiscs in the case of $ZnCl_2$ [133]. For our case, increasing the concentration from 10 mM to 20 mM gives rise to a decrease in the aspect ratio (figure 3.8a), and a concentration of 40 mM gives nanodiscs (figure 3.8b). This test clearly indicates that implementing the cycles, i.e. adding precursors step-wise without washing the solution, is different than simply multiplying the precursor concentration. The cycle approach improves the ZnO nanowire aspect ratio preserving the regime

of the rod-like structure.

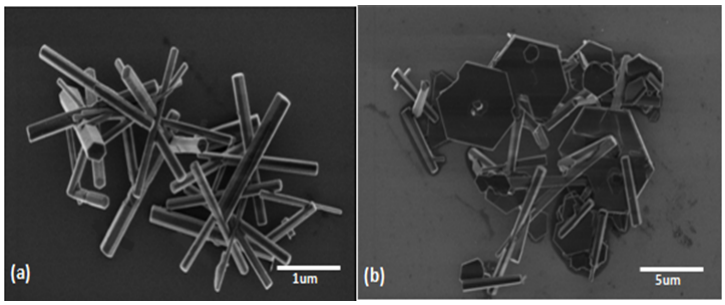

Figure 3.8.: SEM images of single cycle samples grown with (a) twice and (b) four times our reference precursor concentration and growth time.

The demonstrated method shows an increase in the length of the obtained nanowires without a significant change in the diameter up to 3 cycles, thus leading to a direct improvement in the aspect ratio. We believe that this new result for homogeneous growth of ZnO nanowires in liquid phase is due to the interplay of Cl^- counter-ions that act as a limiting agent and $HMTA$ that delivers NH_4^+, promotes vertical growth and limits the action of Cl^-. The involved mechanism could be used not only for growing nanowires with an enhanced aspect ratio but also for growing axial heterostructures for additional functionality [8].

3.4.1. Combining PEG and cycles

As shown and described above, the nanowire length is increased by cycling the injection of precursors. It was already demonstrated that the addition of PEG could also increase the aspect ratio of liquid phase grown ZnO nanowires [133]. We have investigated the effect of PEG on the step-growth method. The fusion of two different concepts enables the shape-controlling of ZnO nanowires and the improvement in their aspect ratio by sequential growth.

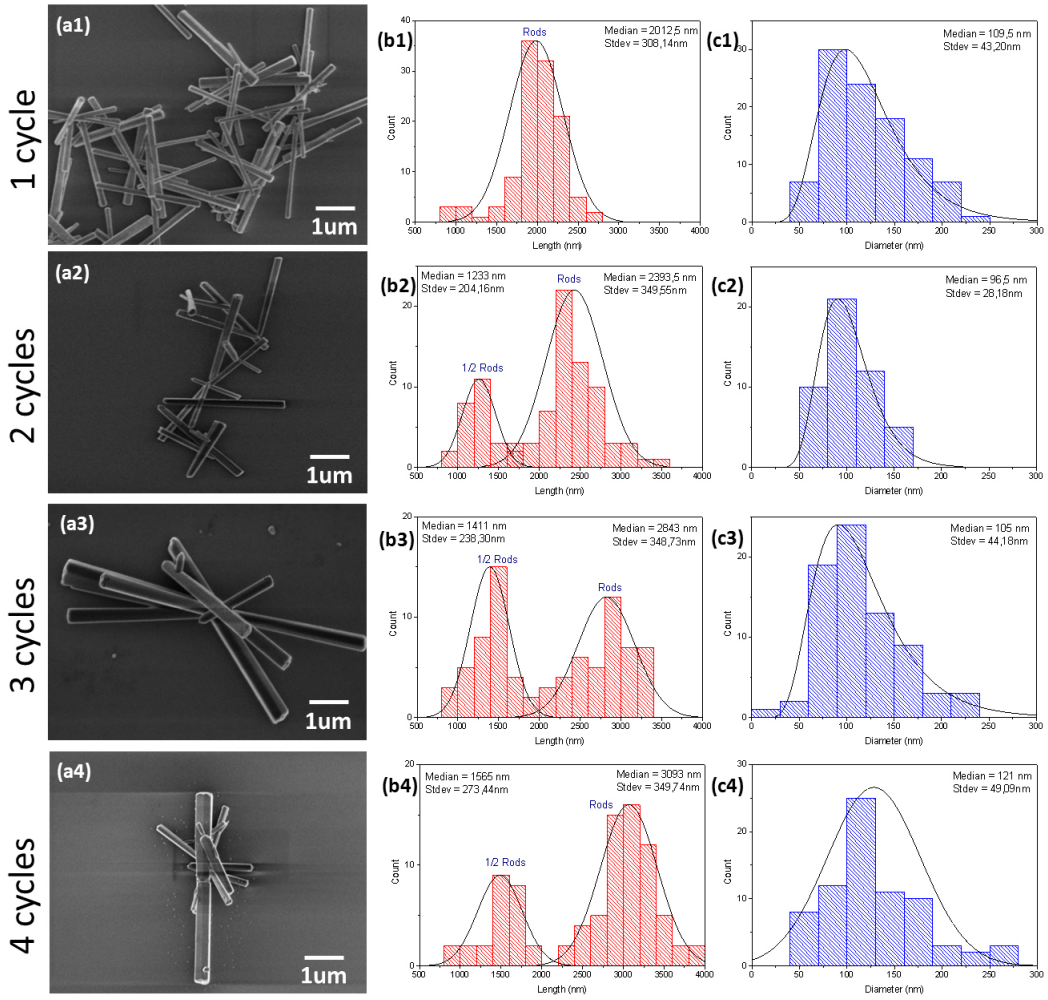

Figure 3.9.: Morphology of ZnO nanowires grown with different number of cycles using PEG as a shape controlling polymer. (a1–a4) SEM images of the nanowires deposited on a SiO_2 substrate for n cycles. (b1–b4) histograms of the length and (c1–c4) histograms of the diameter of the nanowires grown with n cycles. The nanowires length and diameter were extracted by measuring 100 nanowires on a single sample of 1x1 cm^2.

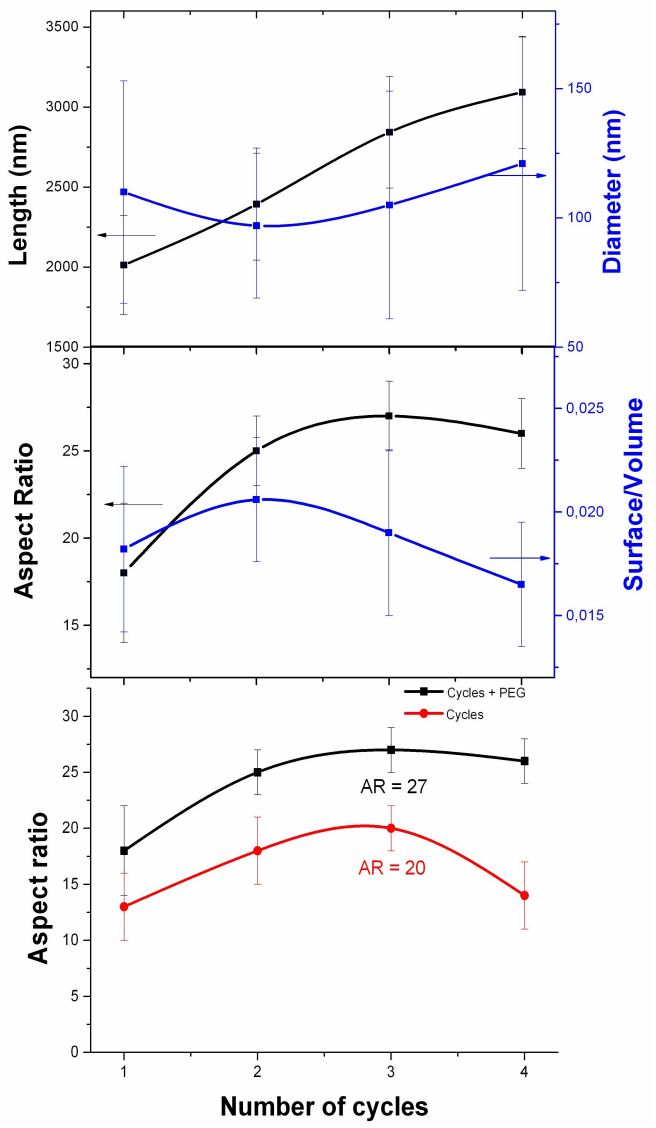

Figure 3.10.: Mean length and diameter (upper panel) and mean aspect ratio and surface-to-volume ratio (middle panel) as a function of the number of cycles using PEG as a shape controlling agent. (Lower panel) Comparison of the aspect ratio of ZnO nanowires grown with and without PEG as a function of the number of cycles. Error bars correspond to the obtained values of standard deviation given in figure 3.9. Length values extracted from the obtained distribution corresponding to an entire nanowire.

Figures 3.9 and 3.10 show the SEM pictures of ZnO nanowires grown using cycles and PEG (a1-a4) and the histograms related to diameter and length (b1-b4, c1-c4) of ZnO nanowires extracted from SEM images. These pictures reveal that with the addition of PEG, the cycles still improve the aspect ratio, and the effect is even enhanced as compared to the case without PEG. In this case, the obtained aspect ratio is around 27 with the addition of the PEG polymer and 20 without it; a comparison of aspect ratio improvement of cycles with and without PEG is shown in 3.10. We note that the breaking of the nanowires grown with PEG occurs already from the second cycle, while it was observed only from the third cycle without PEG. We believe that the reason is the larger length of the nanowires grown by PEG as compared to without PEG, thus leading to more fragile nanowires. We can then estimate a critical length of about 2 µm above which breaking starts to occur.

3.4.2. Growth mechanism

The solution phase synthesis of ZnO nanostructures results from the hydroxylation of Zn^{2+} ions into $Zn(OH)_2$ and $Zn(OH)_4^{2-}$ complexes, followed by the aggregation of complexes and the precipitation of ZnO starting at the center of aggregates when supersaturation is attained [197]. ZnO [0001] polar facets have a higher surface energy than non-polar $[1\bar{1}00]$ and $[2\bar{1}\bar{1}0]$ facets [210], this difference of energies lead to the preferential growth in the c-axis direction, thus rod-like structure. The complex interplay between thermodynamically and kinetically limited reactions leads to the wide variety of observed morphologies for ZnO nanocrystals from 0D to 3D [123]. Such interplay explains the cycle growth proposed hereafter. The three main parameters explaining our mechanism are (i) the use of HMTA as alkaline medium, (ii) the use of Cl^- counter-ion and (iii) the slow addition of the precursor step by step by using the cycling process.
One essential ingredient for the growth of ZnO in solution is the alkaline conditions which control the hydroxylation of Zn^{2+} ions, this is provided by HMTA as it shows several advantages for the growth of ZnO nanowires. First, HMTA acts as a pH buffer. Second, due to its chelat-

ing effect, HMTA binds to Zn^{2+} to limit the rate of Z(OH)2 release avoiding agglomeration and the unwanted rod aggregation [86]. At pH 6.6 and at 25 °C, the degradation of HMTA into ammonia and formaldehyde occurs at a very slow rate. The sticking of HMTA on non-polar facets is thus preserved and favoured. HMTA, thus, regulates the slow delivery of Zn^{2+} ions, provides NH_4^+ ions and preserves the wire facets 3.11.

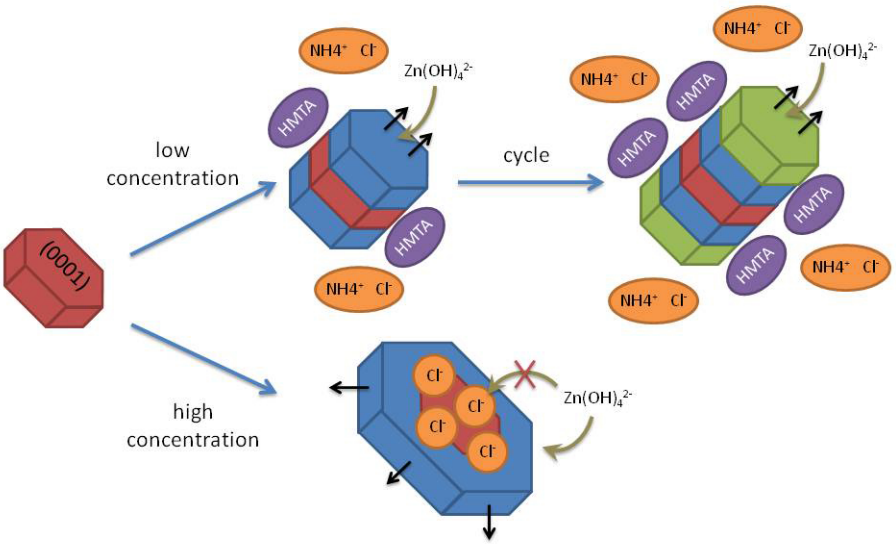

Figure 3.11.: Scheme of the expected mechanism leading to the increase in aspect ratio of the nanowires grown at a low precursor concentration and with cycles, as compared to disks grown at a high precursor concentration.

The case of Cl^- counter-ions is particularly interesting as it can promote rod- or disk-like morphologies depending on its concentration ([133] and figure 3.8). At a high concentration, Cl^- ions act as a capping agent, reducing the interaction of $Zn(OH)_4^{2-}$ ions on the charged polar facets (see figure 3.11, bottom). Cl^- ions are electrostatically attracted by the positively charged [0001]-Zn faces. Since the delivery of $Zn(OH)_4^{2-}$ ions is regulated by HMTA, the kinetics of the Cl^-approaching the surface is faster than $Zn(OH)_4^{2-}$ and will thus block the growth and lead to

lateral growth and disk shaped nanocrystals. At a low concentration of Cl^-, the capping effect is reduced, and the growth nevertheless occurs preferentially from the polar facets, leading to rod-like structures. This preferential growth is enhanced in the presence of HMTA due to its capping properties on the non-polar facets. This mechanism explains the results obtained in figure 3.8, where ZnO large hexagonal discs are obtained when increasing the precursor concentration. In order to increase the aspect ratio, we thus need to reduce the capping effect of Cl^- ions while adding precursors as source of Zn. For this purpose, we believe that the presence of NH_4^+, delivered from degraded HMTA after the release of $Zn(OH)_2$ species, is an important ingredient. The NH_4^+ or HMTA by-product cations interact with Cl^- and decrease the capping effect of Cl^- by decreasing the effective concentration (figure 3.11, top), i.e. acting as a buffer for Cl^- ions. This effect is enhanced since NH_4^+ ions are always in excess as compared to Cl^- (with a ratio of 2 to 1, since HMTA delivers four NH_4^+ ions for each Zn^{2+} ion, i.e. for $2Cl^-$) [197]. The full set of reactions involved in the process can thus be written as follows:

$$ZnCl_2 + 4NH_3 \leftrightarrow [Zn(NH_3)_4]^{2+} + 2Cl^- \tag{3.14}$$

$$[Zn(NH_3)_4]^{2+} 2Cl_2^- + 2H_2O \leftrightarrow Zn(OH)_2 + 2(NH_4^+Cl^-) + 2NH_3 \tag{3.15}$$

The delivery of NH_4^+, which is buffering the Cl^- ions, is a slow process compared to the delivery of Cl^- that occurs during the first steps. For the buffer action to be effective, it is thus required to add the $ZnCl_2$ precursor slowly, in a step-by-step manner, which is exactly what is performed using the sequential or cycle growth. In addition, keeping the critical HMTA concentration during growth enhances the capping effect on the side facets.

3.5. Thermal annealing of ZnO nanowires

The annealing treatment promotes the nanowire crystallization and removes the organic ligands used during the liquid-phase growth. At the same time, annealing can also influence the final density of intrinsic point defects such as zinc vacancy, zinc interstitials, oxygen vacancies, and oxygen interstitials, which play an important electronic role in the performance of the final device [50, 177]. The influence of thermal annealing has shown enhanced conductivity indicating a change on the intrinsic defects [118]. The atmosphere composition is a critical parameter of the annealing process [60, 128, 114, 192]. For example, solution-grown ZnO nanowires are normally annealed in air [107, 193, 197, 56]. However, Mtangi et al. demonstrated that argon atmosphere improves the performance of ZnO nanowire-based devices by reducing the concentration of intrinsic defects [128]. The annealing performed on ZnO nanowires-networks thin films deposited on a substrate, and on prefabricated electrodes in order to test the conductivity. The increasing of the annealing temperature has the purpose of conductivity improvement, when an improvement is not longer observed, further temperatures are not longer studied. The conductivity results of these nanowires will be presented in Chapter 4.

3.5.1. Air annealed ZnO

Figure 3.12a shows the morphology and crystalline characterization of samples annealed under environmental conditions (Air) at different temperatures during one hour time. Figure 3.12a shows the SEM images of ZnO nanowires for as-grown nanowires, annealed 1 h at 100 ^{o}C, 200 ^{o}C, 250 ^{o}C and 300 ^{o}C. From the SEM pictures, no change in the morphology is observed at 100 ^{o}C, 200 ^{o}C and 250 ^{o}C when compared to the non-treated sample, when the temperature is increased above 250 ^{o}C under air conditions, some nanowires are found to be pealing, the ZnO surface is detaching from the nanowire itself. This phenomenon, to our knowledge, has not yet been reported in the literature, and it could be due to a lack of stability of the ZnO nanowires to elevated temperatures. Figure 3.12b shows the normalized XRD analysis of the samples

under different temperatures, from where the wurtzite structure of ZnO is preserved after annealing, the spectra indicates there is no preferred orientation. This XRD pattern is the result of an average signal collected from several random-oriented nanowires thin film with respect to each others and especially to the incident X-ray beam. Therefore, a detailed explanation about the crystallinity improvement with annealing of ZnO nanowires cannot be concluded.
Figure 3.12c and d show a normalized PL spectra regarding the UV peak in order to compare visible light photoluminescence behavior when annealing the samples. Their area ratio for visible peak over UV peak is then calculated for analysis. Two popular mechanisms for this visible emission are still under debate: one is recombination of electrons from the conduction band (CB) with holes in deep traps, and the other is recombination of holes from the VB with a deeply trapped electron [132, 81, 137, 204]. Nevertheless, these models agree that the ZnO visible emission intensity depends on the crystalline defect concentration.The ZnO PL spectra shows a dominant orange emission centered at ∼610 nm, and a weak UV emission at ∼380 nm was observed upon excited by light with a wavelength of 300 nm for as-deposited sample. When the sample is annealed, the UV emission is increased, therefore the ratio in figure d from the two peaks always decreases with air annealing. Previous studies on ZnO reported a luminescence green peak at ∼520 nm, which has been attributed to defects associated with oxygen deficiency [206]. Orange emission is not often discussed, and it does not seem to be fully understood, but some reports pointed out that they are due to interstitial oxygen ions [159]. Regardless of the origin of the orange emission, which is beyond the scope of this thesis, the strong contribution from the visible over the UV emission indicates defective ZnO nanowires and its improvement by annealing.

3.5.2. Ar annealed ZnO

Samples were annealed under a constant Argon flow during one hour at different temperatures. Figure 3.13 shows the morphology and crys-

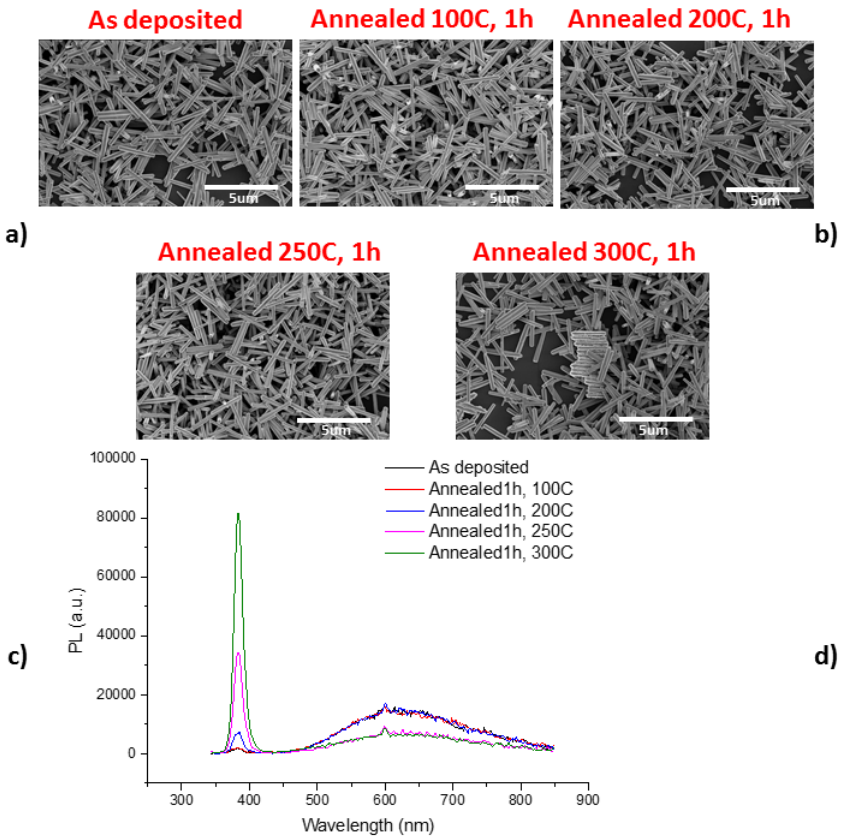

	UV Peak Area	Visible Peak Area	$A_{visible}/A_{UV}$
As deposited	22,34	1574,30	70,47
100C Annealed	22,28	1280,06	57,45
200C Annealed	21,83	438,64	20,09
250C Annealed	17,61	46,89	2,66
300C Annealed	16,45	17,70	1,08

Figure 3.12.: Characterization of ZnO nanowires after annealing under environmental conditions during one hour. a) Morphology of ZnO nanowires after annealing at different temperatures, b) XRD pattern of ZnO nanowires after annealing at different temperatures. The figure curves are normalized to the maximum of the ZnO (100) peak, c) Photoluminescence spectra of ZnO nanowires for each annealed temperature. The curves are normalized to the maximum of the ZnO UV peak at 380 nm; and d) summary table comparing area-under-the-peak ratio from the two peaks contribution.

talline characterization of samples annealed under Ar conditions at different temperatures during one hour time. Figure 3.13a shows the SEM images of ZnO nanowires for as-grown nanowires, annealed 1 h at 100 °C, 200 °C, 300 °C and 400 °C. From the SEM pictures, no change is observed at 100 °C as compared to the non-treated sample, when the temperature is increased above 100 °C under Ar the peeling behavior already discussed and seen for annealed samples under air was again observed, confirming the hypothesis that the peeling could be due to a lack of stability from the ZnO nanowires to elevated temperatures. Samples annealed under a constant flow of Argon also exhibit a porous appearance that was not existent on the as-grown nanowires. This phenomenon has been observed in literature and known as Kirkendall's effect owing to a vacancy diffusion mechanism.

It is well-accepted that diffusion could occur by direct atomic exchange mechanism, in which atoms migrate by switching positions with atoms on adjacent lattice sites or, another possibility involves lattice vacancies, where an atom moves into a vacant lattice site switching places [37, 1, 125]. As a result, from this effect, the presence of pores is stated in the material formed during diffusion. When the vacancies are substantial to stability in a material [154], they can expand to restore equilibrium creating pores on the material. The formation of pores due to Kirkendall effect typically occurs above a temperature threshold, in order to avoid their presence annealing could be performed at lower temperatures [41].

Figure 3.13b shows the normalized XRD analysis of the samples under different annealing temperatures under a constant argon flow, the wurtzite structure of ZnO is preserved after annealing. Figure 3.13c and d show a normalized PL spectra regarding the UV peak in order to compare visible light photoluminescence behavior when annealing the samples. Their area ratio for visible peak over UV peak is then calculated for analysis. The ZnO PL spectra show a dominant orange emission centered at ∼610 nm, and a weak UV emission at ∼380 nm was observed upon excited by light with a wavelength of 300 nm for as deposited sample, when the sample is annealed this UV emission is then increased, therefore the ratio in figure d from the two peaks always

decreases with argon annealing. This trend is observed for temperatures up to 400 °C, when the porosity appears and in this case, the area-under-the-peak ratio increases considerably in comparison with the previous annealing and the lower temperatures. The extended amount of oxygen vacancies explaining the existence of pores due to the kirkendall effect exhibits a considerably increase of defects in the ZnO nanowires, resulting in the visible peak which reveals the behavior of defects, explaining why this ratio increases again after 400°C annealing.

3.5.3. H_2N_2 annealed ZnO

In order to make a complete study of the annealing, a reducting gas such as H_2N_2 is also investigated. Samples were annealed under a gas composed of 5% Hydrogen and 95% Nitrogen during one hour for different temperatures. Figure 3.14 shows the morphology and crystalline characterization of samples annealed under H_2N_2 at different temperatures. Figure 3.14a shows the SEM images of ZnO nanowires for as-grown nanowires, annealed 1 h at 200 °C, 300 °C, 350 °C and 400 °C. From the SEM pictures, no change is observed at 100 °C as compared to the non-treated sample, when the temperature is increased further than 100 °C under H_2N_2 the peeling behavior already discussed and seen for annealed samples under air and Ar was again observed, once again confirming the hypothesis that the peeling could be due to a lack of stability from the ZnO nanowires to elevated temperatures. Samples annealed under a H_2N_2 atmosphere also exhibit a porous appearance as the samples annealed in Ar atmosphere, from SEM images we observe the porosity is different, pores are not uniform and round-shaped. Nonetheless, once the temperature or the concentration of hydrogen are increased, pores are not longer observed but completely reduced nanowires, result that was not encountered when annealing ZnO nanowires at higher temperatures where the nanowires were porous as the once shown in 3.13. Therefore, we could conclude that the porosity present under H_2N_2, besides Kirkendall's effect, is due to the beginning of deterioration of ZnO nanowires.

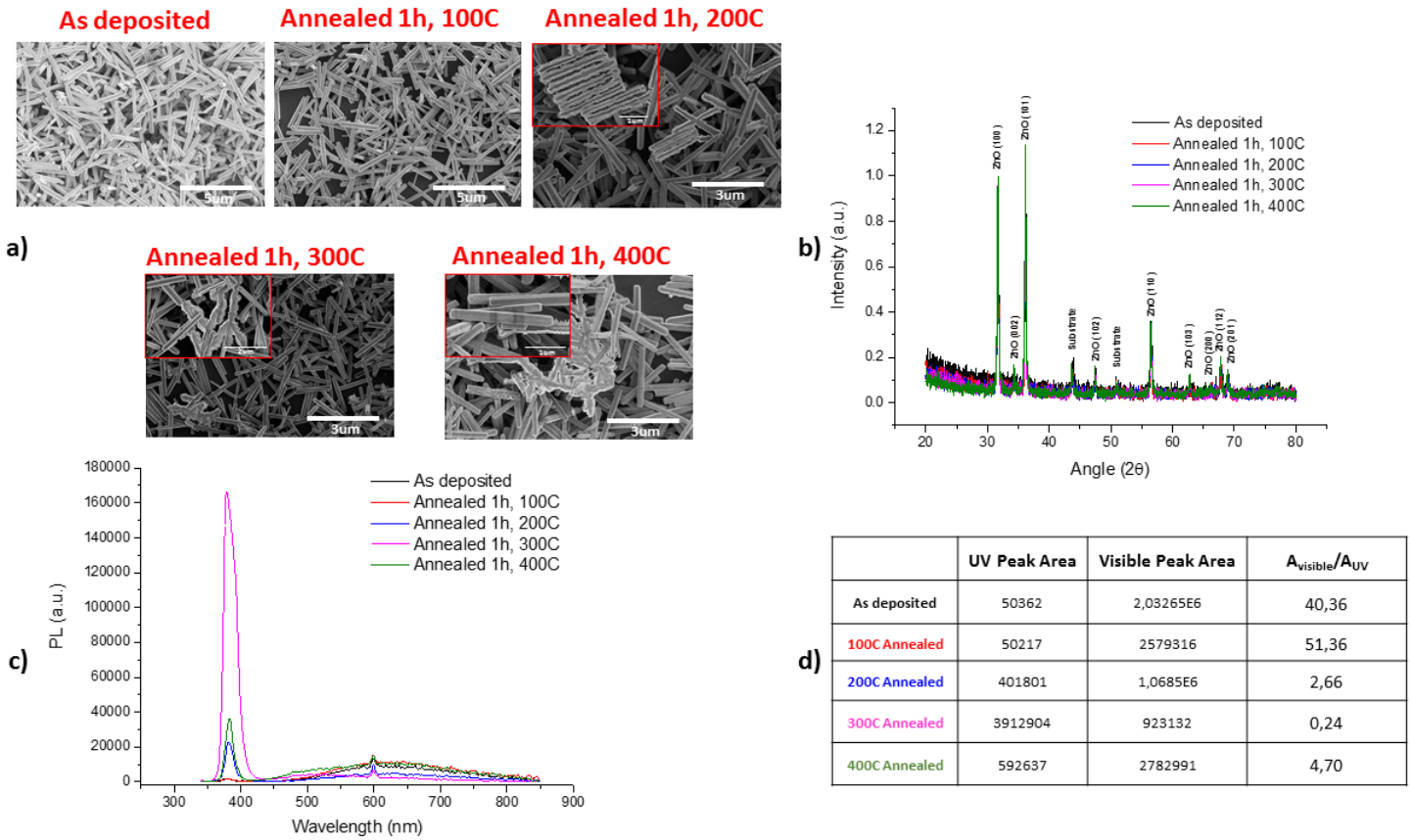

	UV Peak Area	Visible Peak Area	$A_{visible}/A_{UV}$
As deposited	50362	2,03265E6	40,36
100C Annealed	50217	2579316	51,36
200C Annealed	401801	1,0685E6	2,66
300C Annealed	3912904	923132	0,24
400C Annealed	592637	2782991	4,70

Figure 3.13.: Characterization of ZnO nanowires after annealing under a constant flow of Argon during one hour. a) Morphology of ZnO nanowires after annealing at different temperatures, b) XRD pattern of ZnO nanowires after annealing at different temperatures. The figure curves are normalized to the maximum of the ZnO (100) peak, c) Photoluminescence spectra of ZnO nanowires for each annealed temperature. The curves are normalized to the maximum of the ZnO UV peak at 380 nm; and d) summary table comparing area-under-the-peak ratio from the two peaks contribution.

Figure 3.14b shows the normalized XRD analysis of the samples under different anneling temperatures under H_2N_2 gas, the wurtzite structure of ZnO is preserved after annealing. Figure 3.14c and d show a normalized PL spectra regarding the UV peak in order to compare visible light photoluminescence behaviour when annealing the samples. Their area ratio for visible peak over UV peak is then calculated for analysis. The ZnO PL spectra show an orange emission centered at ∼610 nm for as deposited, 200 °C and 300 °C annealed samples and green emission centered at ∼520 nm for samples annealed at higher temperatures; and a UV emission at ∼380 nm was observed upon excited by light with a wavelength of 300 nm. When the sample is annealed, the UV emission is increased, therefore the ratio in figure 3.14d from the two peaks decreases with H_2N_2 annealing at 200 °C and 300 °C. This trend is observed for temperatures up to 300 °C, when green emission is then detected, previous studies on ZnO reported a luminescence green peak at ∼520 nm, which has been attributed to defects associated with oxygen deficiency [206]. Since orange emission is not completely well-understood but it is well-accepted to agree that interstitials defects play a big role in this emission. Samples annealed a lower temperature under H_2N_2 conditions decrease orange-related visible emission related to interstitials and vacancies. The new peak centered at 520 nm appearing when samples are annealed at higher temperatures, could be explained by the creation of oxygen vacancies on ZnO nanowires. The Kirkendall's effect pore creation could be also the reason why nanowires are destroyed after a long exposure to H_2N_2 concentrations or even higher temperatures by the expansion of these pores. Futhermore, this could also help the understanding why the area-under-the-peak increases for temperatures above 300 °C since new defects (oxygen vacancies) could be created.

3.6. Conclusions

The introduction of cycles enables ZnO nanowires created over the first synthesis to behave as ZnO nuclei during the second synthesis, allowing

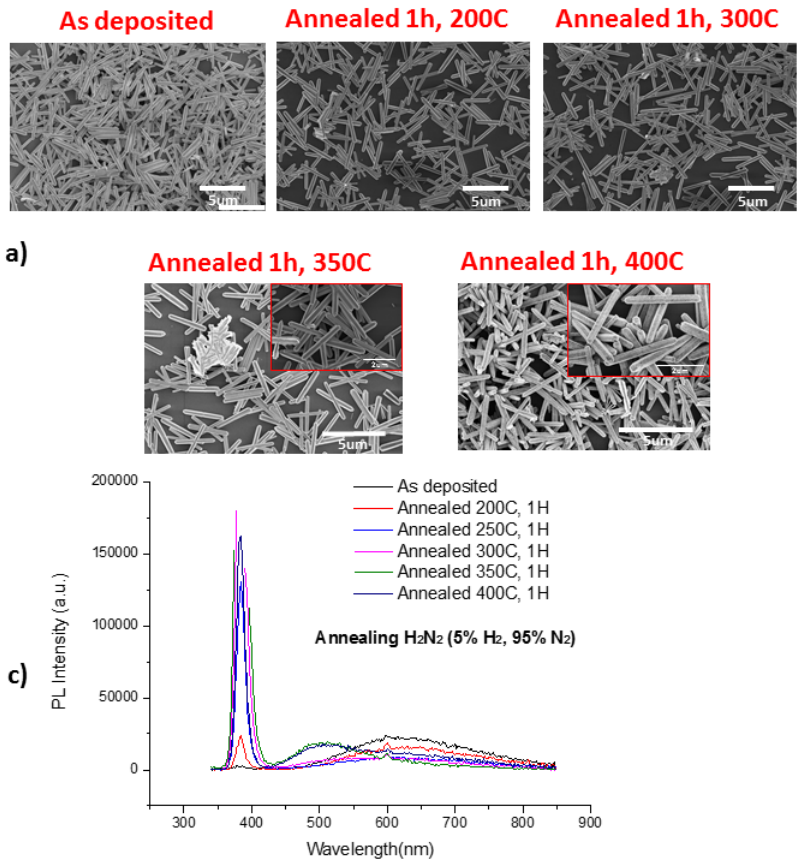

d)

	UV Peak Area	Visible Peak Area	$A_{visible}/A_{UV}$
As deposited	74009	5,03E6	67,96
200C Annealed	365071	3,55E6	9,72
250C Annealed	2,07E6	2,17E6	1,05
300C Annealed	3,75E6	2,56E6	0,68
350C Annealed	3,90E6	3,60E6	0,92
400C Annealed	2,61E6	4,01E6	1,54

Figure 3.14.: Characterization of ZnO nanowires after annealing under H2N2 (5% Hydrogen, 95% Nitrogen), reducting atmosphere, during one hour. a) Morphology of ZnO nanowires after annealing at different temperatures, b) XRD pattern of ZnO nanowires after annealing at different temperatures. The figure curves are normalized to the maximum of the ZnO (100) peak, c) Photoluminescence spectra of ZnO nanowires for each annealed temperature. The curves are normalized to the maximum of the ZnO UV peak at 380 nm; and d) summary table comparing area-under-the-peak ratio from the two peaks contribution.

crystal growth in the c-direction to be improved. Polymers such as PEG allow the control of the size and shape of ZnO, in particular, leading the growth to occur on the c-axis preferentially than any other direction possible due to its attachment to the non-polar facets of the crystal. Viscosity is an important parameter which inhibits growth on an aqueous solution; for this reason, nucleation of ZnO nanowires is affected by the PEG concentration. The combination of cycles with the shape controlling agent PEG enhances the ZnO nanowire aspect ratio up to 27 instead of 20 in the case of the normal growth aspect ratio. Furthermore, a new hypothesis explaining the growth mechanism of rod and disc formation is fully discussed. While we have demonstrated that the involved mechanism can improve the aspect ratio when a single metal precursor is used, the cycle growth could be extended to the growth of axial heterostructures when using cycles with different metal precursors, which is a challenge in liquid phase with homogeneous nucleation. Optimum thermal annealing parameters in terms of temperature, atmosphere and duration are studied. We have chosen to compare non-treated ZnO nanowires and argon-annealed ZnO nanowires at 250 °C during one hour in the next chapters. Argon atmosphere at 250 °C achieves the best results in terms of conductivity without affecting their initial morphology. Therefore, this atmosphere is chosen as ZnO nanowires annealing treatment in Chapters 4 and 5.

4. Electrical transport analysis

Two semiconducting interfaces in contact by a junction would have either an Ohmic or Schottky behavior when a voltage is applied. It is mostly accepted that the non-linear I-V characteristics are strongly attributed to the microstructure composed of n-type semiconducting ZnO grains, and therefore, creating Schottky contact [52, 120]. In this chapter, a short review of conduction in polycrystalline ZnO based on grain-to-grain junctions potential barriers is discussed. Inspired by the conduction models of polycrystalline ZnO, we propose an electrical transport model for a ZnO-based nanowire network, supposed to be crystalline nanowires, which is mainly determined by the potential barrier (Φ_B) generated by nanowire-to-nanowire junctions. This model is validated by investigating the different contact geometries described in Chapter 2. The purpose of this chapter is to go further in the study of ZnO nanowire network and the understanding of the behavior of potential barrier created by nanowire-nanowire contact and of the series resistance of the network-based ZnO thin film through a conductive model in order to improve the state-of-the-art of ZnO nanowires-based conductometric gas sensors. The controlled obtained structures in Chapter 3, ZnO nanowires with aspect ratio of 14, will allows us to propose an accurate conduction model for an uniform network-based thin film.

4.1. Review of non-linear electrical transport

4.1.1. Grain-to-grain conduction model approach

Due to their unusual electrical properties, granular semiconductor materials are used in a wide range of devices, such as varistors or gas sensors.

ZnO is an n-type semiconductor due to an excess of Zinc metal that goes twice through ionization. These generates two types of intrinsic donors that could be assigned to Zn interstitials (Frenkel defects) [73], or to the oxygen vacancies (Schottky defects) [101, 120]. However, the major contribution of these two are the oxygen vacancies generated during the synthesis which control mainly the conductivity. ZnO granular thin films conductivity models are widely studied inspired by accepted models for varistors and then applied to metal oxide-based granular thin films understanding [30, 152, 153, 121]. Varistors are widely known as components with electrical resistance which depends on the applied voltage. It is characterized for its non-linear IV behavior, similar to the one known for diodes. The main difference between a diode and a varistor is the asymmetric I-V characteristics for diodes, while they are symmetric in the case of varistors, such that at low voltages the electrical resistance is very high and decreases as the voltage is raised. Metal-oxide varistors are the most common type of semiconductor devices with highly non-linear current-voltage characteristics composed by zinc oxide grains and other metal oxides inside two metal plates acting as electrodes. Zinc oxide conductive grains with grain boundary potential barriers formed during their sintering exhibit non-linear conduction. The boundary between the grains forms a junction, resulting in a symmetric potential barrier where electrical current flows. When a small or moderate voltage is applied across the electrodes, only a tiny current flows, caused by the grain boundary potential of the junctions. When a larger voltage is applied, the junction breaks down due to a combination of thermionic emission and electron tunneling, resulting in a large current flow through the potential barrier [108, 121]. The origin of this non-linear behavior present in varistors is controlled by the potential barriers between grain-to-grain interfaces and follows a conduction mechanism related to thermionic emission principle [152].

Gas sensing metal oxides are also granular semiconductors, their electrical conductivity is controlled by potential barriers associated with grain-to-grain boundaries [16]. Assuming that each grain contributes to the conductivity of the whole gas sensing film, it can be modeled by assuming identical grain boundaries are connected in series where the

conductivity depends exponentially on the barrier height [16]. For the electrons conductivity, the grain-boundary potential barrier limits their motion considerably, this leads to a bending of the band structure. The band bending, often called double Schottky barrier structure, gives rise to the depletion of conduction electrons near the surfaces of the grains and the grain boundary. The total voltage applied across the sample, dominated by the junctions produced by the grain boundaries between grains, will be equal to the contribution from each grain boundary and the thin film itself by applying Kirchhoff's and Ohm's laws.
Varpula et al. have reported the granular thin films conductivity based on grain boundary barrier limited models concluding that I–V curves from granular thin films present four characteristic regions: linear, sub-linear, super-linear and series resistance limited [91]. Figure 4.1 presents the four different regions of a typical non linear I-V characteristics of a ZnO granular thin film. At low voltages, current is limited by the potential barriers created by the grain-to-grain boundaries thus the behavior is linear [120]. Then a sub-linear region appears when the current increases with voltage more slowly than in the linear region, dominated by the thermionic emission or the tunneling of carriers through the grain boundary potential barrier [108, 121]. At higher voltages, the sub-linear region changes into the super-linear region, where this barrier decreases when increasing the voltage and the current increases exponentially. In the series resistance limited region, which lies at very high voltages, the current flow is only limited by the series resistance and the I-V curve returns a to linear behavior [109][170, 171, 172, 173].

4.1.2. Nanowires network-based models

The first studies made on network-based systems started not so long ago and for carbon nanotubes network systems as done by Yanagi et al. Nevertheless, these studies are on-early stages and the conduction mechanism is not well-understood [201]. Thus, a fundamental understanding of the electrical transport properties in such networks is critical. Recently, some studies based on nanowires network conduction models have been published on Ag nanowires. To our knowledge, the contribu-

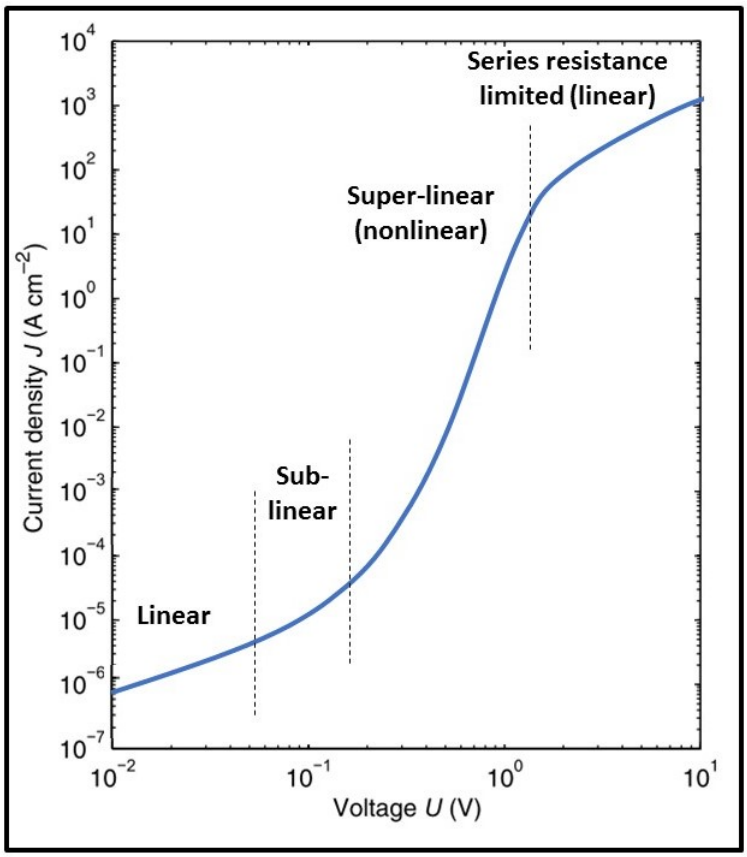

Figure 4.1.: Current density vs. Voltage non-linear characteristic behavior for ZnO granular films.

tion from thin films nanowire-based network has never been specifically investigated for its optimization for semiconductor materials.
In 2015, Bellew et al. manage to measure the junction resistance, for the first time, for the junction between two Ag nanowires in contact on a network (11 Ω), comparable to the resistance associated with the wire segments within a nanowire network. Junctions are the base when building any network. It is frequently assumed that the junction resistance is significantly larger than the contribution of the nanowires, neglecting the nanowire resistance contribution completely. Their research was based on a rigorous computational model based on real Ag nanowire networks in which the wire junctions and wire length segments

are mapped to create a near-perfect replica [22].

4.2. Junction-based non-linear model for semiconductor nanowires network

Based on what is proposed in the state-of-the-art for non-linear granular thin films and by assuming our ZnO nanowires as monocrystalline semiconductors, we propose a conductive model for un-doped ZnO nanowires network-based electrical transport using liquid phase synthesis [31] where the conductivity is controlled by the potential barriers (grain-to-grain boundaries) and its exponential behavior as a function of the barrier height (figure 4.2a,b and c). Figure 4.2d presents the non linear I-V characteristics of ZnO nanowires network, which can be compared to the non-linear behavior of polycrystallin films in figure 4.1. Our I-V curves are located in the super-linear (or non linear) region towards the series resistance limited region for the last values of V. In this manner, we describe the junction properties of ZnO nanowires films and study their resistance in order to draw conclusions about the network optimization and its performance, which for gas sensing hasn't been studied yet.

Taking a similar approach than for granular thin films, Kirchhoff law is applied:

$$U = N_{gb}U_{gb} + R_S I \tag{4.1}$$

Where U is total voltage applied accross the network, indicating the conduction is driven by the number of nanowires junctions (Ngb) in the nanowire-based thin film and their series resistance (Rs) which includes the contact resistance and the nanowire resistance contribution.

4.2.1. Fitting

The forward I–V characteristics in vacuum were measured for multiple devices with different geometries from -20 V to 20 V (shown in Figure 4.2d). The I-V curves were fitted to the relation for thermionic emis-

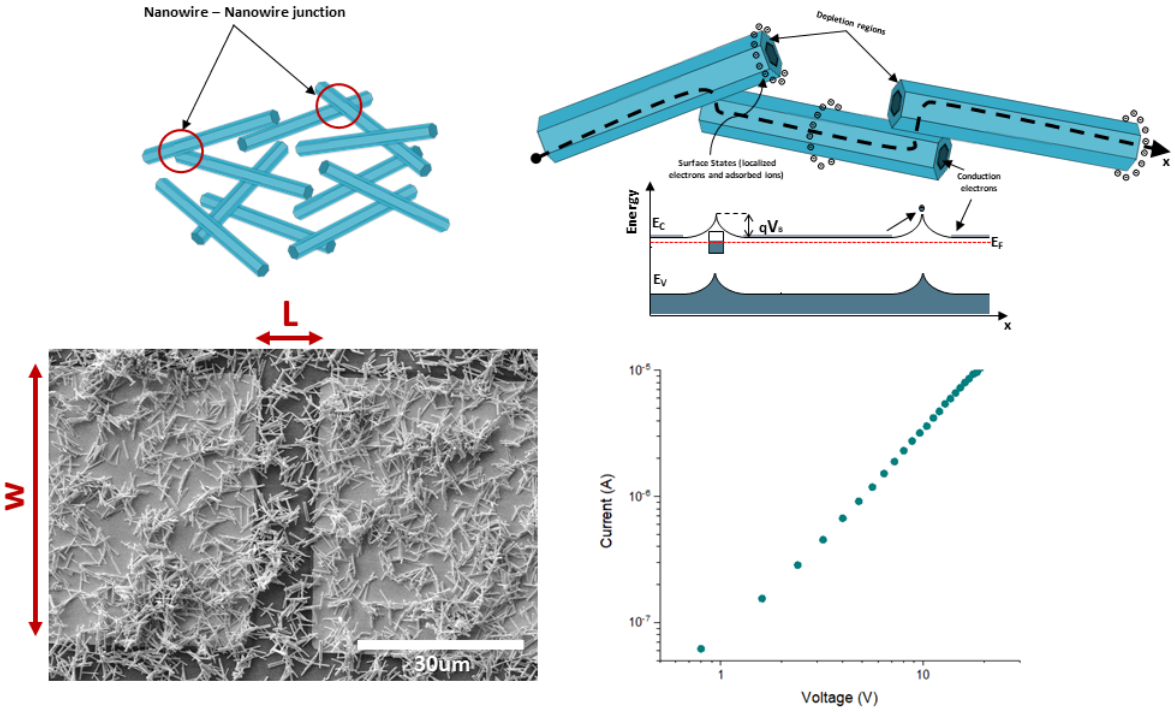

Figure 4.2.: Nanowires electrical transport behavior. a) Top view of nanowire-to-nanowire junction on network-based film, b) Schematic cross sectional view of network-based sensing film with electronic-energy bands representation of semiconductors in equilibrium, where E_c and E_v are the conduction and valence bands, B grain boundary energy and E_F the fermi level, c) ZnO nanowires deposited onto pre-fabricated substrate, where L= gap between the electrodes and W= Contacts width. and; d) I–V characteristics for ZnO nanowires network-based thin film under vacuum at room temperature.

sion over a barrier (relation below). The two terms of this equation correspond to the two-sided junction (negative and positive voltages) to simulate a symmetric junction.

$$I(U) = I_1(e^{\frac{q(U-IR_S)}{n_1 N_{1,gb} K_B T}} - 1) - I_2(e^{-\frac{q(U-IR_S)}{n_2 N_{2,gb} K_B T}} - 1) \tag{4.2}$$

where

$$I_{1,2} = AT^2 e^{-\frac{\varphi_b}{K_B T}} \tag{4.3}$$

$I_{1,2}$ is the amplitude of the current dependent of the Richardson constant from ZnO and the effective area of the junction-based thin film, $n_{1,2}$ is the ideality factor that is a quantity for describing the deviation of the diode from an ideal Schottky barrier, for which n = 1, K the Boltzmann constant, T the absolute temperature, q is the charge which dominates the conduction (electrons), Φ_B the grain boundary potential barrier and, I and V the current measured and applied voltage.
It is widely known in literature that one side of equation 4.2 is solved using LambertW function (equation 4.4) as follows:

$$z = f^{-1}(ze^z) = W(ze^z) \tag{4.4}$$

where e^z is the exponential function and z is any complex number.

$$I(U) = \frac{nN_{gb}K_B}{qR_S} lambertW(\frac{qI_{1,2}R_s}{nN_{gb}K_B} e^{\frac{q(U+I_{1,2}R_S)}{nN_{gb}K_B}}) \tag{4.5}$$

Equation 4.5 gives a non-linear dependence between I and V, for a given number of junctions in a thin film. This relation will be used as a fit for the collected experimental data of our devices. From this fit, parameters nN_{gb} and R_s are determined and their behavior with different geometries is evaluated.

4.2.2. Influence of geometry of contacts

From a first fit, the data appearing in figure 4.2d are fitted using equation 4.5, this allows to determine the behavior of some parameters as a function of the pre-determined contact geometries. The following ex-

pected hypotheses are described as follows:

- The number of grain boundaries times the ideality factor will be influenced by the gap in between the electrodes (L), since more junctions will be created, and independent on the contact width (W) of the device as the shortest (horizontal) junctions path is considered to contribute.

- The series resistance of the system will be dominated by the contact resistance depending inversely with the W and not with L since when larger current is allowed from nanowires junction, the contribution will be reduced. The nanowire resistance itself will be dependent on L and not on W, as only horizontal paths are more likely to contribute in conductivity.

I-V characteristics of ZnO nanowire network-based sensors were obtained under primary vacuum conditions (10^{-3} mbar) using Cryogenic two probe station (figure 2.12). The contacts geometries were changed as indicated in figure 2.2 where the gap (L) varies between 2-20 μm and the contact width (W) from 10-300 μm. The analyzed devices geometries for a fixed L are at W=10 μm due to the high current contribution at higher W a break down was observed. For different W, the L was fixed at 20 μm since the higher nanowire-to-nanowire junction contribution comes from higher contact gaps. The data collected from the different devices was fitted using relation 4.5 to obtain $nNgb$ and Rs parameters according to contact geometries in order to confirm the hypothesis explained above. The left and right upper panels from figure 4.3 present the behavior of $nNgb$ of as-grown and argon-annealed nanowires with the contact geometries L and W. The bottom panels of figure 4.3 exhibit the Rs trend with and without annealing. Argon-annealed samples were studied since they show higher conductive behavior without damaging ZnO nanowires as compared to other annealing studied. These behaviors confirm the hypothesis explained above, a linear dependence from the ideality factor times the number of grain boundaries involved in the conduction path to the gap between the electrodes and remaining constant with the contact width. The series resistance is shown at the figure 4.3 (lower

panel) confirming its inverse dependence on the contact width. Therefore, we can conclude that the main conductivity contribution comes from created network junctions in which the argon-annealed sample improves conductivity by decreasing the contact resistance. This leads the nanowire resistance to appear, showing a linear dependence with L, as it is expected since the number of junctions increases.

4.3. Model Validation

For a validation of this model and fitting accuracy, a device of 20 μm gap and 300 μm contact width is selected due to its maximal junction's contribution between the contact's gap and the maximal contact width to enhance current contribution and avoid any noise. Figure 4.4. presents the obtained experimental data, fitted by using the thermionic emission voltage over a junction relation between the nanowires. As seen before (in figure 4.2d), this result reflects a reproducible accurate fitting with the experimental data. In order to validate that the current contribution comes mainly from the nanowires junction, two curves are plotted with the obtained fitting parameters but the series resistance, which is fixed at 0 Ohms (assuming there is no contribution from the nanowire itself or the contact resistance) and, considering the obtained resistance is ten times larger than the value obtained with the fit. When Rs = 0 Ohms, for few volts applied, the current increases exponentially with the voltage as an ideal diode but when the Rs is increased, the amount of current passing through the device is then limited and therefore not exponentially dependent on the voltage. Consequently, from this graph we can conclude that the conduction mechanism is mainly controlled by the grain-to-grain boundaries or nanowires junctions on the network-based thin film and not by the series resistance coming from the nanowires themselves and the contact resistance.

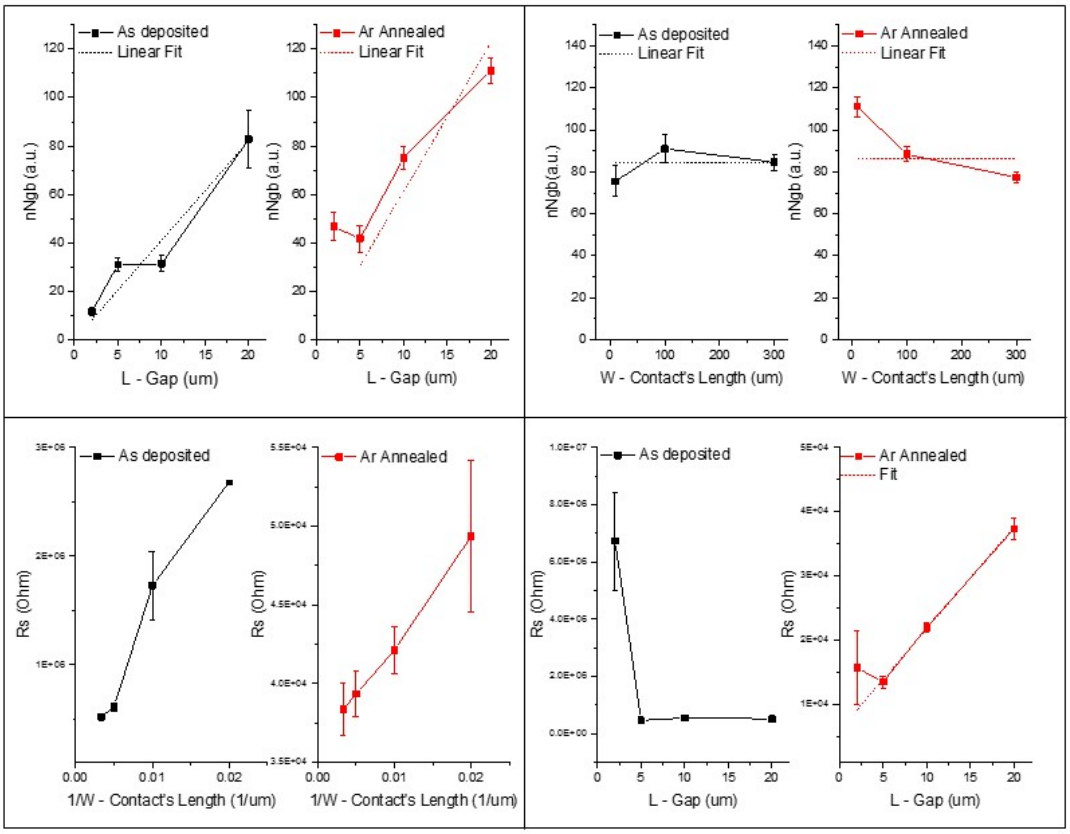

Figure 4.3.: nNgb and Rs parameters behaviour with contact geometries (L,W) for samples as-deposited (or as-grown nanowires) and AR-annealed. a) nNgb linear dependence with L for W = 10 μm, b) nNgb constant behaviour with W for L= 20 μm, c) series resistance depending inversely with W for L=20 μm, representing contribution from contacts and d) series resistance dependence with L for W= 10 μm, indicating nanowire resistance contribution. The used ZnO nanowires used for the analysis correspond to 1 cycle (length =3 μm, diameter= 250 nm). Error bars correspond to the obtained standard deviation of the mean generated by the fit for each value.

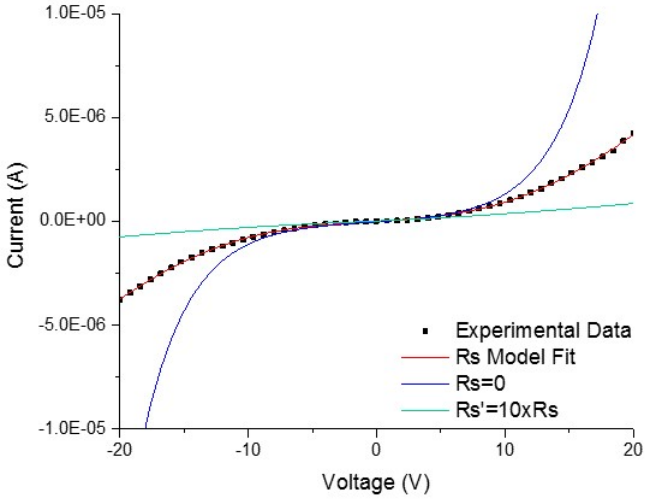

Figure 4.4.: I–V characteristics for as-grown ZnO nanowires network-based thin film under vacuum at room temperature. Model Validation with a L = 20 μm gap between the electrodes and W = 300 μm contact width device.

4.4. Influence of temperature

Figure 4.5 presents the I-V characteristics at various temperatures mesurements with a non-linear behaviour from -20 V to 20 V. These I–V curves were obtained at 100, 160, 220, 280, 300, 340, and 400 K, respectively. The measured current increases when increasing the temperature from 300 to 400 K, which is commonly accepted for ZnO n-type semiconductor behaviour. The resistivity of the nanowires is thus increased when the temperature decreased from 300 to 100 K, showing a typical semiconductor R vs. T characteristic, which according to the thermionic emission, the higher temperature allows carriers to flow over the potential barrier created between the ZnO nanowire-based network film. Since the oxygen vacancies and zinc interstitials are responsible for conductivity in surface, and our ZnO nanowires present high density of these defects characterized by PL measurements in our previous work [31], we can could conclude the conductivity contribution may come from surface rather than bulk.

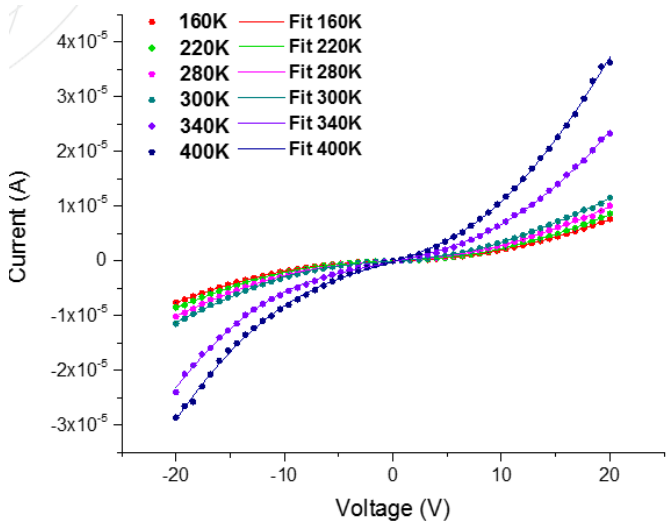

Figure 4.5.: Temperature dependence I–V characteristics for ZnO nanowires network-based thin film under vacuum. The measured device corresponds to L = 20 μm and W =300 μm.

From equation 4.5, the obtained parameter $I_{1,2}$ from this first fit, is then plotted in function of the absolute temperature, revealing a clear exponential dependence behaviour with the temperature (figure 4.6).

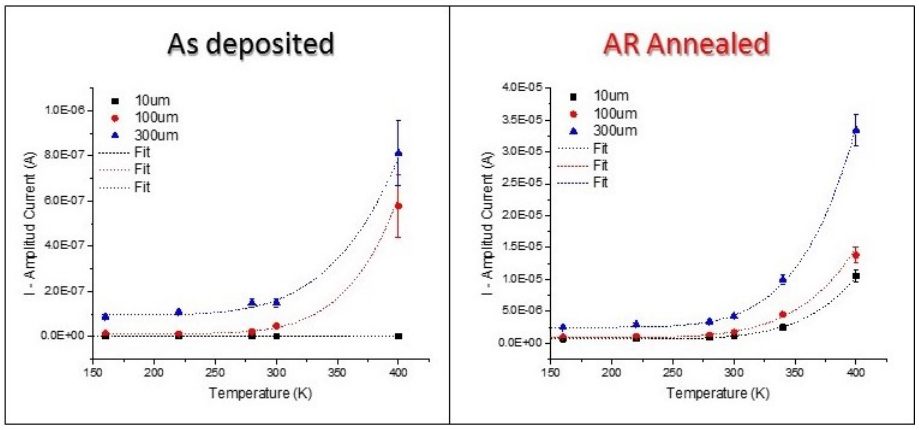

Figure 4.6.: $I_{1,2}$ extracted from first fit dependence with temperature (T). The used ZnO nanowires used for the analysis correspond to 1 cycle (length =3 μm, diameter= 250 nm). Error bars correspond to the obtained error generated by the fit.

From this result, a second fit then realized in order to extract parameters A and Φ_B (equation 4.3) for the different tested geometries. The extracted parameters and the resulting dependence is shown below:

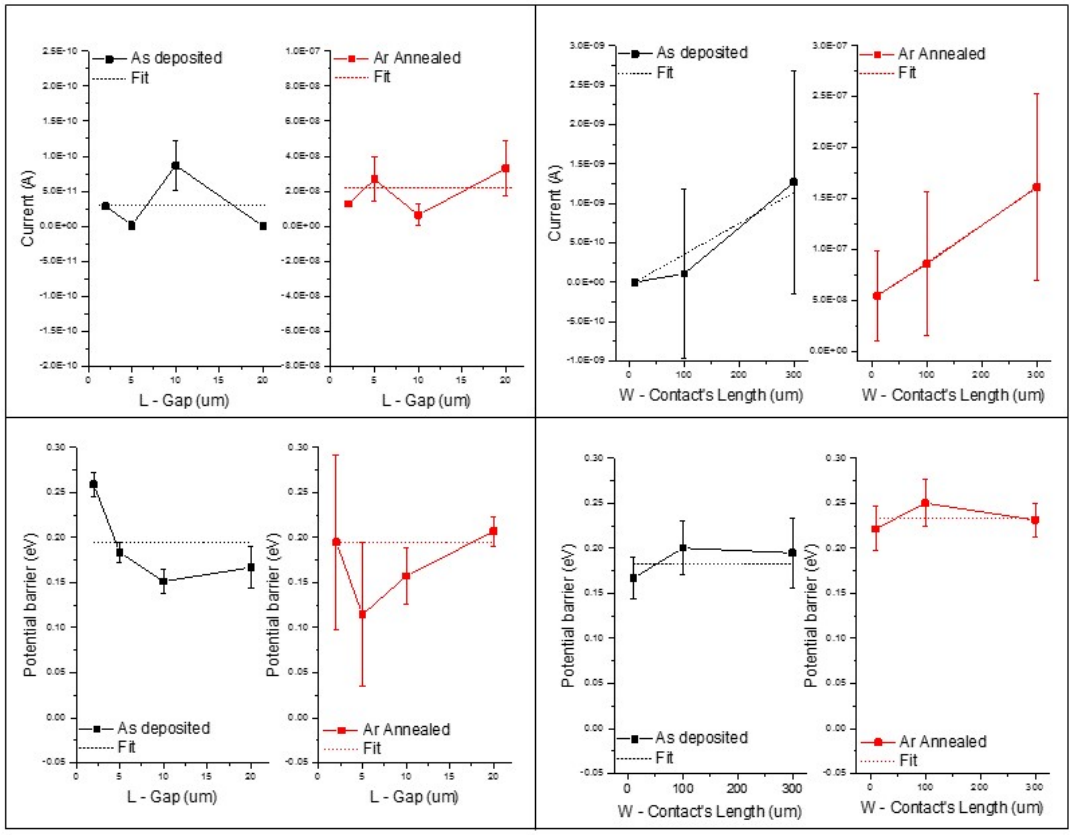

Figure 4.7.: Second fit A and B parameters behaviour with contact geometries (L,W). a) A dependence with L, remaining constant, W=10 μm is kept constant since the junction contribution is mostly the same in each case, b) linear dependence of A with W fixed at L=20 μm when more junctions are involved in current measurements then the contribution is higher, c) Φ_B non-dependence with L for W=10 μm and, d) Φ_B independent with W for L=20 μm.The used ZnO nanowires used for the analysis correspond to 1 cycle (length =3 μm, diameter= 250 nm). Error bars correspond to the standard deviation of the mean generated by the fit for each value.

From figure 4.7, A parameter is completely dependent on W since the current is higher, when the sample is annealed, this contribution is improved, indicating the sample is more conductive. The intersection with y-axis will indicate the leakage current for the device, since the conductivity is improved when annealed, this one is as well increased. Leak current for sample as deposited is almost negligible. The potential barrier doesn't show any dependence neither on L or on W, meaning the potential barrier (Φ_B) originating from nanowire-to-nanowire junctions boundaries are independent of the contact geometries. Parameters A and Φ_B show higher error bars than the ones in figure 4.3 indicating higher uncertainty. Certainly, performing a fit gives an average of the data and is therefore expected to improve accuracy. But, when several parameters are to be determined by a fit, even when accurate, the fact of value compensation from one parameter to another cannot be avoided and thus, a second fit with these parameters, could carry out this compensation effect into a second fit generating more uncertainty. The potential barrier (Φ_B) does not seem to change depending on the surface treatment applied and since the nanowires are the same, the annealing doesn't change the nature of the junction. This means that probably, surface treatment applied could remove surface contamination or organic residues, increase the doping of native defects such as oxygen vacancies in the surface which originates higher conduction without changing the potential barrier of the nanowire junctions. The obtained values correlate with the accepted values for barrier heights since Au diodes on ZnO can range from 0 to 1.2 eV, depending on the crystal, the surface preparation, and the conditions under which the contact is formed [26].

Figure 4.8 summarizes all the obtained parameters resulting from the proposed electrical transport model of the two samples, as-deposited and Ar-annealed at 250 °C, indicating the ideality factor per unitary junction (obtained by normalizing $nN_{gb}/L = n/L_o$) is increased when the sample is annealed. If we assume that the unitary junction remains constant in each sample, this leads to an increase of the ideality factor from one sample to another; and vice-versa, if the unitary junction could change from a sample to another and assuming ideality factor equal to 1, then

the obtained unitary junctions length are 250 nm and 160 nm, respectively. However, this analysis is established assuming ZnO nanowires thin film devices are deposited uniformly and their dispersion is similar in each sample.

The A amplitude, depending on the thin film properties (such the area and the current contribution) and the Richardson constant for ZnO, is increased when annealing. This behavior is expected since when performing an annealing, organic residues desorb from the surface which improves the thin film conductivity. The improvement from air-annealed sample towards the as-deposited sample could be explained by the organic residues desorption on the surface. Nonetheless, argon-annealed sample show a higher improvement of about three order of magnitude. This could be explained by better crystallization after this annealing or, from the PL results at 400 °C, the possible creation of oxygen vacancies leading to a higher conductivity.

The potential barrier remains mostly constant for non-treated and Ar-annealed nanowires, showing no modification of nanowires junctions. On the other hand, for air-annealed sample, the calculated potential barrier is very small as compared to the other samples. A possible explanation would be a Fermi energy level shift due to lack or excess of defects after air annealing, thus decreasing the potential barrier. Unfortunately, PL spectra do not provide detailed information in order to make a more precise conclusion.

Finally, the series resistance for the as-deposited sample indicates the contact resistance is highly dominant over the thin film resistance. When annealing at 250 °C, the contact resistance decreases which allows the resistance corresponding to the nanowires contribution to be determined. This could be due to the organic residues desorption on the annealed samples as well as an improvement of crystallinity of the nanowires.

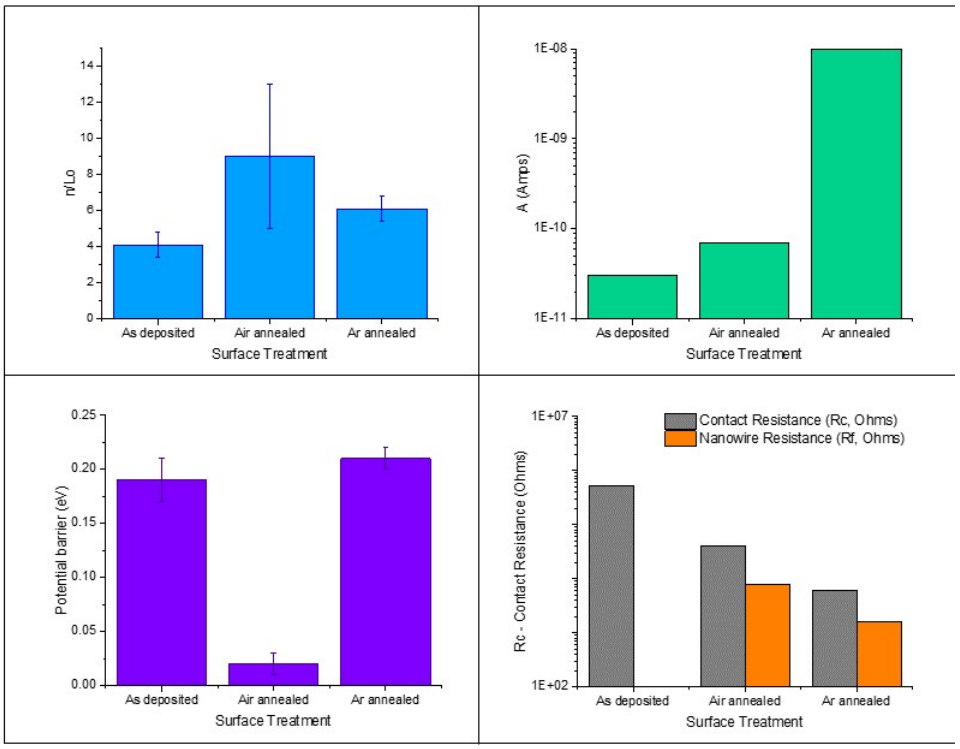

Figure 4.8.: Recapitulative figure summarizing all results obtained for the different parameters including the analyzed samples. a) Ideality factor per junction length for sample as-deposited and Ar-annealed, b) A amplitude factor in function or as-deposited and Ar-annealed, c) Potential barrier for the different samples and d) Series resistance (linear dependence with L) for the sample indicating after the annealing the contact resistance (linear dependence with $1/W$) is reduced and the nanowire resistance plays a role as well. Error bars correspond to an average of the obtained error generated by the fit.

4.5. Conclusions

The fabricated ZnO nanowire-based networks devices achieve high conduction with high sensitive surface making it suitable for sensing devices. Nevertheless, few studies have been published on gas sensing of one-dimensional materials network. The different contact geometries used allows the determination of the number of junctions present in a

contact gap, therefore, the density of the thin film by drop casting. The conductive model allows a good understanding of the series resistance contribution, the one related to the contact resistance which is reduced when annealing the sample and; the nanowire resistance that appears just after annealing the nanowire. The influence of temperature on these samples correlate with the thermionic emission conductive model used to predict the electrical transport of these nanowires, and enables the possible determination of the potential barrier of each nanowire-to-nanowire junction.

5. Low temperature response of ZnO nanowires network-based sensors

ZnO nanowires network-based sensing activities for an oxidant (O_2) and reducing gas (CO_2) towards ZnO with different response mechanisms are studied and discussed in this chapter. The influence of gas concentration and temperature under the presence of these two gases are also fully discussed. Annealed samples responses (from Chapter 3) were compared to non-annealed nanowires response under oxidant and reducing atmospheres. The model proposed in Chapter 4 is applied to the as-grown nanowires corresponding to 1 cycle under different concentrations of oxygen. The used geometry corresponds to 20 μm of contacts gap which lets a maximum number of junctions to contribute in the nanowire network film and 1050 μm contact width corresponding to the highest fabricated value leading to higher current contribution. The controlled ZnO nanowires structure of aspect ratio 14, and, the conduction model proposed in Chapter 4 allows us to correlate in this chapter the electronic sensor performance and transport mechanisms with its physico-chemical properties. Nitrogen is used as carrier gas to study the chemical kinetics of the interaction between a target gas and the metal oxide surface.

5.1. ZnO sensing activities

ZnO is well known as an electrophilic semiconductor, when oxygen molecules interact with ZnO surface, oxygen acts as an electron acceptor and gets ionized by adsorbing and capturing free electrons on the

surface from the conduction band forming chemisorbed oxygen species (O_2^-, O^- and O^{2-}). In the adsorption process, oxygen molecules get an electron from the ZnO surface by occupying the oxygen vacancies present in ZnO nanowire's surface. Hence, the chemisorption of oxygen molecules reduces the mobility of electrons leading to a lower conductance of ZnO resulting in a resistance increase. The chemisorption reaction of oxygen on the metal oxide surface is described in equations 1.1 and 1.2. On the other hand, when ZnO nanowire surface interacts with a reducing gas, the gas molecules act as electron donors. During this interaction, the reducing gas desorbs or removes the oxygen ions and physisorbed hydroxyl ions from the ZnO surface. The oxygen ions on the surface react with the gas molecules and giving up electrons to the conduction band increasing the electron mobility and decreasing the resistance. The gas sensing response could be correlated to active centers obtained from the oxygen vacancies present on the nanowires typical from ZnO nanostructures created by liquid phase synthesis.
The response to a gas is then defined as the relative resistance ratio with respect to the one under neutral conditions such as room temperature under nitrogen gas (R_o) and when exposed to the targeted gas (R_g).

$$S_g = \frac{R_g}{R_0} \tag{5.1}$$

5.1.1. Oxygen sensing

The response to 5% concentration of oxygen in nitrogen was recorded as a function of time. The figure 5.1 shows a gas sensor device composed of non treated ZnO nanowires with a rapid response and slower recovery time to 5% oxygen gas molecules over 95% nitrogen gas. The sensor is left under 100% nitrogen during 600 s to stabilize the response and then exposed to oxygen for one hour where the resistance increases due to the known absorption of oxygen molecules on the surface of ZnO. After, oxygen flow is then stopped and the sensor is under 100% nitrogen again, which allows the desorption of the absorbed oxygen resulting in a resistance decrease. The recovery of ZnO sensors due to oxygen des-

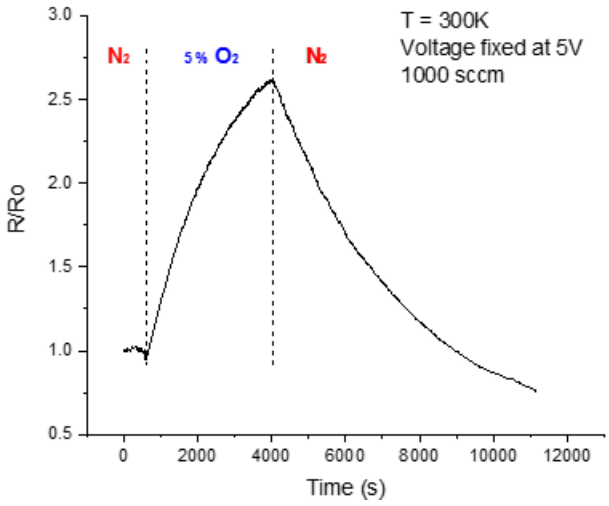

Figure 5.1.: Dynamic sensing characteristics of the as-grown ZnO nanowires (corresponding to 1 cycle) network sensors to 5% concentration of oxygen at 300 K. Voltage bias was fixed at 5 V.

orption takes at least twice the time of response to recover and reach its initial state. The measurements were performed under a fixed bias at 5 V.

Yadav et al. recently reported pure ZnO nanowires prepared by Chemical Vapor Deposition (CVD) with faster response times of about 1.5 min towards oxygen gas [198]. Our oxygen ZnO nanowire network-based sensing device was exposed to oxygen gas during 3600 s showing greater sensitivity but slower response time. One of the factors that could explain this result could be the sensing chamber used in our case, which is bigger in volume and its filling time is of about 20 min with a flow of 1000 sccm. Another factor is the synthesis technique used in each case, CVD techniques are known for providing higher aspect ratio nanowires (which is related to higher sensitive surface exposed thus faster response times) and higher crystalline structures (leading to a better quality nanowire-to-nanowire junctions thus reducing junction-to-junction barrier). Better quality nanowire thin films with higher surface-to-volume ratio and crystallinity will reduce the contribution of the nanowire resistance itself

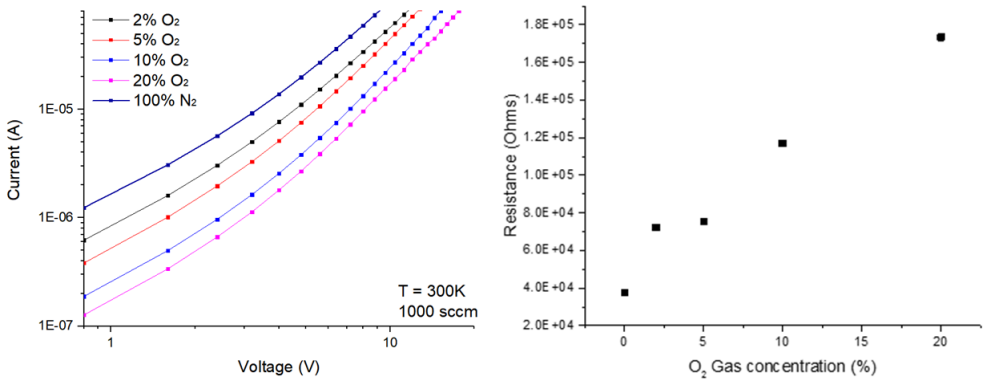

Figure 5.2.: Left side: I-V characteristics of ZnO nanowires sensor reaction to different concentrations of oxygen molecules. Right side: Nanowire network thin film resistance variation with oxygen gas concentration. Resistance was calculated at 5 V and measurements were performed at 300 K.

as compared to the contribution to the series resistance.

Influence of oxygen concentration

The influence of the oxygen concentration with the sensing response at room temperature was also investigated. I-V characteristics for as-deposited nanowires network could be observed in figure 5.2 (left side) showing that the sensor resistance increases when exposed to oxygen molecules during 3600 s as compared once is exposed under 100% nitrogen. The right side of figure 5.2 indicates that ZnO nanowires decreased their resistance when exposed to lower concentration of oxygen molecules. This result is in agreement and follows the typical response of ZnO to oxygen expected sensing behavior.

Influence of temperature

As-grown ZnO nanowires under oxidant conditions are studied using different temperatures considering the significant impact of the oper-

ating temperature on the sensitivity of ZnO gas sensors. Figure 5.3 (left panel) shows the same as-deposited ZnO nanowires sensor oxygen response and recovery under different temperatures under atmospheric pressure. The response characteristic times (τ) of ZnO nanowire-based sensors are 1952 s, 1403 s and 1177 s for temperatures 300 K, 330 K and 360 K, respectively, while the recovery characteristic times (τ') are 3561 s, 2381 s and 1923 s for temperatures 300 K, 330 K and 360 K, respectively. Clearly, the response and recovery times at higher temperatures are shorter than those kept at lower temperatures, which confirms ZnO sensing behavior described by literature.

The right panel of figure 5.3 exhibits a I-V characteristic curve measured in presence of 5% oxygen after one hour exposure. The I-V characterisics confirms what is shown on the left panel, the magnitude of the response increases as a function of temperature, thus, resistance increases with the operating temperature increase. This behavior of the magnitude and time scale of the response as a function of the operating temperature is usually explained with regard to the kinetics and mechanics of gas adsorption and desorption on the surface of ZnO or similar semiconducting metal oxides [64]. At high operating temperatures, the resistance increases as a result of oxygen adsorptions on the ZnO nanowires surface. At this stage, there are two phenomena present on the ZnO nanowires, the oxygen chemisorption and the thermionic emission of electrons. This continues until there is a complete coverage of the ZnO surface with chemisorbed oxygen species, where sensors show the highest sensitivity. Normally, beyond 150 °C, the sensitivity is at its maximum and starts to decrease due to the effect of the dominant thermal excitation of electrons and the saturation of oxygen adsorption on the resistance of the ZnO sensors.

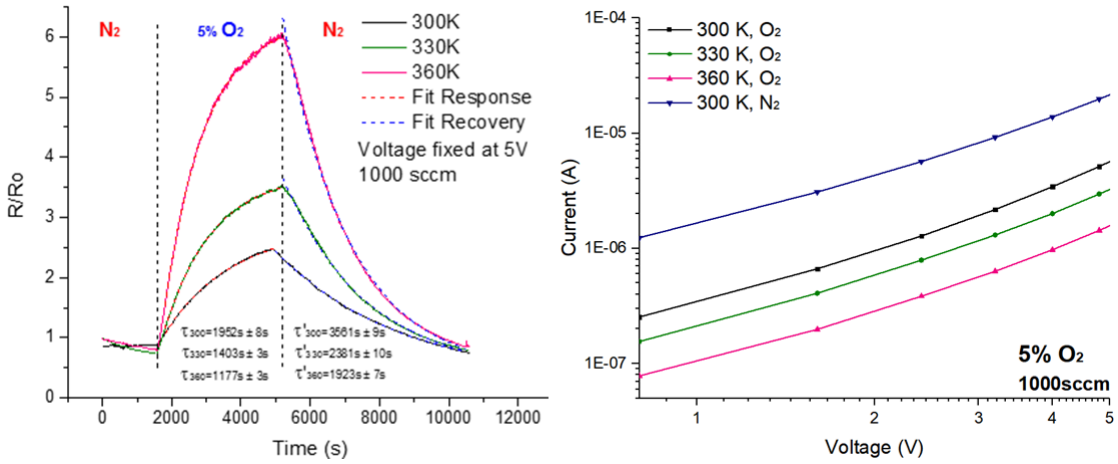

Figure 5.3.: Left side: Dynamic sensing characteristics of the as-grown ZnO nanowires network sensors to 5% concentration of oxygen for different temperatures, with voltages was fixed at 5 V. τ and τ' are the characteristic response and recovery times calculated by fitting the data. Right side: I-V characteristics of ZnO nanowires sensor reaction to different temperatures for 5% oxygen molecules after exposure of 3600 s and at a fixed voltage 5 V.

Figure 5.4 shows an Arrhenius plot that is based on the values obtained during the dynamic sensing τ and τ' which corresponds to characteristic response /recovery times and the operating temperature. The slope obtained from the linear regression allowed the calculation of activation energy for the chemisorption reaction of oxygen at the surface of ZnO nanowires. The activation energy of the response to oxygen is 0.08 eV and to recover from oxygen is 0.098 eV. The difference between of the activation energy to recover from the response could explain the longer recovery needed for ZnO nanowires to recover from oxygen exposure in N_2. The low activation energy obtained for ZnO nanowires oxidation is smaller than most activation energies values for ZnO structures to be between 0.6 and 5 eV [14, 208, 61].

The obtained activation energy values are smaller than previously reported values in literature, which correlates with the high sensitivity of our devices toward oxygen gas molecules at low temperatures. A hypothesis to explain this sensitivity could be due to different surface

states created using liquid phase synthesis as compared to other fabrication techniques, which lead to more defective ZnO nanowires that are highly reactive to oxygen even at low temperature.

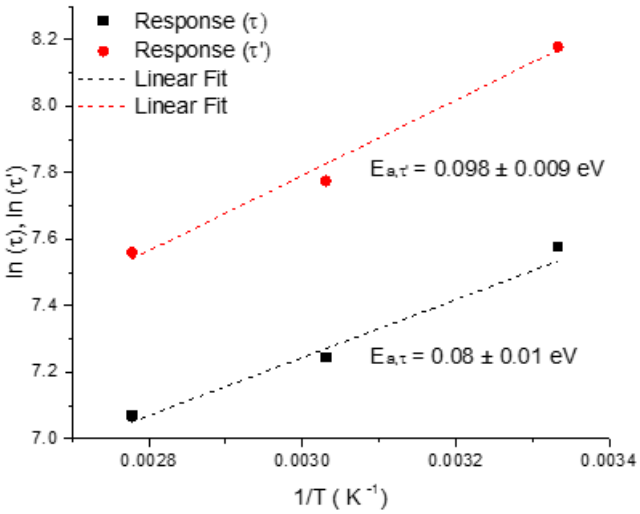

Figure 5.4.: Arrhenius plot of dynamic sensing characteristics of the as-grown ZnO nanowires network sensors under 5% concentration of oxygen for different temperatures. The activation energy can be calculated from slope = Ea/K_B of the graph.

Influence of annealing atmosphere

Considering the influence of defects on the sensing mechanism ZnO nanowires, three other different gas sensors have been fabricated and tested: air annealed and argon annealed to be compared to the as grown nanowires device sensing mechanism. These sensors are based on nanowires based network with different annealings atmospheres peformed at 250 °C during one hour under the already described in Chapter 2.

Figure 5.5 shows the I-V characteristics of the three different sensors to 5% Oxygen at atmospheric pressure after one hour. Since the analyzed samples contain different annealed nanowires and nanowire-network based thin film cannot be guaranteed equal in all samples, a precise compari-

son cannot be made. In order to estimate different annealing treatments and their influence on the sensing mechanism at different temperatures, the current ratio between the sample at 5 V under 100% Nitrogen and when is exposed to 5% Oxygen is calculated. The current ratios for the as-deposited, air-annealed sample and Ar-annealed sample are 3.71, 4.97 and 11.89, respectively. This ratio is a factor that indicates the influence of oxygen gas molecules on each sample at 300 K, this factor is higher for argon and air-annealed samples. An explanation for the results observed in figures 5.3 and 5.5, could be the desorption of organic residues on nanowires network junctions of the annealed samples, which lead to a better response than as-deposited sample. Argon-annealed sample shows the highest ratio which could imply the formation of defects such as oxygen vacancies that will increase the sensing response to oxygen gas, such hypothesis is supported by the PL characterization for argon-annealed sample at 400 °C in Chapter 3.

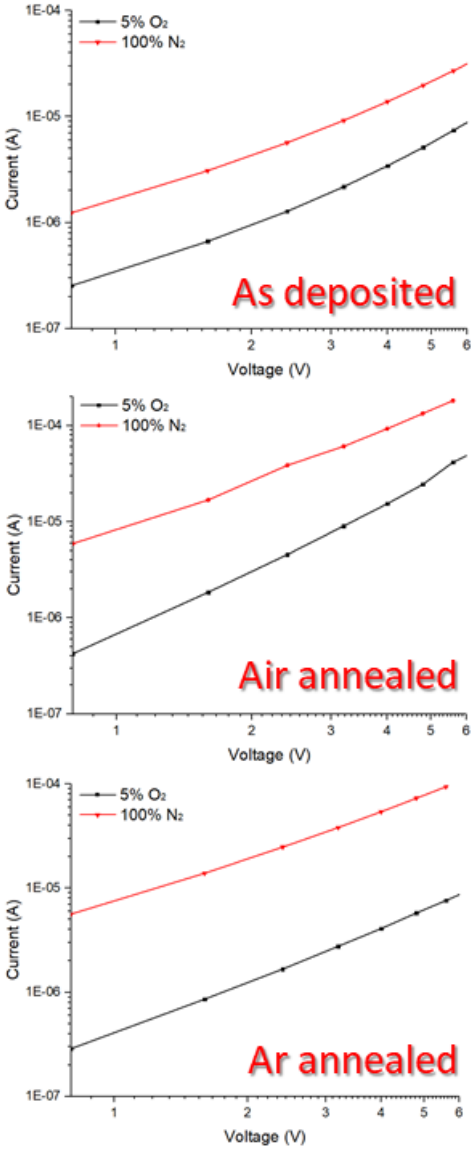

Figure 5.5.: I-V characteristics of ZnO nanowires sensor reaction at 300K for 5% oxygen molecules. Upper panel, sample as-grown nanowires. Central panel, sample annealed under enviromental conditions. Lower panel: sample annealed under a constant flow of argon.

5.1.2. CO_2 sensing

The response to 1000 ppm concentration of CO_2 mixed with N_2 was recorded as a function of the time. A concentration of 1000 ppm CO_2 is considered as the limit of acceptable exposure allowed for humans without carrying side effects, therefore we chose this concentration to carry out our experiments. The figure 5.6 shows a gas sensor device composed of non treated ZnO nanowires with a rapid response and slower recovery time to 1000 pm of CO_2. The sensor is left under 100% nitrogen during 600 s to stabilize the response and then exposed to 1000 ppm of CO_2 during one hour where the response increases. After, CO_2 flow is then stopped and the sensor is left under air to induce recovery. The air defined as 80% nitrogen and 20% oxygen, which allows the rapid absorption of oxygen and in consequence, the resistance increases rapidly returning to its original state. The recovery of ZnO sensors exposed to CO_2 involves the oxygen absorption which is faster than the response to the CO_2 gas itself. Latter to this recovery induced by air after CO_2 injection, the sensor must be exposed to N_2 in order to reach its initial conditions. The measurements were performed under a fixed bias at 5 V.

The sensing mechanism of ZnO-based materials towards CO_2 is still unclear. CO_2 is an oxidant gas that in contact with ZnO surface acts as a reducing gas. Among many hypothesis, recent work has been published claiming CO_2 reacts with hydroxyl group ($-OH$) at the surface of zinc oxide to form carbonates and hydroxycarbonates [156]. These species will then react with oxygen on the ZnO surface creates oxygen vacancies as new donor states, releasing electrons resulting in a decrease of the resistance. This behavior is attributed to the adsorption–desorption sensing mechanism based on a reversible chemisorption of the carbon dioxide on the ZnO surface.

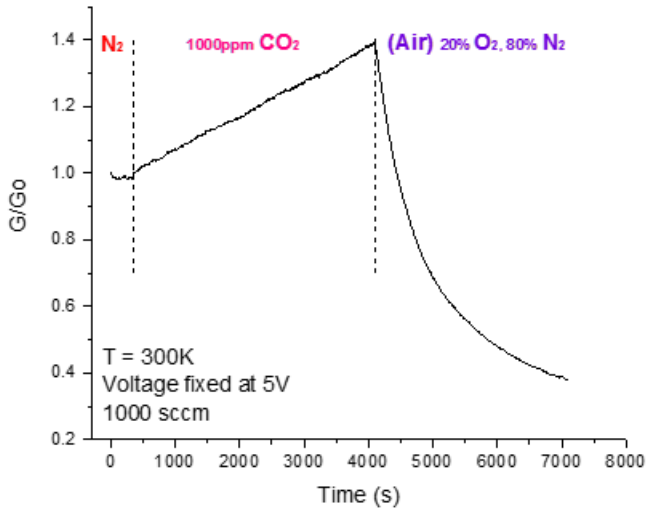

Figure 5.6.: Dynamic sensing characteristics of the as-grown ZnO nanowires network sensors towards 1000ppm concentration of CO_2 at 300K. Voltage bias was fixed at 5 Volts.

Influence of CO_2 concentration

As investigated with oxygen, the influence of the CO_2 concentration in the sensing response at room temperature was also studied. I-V characteristics for as deposited nanowires network could be observed in figure 5.7 presenting a sensor resistance decrease when nanowires are exposed to CO_2 molecules. ZnO nanowires increased their resistance when exposed to lower concentration of CO_2 molecules. The injection of produced electrons from the surface to the bulk of semiconducting layer induces consequently a decrease of the sensor resistance proportional to CO_2 concentration. Recent work have been done on sensing devices based on ZnO structures towards CO_2, however, to our knowledge, there no reports on non-doped ZnO nanowire network based sensors showing sensitivity to CO_2 at 300 K.[169, 139, 147, 77, 19, 65, 156].

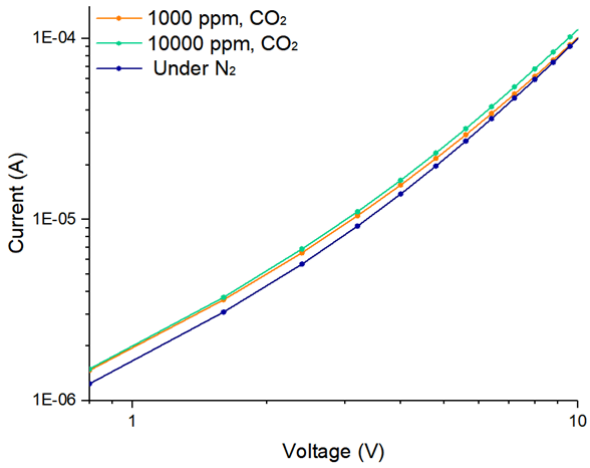

Figure 5.7.: I-V characteristics of ZnO nanowires sensor reaction to different concentrations of CO_2 molecules at 300K.

Influence of temperature

As-grown ZnO nanowires under reducing conditions are studied using different temperatures considering the significant impact of the operating temperature on the sensitivity of ZnO gas sensors. Figure 5.8 (left panel) shows the same as-deposited ZnO nanowires sensor CO_2 response and recovery under different temperatures at atmospheric pressure. Although, the CO2 sensing do not correspond to an expected behavior, the response is determine as used for oxygen sensing. The response characteristic times (τ) of ZnO nanowire-based sensors are 12002 s, 4867 s and 2540 s for temperatures 300 K, 330 K and 360 K, respectively, while the recovery characteristic times (τ') are 813 s, 535 s and 446 s for temperatures 300 K, 330 K and 360 K, respectively. Clearly, the response and recovery times at higher temperatures are shorter than those kept at lower temperatures, confirming the CO_2 detection is improved when increasing the temperature.

The I-V characteristics reveal curves measured in presence of 1000 ppm CO_2 after one hour exposure (right panel of figure 5.8). A major resistance decrease once the temperature increases is observed. At a low operating temperature, the response of the films to CO_2 is restricted by the speed of the chemical reaction because the gas molecules do not

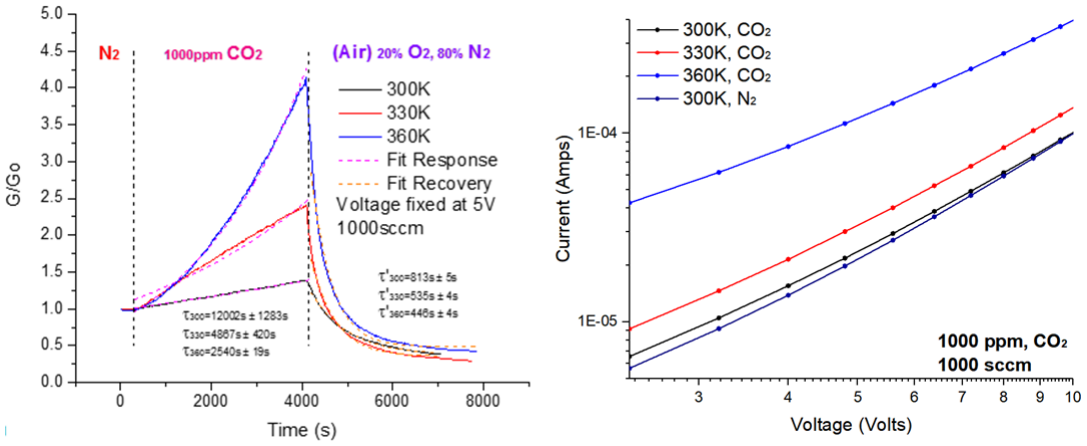

Figure 5.8.: Left side: Dynamic sensing characteristics of the as-grown ZnO nanowires network sensors towards 1000 ppm concentration of CO_2 for different temperatures, with voltage fixed at 5 V. Right side: I-V characteristics of ZnO nanowires sensor reaction to different temperatures for 1000 ppm of CO_2 molecules at a fixed voltage 5 V.

have enough thermal energy to react with the surface adsorbed oxygen species.

Figure 5.9 shows an Arrhenius plot that is based on the values obtained during the dynamic sensing τ and τ' obtained while exposing the sensor under CO_2. The activation energy of the response to CO_2 is 0.236 eV and to recover from CO_2, under 20% oxygen, is 0.097 eV. The difference between of the activation energy to recover from the response could explain the longer reaction time towards CO_2 in comparison to oxygen gas, leading to faster recovery under air conditions. Many studies have been realized in order to calculate the activation energy obtained for ZnO nanowires under CO_2 gas. Our result, to our knowledge, is smaller than most activation energies reported to be from 0.9 to 2 eV [61, 119, 74].

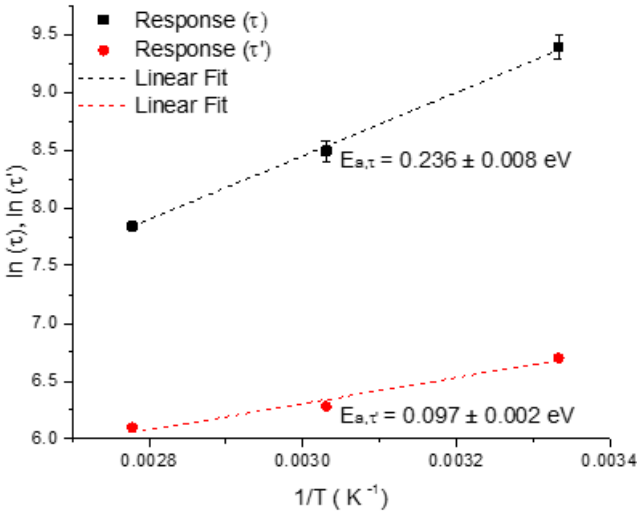

Figure 5.9.: Arrhenius plot of dynamic sensing characteristics of the as-grown ZnO nanowires network sensors under 1000 ppm of CO_2 for different temperatures. The activation energy can be calculated from slope = Ea/K_B of the graph.

Influence of annealing atmosphere

The same study as under oxygen gas molecules is now performed under 1000 ppm of CO_2 to analyze the influence of defects on the sensing mechanism ZnO nanowire. Figure 5.10 shows the I-V characteristics of the three different sensors to 1000 ppm of CO_2 at atmospheric pressure after one hour. Since CO_2 is a reducing gas, the ratio of the current measured once exposed to CO_2 over the initial measured value at 5 V is then considered. The ratio for the as-deposited, air-annealed sample and Ar-annealed sample are 1.10, 1.64 and 2.04, respectively. This ratio is a factor that indicates how the resistance decreases once exposed to CO_2 gas molecules at 300 K, the factor of the argon-annealed sample is bigger than the as-deposited nanowires and air-annealed samples, indicating this one is more suitable to be used as a CO_2 sensor.

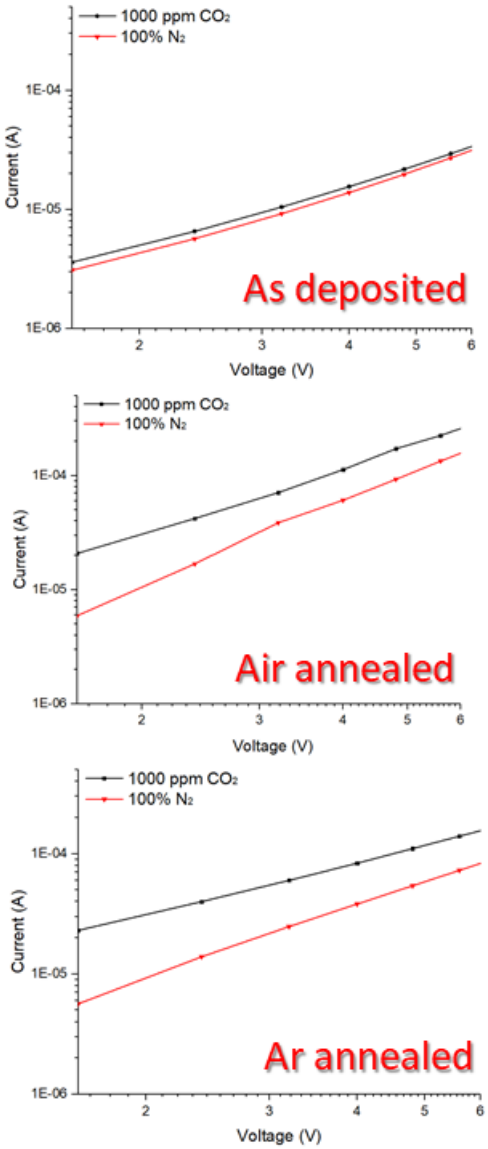

Figure 5.10.: I-V characteristics of ZnO nanowires sensor reaction to different temperatures for 1000ppm of CO_2 molecules at 300 K. Upper panel, sample as-grown nanowires. Central panel, sample annealed under enviromental conditions. Lower panel: sample annealed under a constant flow of argon.

Conclusions

Following the sensing activities of ZnO nanowires, the main conclusion is that argon-annealed ZnO nanowires networks at room temperature seem to deliver the best results and to be the most optimum among all devices for sensing analysis. In order to take a further step in the sensing field, we have decided to apply the electrical transport model created for ZnO network based nanowires in the sensing characteristics in order to induce a better understanding for these types of sensors. Next section overcomes a big limitation in the sensing field, due to the interpretation of results based only on the resistance. The key parameters that are intrinsic of the sensors such as potential barrier and series resistance are determined in next section as well as their role in the sensing response. Therefore, we have used our conduction model proposed in Chapter 4 to extract the corresponding these physical parameters to further analyze and discuss the mechanisms governing the sensor responses.

5.2. Application of electronic transport model

For this analysis, non-treated nanowires networks at 300 K under oxygen conditions (since ZnO sensors have shown better response towards oxygen) are considered. The figure 5.11 shows the same plot to the oxygen concentration behavior explained previously in figure 5.2, except that this graph exhibit the fit of the conduction model validated in Chapter 4 for ZnO nanowire-based network devices. At 300 K, the resistance increases once oxygen molecules are present and when the concentration is increased, the resistance keeps increasing. Table 5.1 summarizes the obtained parameters from fit of curves shown in figure 5.11. From this table, V_1 and V_2 remain mostly constant, the series resistance is increased with gas concentration and; parameters I_1 and I_2 decrease.

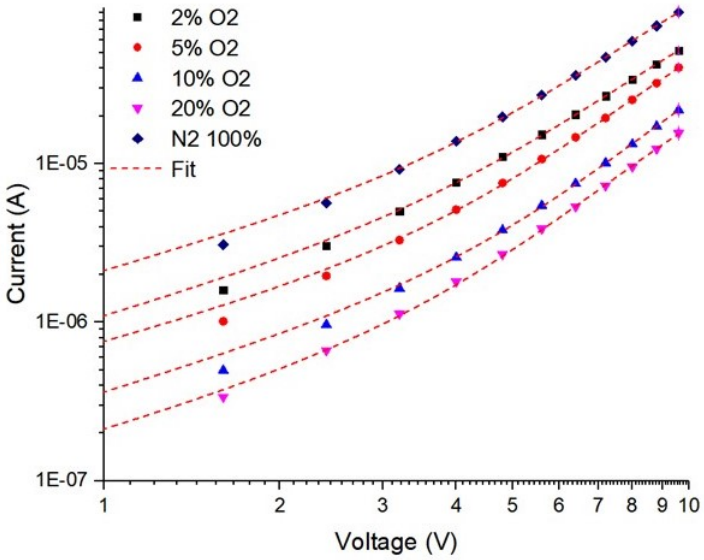

Figure 5.11.: I–V characteristics for as-grown ZnO nanowires network-based thin film under different oxygen concentrations at room temperature. Model validation with a 20 μm gap between the interdigitated electrodes of 1050 μm contact width.

	N_2 -100%	2% O_2	5% O_2	10% O_2	20% O_2
$\mathbf{V_1(V)} = \frac{\eta_1 N_{1,GB} K_B T}{q}$	1.92 ± 0.05	1.92 ± 0.05	1.82 ± 0.06	2.00 ± 0.07	1.7 ± 0.4
$\mathbf{V_2(V)} = \frac{\eta_2 N_{2,GB} K_B T}{q}$	1.89 ± 0.05	1.82 ± 0.05	1.99 ± 0.06	2.03 ± 0.06	1.6 ± 0.3
$R_s(Ohms)$	26525 ± 990	45294 ± 1770	52271 ± 2670	74259 ± 5578	142909 ± 42093
$I_1\,(A)$	2.06E-6 ± 1.5E-7	1.18E-6 ± 8.7E-8	6.39E-7 ± 6.2E-8	4.01E-7 ± 3.9E-8	1.92E-7 ± 1.3E-7
$I_2\,(A)$	2.15E-6 ± 1.6E-7	9.52E-7 ± 7.9E-8	7.72E-7 ± 6.3E-8	3.46E-7 ± 3.2E-8	1.40E-7 ± 9.6E-8

Table 5.1.: Summary table of obtained fit parameters from the I-V characteristics performed in figure 5.11.

V_1 and V_2 are dependent on the number of junctions involved and the ideality factor of the sensing device. From table 5.1 we can conclude that the number of nanowire-to-nanowire junctions present in the thin

film and their ideality factor remain constant when exposing to a gas. These results are expected, the number of junctions on the nanowire thin film is a geometrical parameter that is not expected to change in contact with gas. However, recent studies have shown changes on the ideality factor towards different environments or operating temperature [87, 129, 113, 209]. If no change is observed on the ideality factor for this case, this would mean the nature of the ZnO nanowire network-based thin films junctions remains the same. The series resistance evolution with gas concentration indicated in figure 5.12 is increased once oxygen molecules are exposed and continues to increase with concentration which correlates with previous results and literature-predicted behavior under oxidant conditions as discussed earlier. This linear dependence, which involves the nanowire surface, towards gas concentration reflects high response and sensitivity to oxygen molecules.

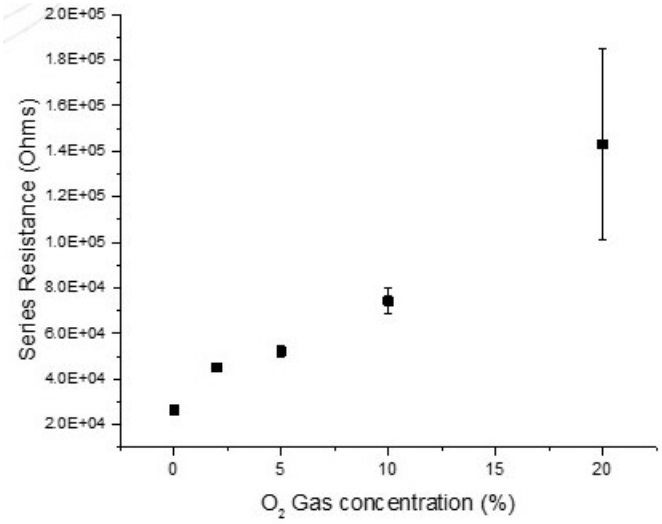

Figure 5.12.: Series resistance variation with oxygen gas concentration taken from table 5.1 calculated from fit parameters. Measurements were performed at 300 K.

Parameters I_1 and I_2 are plotted in function of the oxygen gas concentration in figure 5.13. I_1 and I_2 are given by the equation 4.3 where K and T are constants and A depends on the Richardson constant and the

working area of the device, which are geometrical parameters that do not change in presence of gas. From this equation, we could conclude that according to I_1 and I_2 results towards oxygen concentration, the potential barrier behavior could be predicted from these parameters. I_1 and I_2 values decrease exponentially when exposing to larger concentration of oxygen molecules, following 4.3 for I_1 and I_2 and the potential barrier, leads to the conclusion the potential barrier increases with the concentration of oxygen. This means oxygen absorbed ZnO nanowires not only reduces the electrons producing conductivity but it affects the junction properties by increasing the junction barrier formed by the nanowire-to-nanowire contact. This conclusion also allows to predict the behavior of the parameter A, which is dependent on the Richardson constant from ZnO and the effective area of the junction-based thin film, decreases when exposed to higher concentration of oxygen molecules. This could only mean the effective area of the thin film decreases, which leads us to conclude there are less network-based paths involves in the conduction. From this analysis, we could conclude, the potential barrier which increases with gas concentration dominating the response at very low voltages. At higher voltages, such at 5 V (see figure 5.2), the response mechanism is mainly dominated by the series resistance which, in this case, corresponds to the nanowire resistance. We found a good compromise to work at 5 V which maximizes sensitivity and contribution from the nanowire resistance. Higher voltages could lead to the contribution of contact resistance and further domination of conductivity.

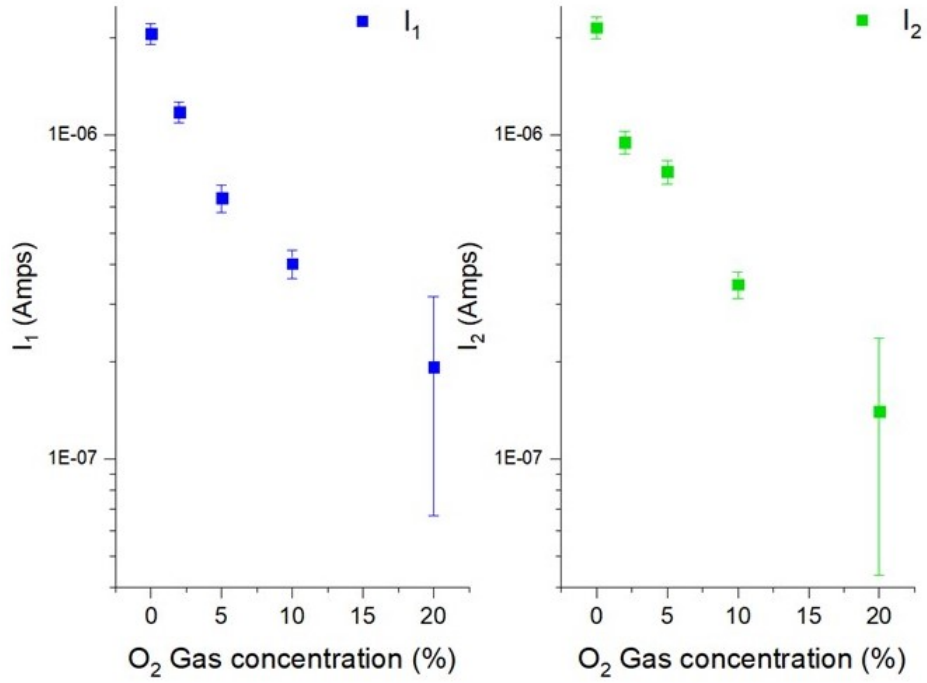

Figure 5.13.: I_1 and I_2 variation with oxygen gas concentration taken from table 5.1 calculated from fit parameters. Measurements were performed at 300 K.

5.3. Conclusions

The electrical transport model proposed for ZnO network based nanowires in Chapter 4, correlates with the sensing expected characteristics of ZnO nanowires. The application of this model to our sensing devices gives a one step further in the understanding of the sensing mechanism of ZnO nanowires network in terms of its physical parameters such as the potential barrier and series resistance of the nanowire thin film. These parameters determination and contribution towards the sensing response are discussed. These results, and in particular, our conduction model, pave the way for a better sensing mechanism comprehension in the field of gas sensors. The influence of ZnO nanowires with higher aspect ratio on the sensing activities towards different gases is to be studied. Also, it could be extended or adapted to other gases or non-linear devices.

6. Conclusions and perspectives

In this chapter, a summary of the PhD work and important achievements are presented. ZnO nanowires synthesis and characterization are discussed. Electrical transport conduction model, main results and its implementation on the sensing mechanism of ZnO nanowire network-based devices are fully discussed. Following the summary and conclusions, the perspectives of this work and improvements are sketched.

6.1. Summary and conclusions

The increased awareness over a need to monitor environmental polluting gases has been a great concern over the last decades. Several devices and methods are now available in the sensor technology. However, a reasonable understanding of the gas sensing mechanisms is controversially emerging in the published literature. Despite the fact that the chemical sensors and especially ZnO gas sensors would not solve the environmental pollution, it may help the monitoring control of the contaminant gases composition, which is related to this global challenge. ZnO nanowires-based gas sensors are widely studied and investigated over the years. Nevertheless, ZnO nanowire-based networks as sensing devices lack of investigation and their electrical transport mechanism have never been studied and connected to their sensing mechanism.
This thesis was conducted in the framework of NANOSENSE project agreed upon between the LIST, CNES and ESA. Within this framework program, this PhD thesis focuses on the physical-chemistry fabrication and on the semiconductor physics of the elaborated sensing devices based on horizontal nanowires network, their characterization and electrical transport comprehension mechanism in order to fully understand the sensing behaviour. Original, simple and low-cost methods were used to

fabricate ZnO nanowire networks. ZnO nanowires network-based thin films were synthetized by liquid phase synthesis technique to be used as a sensitive layer for the final sensing device. This synthesis was made a low temperature (85 ^{o}C) and for a short time of 100 min. The ZnO structure could be tuned by changing different parameters as precursors ratio concentration, reaction time, temperature, etc. The aspect ratio of these structures could be improved by implementing cycle growth which consists in cycling the precursors enabling ZnO nanowires created over the first synthesis to behave as ZnO nuclei during the second synthesis, allowing crystal growth in the c-direction to be improved. The used of a shape control agent such as PEG with the cycle growth method, in particular, enhance aspect ratio results from 20 to 27, due to the attachment to the non-polar facets of this polymer. Viscosity influence over the nucleation of aqueous solutions using PEG is for the first time discussed. Furthermore, a new hypothesis explaining the growth mechanism of rod and disc formation is fully discussed.

ZnO nanowires exhibit a typical wurtzite ZnO structure. Optical analysis revealed that they are highly defective. The electrical properties originating from the oxygen vacancies defects and organic residues. These have been optimized by performing a thermal annealing of the samples under different atmospheres. On-wafer electrical measurements were performed on the network electrical behavior before and after thermal annealing. A study is made to find the optimum thermal annealing parameters in terms of temperature and duration. The thermal process includes a first stage where most of the organic residues from the deposition desorb from the nanowire junctions, so the electrical contact is improved. Thermal annealing parameters (duration and temperature) must be carefully adapted to optimize the networks without degrading them. The measured current of ZnO thin films at room temperature could reach uAmps (10^{-6}) without further treatment.

Nanowire-to-nanowire junctions were created by drop casting (instead of spin coating) the synthetized ZnO nanowires several times in order to form an uniform thin film based on ZnO nanowire network avoiding agglomerates in the network. These networks achieve high conduction and high sensitive surface making it suitable for sensing devices. Although,

few studies have been published on gas sensing of one-dimensional materials network; this thesis went one step further in the understanding of ZnO nanowire network sensing mechanism and the intrinsic properties of the network such as its junction potential barriers and series resistance using different contact geometries. The different contact geometries used allows the determination of the number of junctions present in a contact gap, therefore, the density of the thin film by drop casting. The conductive model allows a good understanding of the series resistance contribution, the one related to the contact resistance which is reduced when annealing the sample and; the nanowire resistance that appears just after annealing the nanowire. The influence of temperature on these samples correlate with the thermionic emission conductive model used to predict the electrical transport of these nanowires and able to determine possible values of the potential barrier of each nanowire-to-nanowire junction.

ZnO nanowires network-based sensing activities were studied under different gases. They showed high sensitivity towards oxygen gas and its improvement when increasing the gas concentration, a faster response and recovery was also observed when the operating temperature is increased, correlating well with what has been already published in literature. Annealed samples were also tested and compared to the as-grown nanowires sample, argon-annealed showed the best sensitivity among all others which is expected since this annealing should increase the number of oxygen vacancies on ZnO nanowires. ZnO nanowires were also exposed to 1000 ppm CO_2 reducing gas, they exhibit great sensitivity even at room temperature which to our knowledge has never been reported for ZnO nanowires. Nanowires sensitivity also increased when increasing the CO_2 gas concentration. Argon-annealed nanowires exhibit greater sensitivity towards CO_2 than any other tested sample. The proposed conductive model was applied on the nanowires exposed to oxygen gas molecules, revealing that the series resistance and the potential barrier of a nanowire-to-nanowire junction increases when exposed to a larger concentration of oxygen molecules.

This work and the obtained results along these four years of PhD achieve a better understanding on the electrical transport and material proper-

ties of ZnO nanowire network-based sensor towards gases such as O_2 or CO_2, which is one step forward in the development of a simple and low-cost device for environmental pollution monitoring. This thesis completed a milestone further in order to achieve a better understanding on nanowire-based semiconductor networks and junction-based devices conduction.

6.2. Perspectives

Despite the interesting results this PhD. accomplished, the following aspects can be taken into considerations to enhance device performance for sensing applications.

6.2.1. Functionalization of ZnO nanowires

One of the perspectives of this work is to develop a selective ZnO nanowires network-based sensing device towards SVOC. This selectivity could be achieved by functionalizing ZnO nanowires using highly selective specific chemical grafting to the targeted gas species. This chemical grafting will be used as a molecular tweezer that will interact directly with the targeted molecule avoiding other molecules present in the environment.

6.2.2. UV excitation on I-V characteristics

Working with the optical properties of ZnO with an optical bandgap of 3.34 meV. Illumination with UV at 365 nm on ZnO nanowires will send photons to excitate electrons on the valence band to the conduction band increasing the measured current thus the conductivity of the material. This principle could be also adapted while sensing to improve response and recovery times.

6.2.3. Piezoelectric effect

ZnO is characterized as being an excellent compound semiconductor with flexoelectricity response leading to a piezotronic effect by applying

a supplementary stress on the ZnO nanowires. ZnO transport properties could thus be tuned due to strain induced causing piezoelectric polarization inside the material. The piezoelectronic effect on ZnO sensors may lead to a performance improvement in strain sensors by largely increasing the resolution, detection limit and sensitivity. Since nanowires and the substrate are bond together by van der Waals forces, a flexible substrate which could replace Si/SiO_2 rigid substrate. This flexible substrate could be then bended and add stress to the device.

Other areas of future work could include:

6.2.4. Heterostructures growth

Liquid phase synthesis cycle growth method could be implemented for heterostructures with different precursors. While we have demonstrated that the involved mechanism can improve the aspect ratio when a single metal precursor is used, the cycle growth could be extended to the growth of axial heterostructures when using cycles with different metal precursors, which is a challenge in liquid phase with homogeneous nucleation.

6.2.5. Photocatalysis for pollutant degradation

Many semiconductor materials are widely studied for water cleaning purposes using solar energy. The implementation of photocatalytic materials for the purification of water remains innovative. Among them, ZnO seems to be a good photocalayst due to its intrinsic properties as direct band gap and and its exciton energy of 60 meV. Widely known for absorbing UV light and its luminescence properties at room temperature. Due to the difference in the growth mechanism, precursors used or growth temperature for all synthesis processes, particular defects can be created in the ZnO structure using liquid-phase synthesis meaning that the obtained ZnO nanowires are rich in defect such as oxygen vacancies. When depositing ZnO nanowires networks on substrates, liquid-phase nanowires powder has an excellent advantage due to the improvement

of the specific surface and therefore, improving photocatalytical activities.

Bibliography

[1] A. D. Smigelskas and E. O. Kirkendall. Zinc Diffusion in Alpha Brass. *Transactions of AIME*, 171:130–142, 1947.

[2] A. K. Geim & K. S. Novoselov. The rise of graphene. *Nature Materials*, 6:183–191, 2007.

[3] S. Ahlers, G. M??ller, and T. Doll. A rate equation approach to the gas sensitivity of thin film metal oxide materials. *Sensors and Actuators, B: Chemical*, 107(2):587–599, 2005.

[4] Faheem Ahmed, Nishat Arshi, M.S. Anwar, Rehan Danish, and Bon Heun Koo. Mn-doped ZnO nanorod gas sensor for oxygen detection. *Current Applied Physics*, 13(4):64–68, jul 2013.

[5] Heejoon Ahn, Amol Chandekar, Bongwoo Kang, Changmo Sung, and James E Whitten. Electrical Conductivity and Vapor-Sensing Properties of ω - (3-Thienyl) alkanethiol-Protected Gold Nanoparticle. (11):3274–3278, 2004.

[6] I. S. Ahuja, C. L. Yadava, and Raghuvir Singh. STructural information on manganese(II), cobalt(II), nickeL(II), zinC(II) and cadmium(II) sulphate complexes with hexamethylenetetramine (a potentially tetradentate ligand) from their magnetic moments, electronic and infrared spectra. *Journal of Molecular Structure*, 81(3-4):229–234, 1982.

[7] Tarek Alammar and Anja Verena Mudring. Facile ultrasound-assisted synthesis of ZnO nanorods in an ionic liquid. *Materials Letters*, 63(9-10):732–735, 2009.

[8] Mohammad R Alenezi, Simon J Henley, Neil G Emerson, and S Ravi P Silva. From 1D and 2D ZnO nanostructures to 3D hierarchical structures with enhanced gas sensing properties. *Nanoscale*, 6(1):235–47, 2014.

[9] P. Althainz, J. Goschnick, S. Ehrmann, and H.J. Ache. Multisensor Microsystem For Contaminants In Air. *Proceedings of the International Solid-State Sensors and Actuators Conference - TRANSDUCERS '95*, 1:72–76, 1995.

[10] G. Amin, M. H. Asif, A. Zainelabdin, S. Zaman, O. Nur, and M. Willander. Influence of pH, Precursor Concentration, Growth Time, and Temperature on the Morphology of ZnO Nanostructures Grown by the Hydrothermal Method. *Journal of Nanomaterials*, 2011:1–9, 2011.

[11] Sadik Antwi-boampong, Kristina S Mani, Jean Carlan, and Joseph J Belbruno. A selective molecularly imprinted polymer-carbon nanotube sensor for cotinine sensing. (June 2013):57–63, 2014.

[12] Michael N R Ashfold, Frederik Claeyssens, Gareth M Fuge, and Simon J Henley. Pulsed laser ablation and deposition of thin films. *Chem. Soc. Rev.*, 33(1):23–31, 2004.

[13] Michael N R Ashfold, Rachel P. Doherty, N. George Ndifor-Angwafor, D. Jason Riley, and Ye Sun. The kinetics of the hydrothermal growth of ZnO nanostructures. *Thin Solid Films*, 515(24 SPEC. ISS.):8679–8683, 2007.

[14] Madeha Ahmed Awad, Eslam Mohamed Mohamed Ibrahim, and Ahmed Mohamed Ahmed. Synthesis and thermal stability of ZnO nanowires. *Journal of Thermal Analysis and Calorimetry*, 117(2):635–642, 2014.

[15] A M Azad, S A Akbar, S G Mhaisalkar, L D Birkefeld, K S Goto, A M Azad, S A Akbar, S G Mhaisalkar, L D Birkefeld, and K S

Goto. Solid â State Gas Sensors : A Review Solid-State Gas Sensors : A Review. 139(12):3690–3704, 1992.

[16] Nicolae Barsan and Udo Weimar. Conduction model of metal oxide gas sensors. *Journal of Electroceramics*, 7(3):143–167, 2001.

[17] Sunandan Baruah and Joydeep Dutta. Hydrothermal growth of ZnO nanostructures. *Science and Technology of Advanced Materials*, 10(1):013001, 2009.

[18] Sunandan Baruah, Mohammad Abbas Mahmood, Myo Tay Zar Myint, Tanujjal Bora, and Joydeep Dutta. Enhanced visible light photocatalysis through fast crystallization of zinc oxide nanorods. *Beilstein Journal of Nanotechnology*, 1(1):14–20, 2010.

[19] Mohamed A. Basyooni, Mohamed Shaban, and Adel M. El Sayed. Enhanced Gas Sensing Properties of Spin-coated Na-doped ZnO Nanostructured Films. *Scientific Reports*, 7(December 2016):41716, 2017.

[20] Matthias Batzill. Surface Science Studies of Gas Sensing Materials: SnO2. *Sensors*, 6(10):1345–1366, oct 2006.

[21] E Bekyarova, M Davis, T Burch, M E Itkis, B Zhao, S Sunshine, and R C Haddon. Chemically Functionalized Single-Walled Carbon Nanotubes as Ammonia Sensors â . pages 19717–19720, 2004.

[22] Allen T Bellew, Hugh G Manning, Claudia Gomes, and Mauro S Ferreira. Resistance of Single Ag Nanowire Junctions and Their Role in the Conductivity of Nanowire Networks. *ACS nano*, (11):11422–11429, 2015.

[23] Kushal D. Bhatte, Dinesh N. Sawant, Rahul A. Watile, and Bhalchandra M. Bhanage. A rapid, one step microwave assisted synthesis of nanosize zinc oxide. 2012.

[24] G. Bher and W. Fliegel. Electrical properties and improvement of the gas sensitivity in multiple-doped SnO2. *Sensors and Actuators B: Chemical*, 26(1-3):33–37, jan 1995.

[25] Diganta Bhuyan, Banajit Malakar, Sudhir S. Arbuj, and Lakshi Saikia. Flower shaped homocentric pencil like ZnO nanorod bundles: synthesis, characterisation and study of their photocatalytic activity. *RSC Advances*, 4(16):8256, 2014.

[26] Leonard J. Brillson and Yicheng Lu. ZnO Schottky barriers and Ohmic contacts. *Journal of Applied Physics*, 109(12):1–34, 2011.

[27] V. Brinzari, G. Korotcenkov, and V. Golovanov. Factors influencing the gas sensing characteristics of tin dioxide films deposited by spray pyrolysis: Understanding and possibilities of control. *Thin Solid Films*, 391(2):167–175, 2001.

[28] V. Brynzari, G. Korotchenkov, and S. Dmitriev. Simulation of thin film gas sensors kinetics. *Sensors and Actuators B: Chemical*, 61(1):143–153, 1999.

[29] Yuan Liu Bs, Sadik Antwi-boampong Bs, Joseph J Belbruno, Mardi A Crane, and Susanne E Tanski. Detection of secondhand cigarette smoke via nicotine using conductive polymer films. pages 1–8, 2013.

[30] J. Bwrnasconi, S. Strässler, B. Knecht, H.P. Klein, and A. Menth. Zinc oxide based varistors: A possible mechanism. *Solid State Communications*, 21(9):867–870, mar 1977.

[31] N. Caicedo, J.-S. Thomann, R. Leturcq, and D. Lenoble. Aspect ratio improvement of ZnO nanowires grown in liquid phase by using step-by-step sequential growth. *CrystEngComm*, 18(29):5502–5511, 2016.

[32] H L Cao, X F Qian, Q Gong, W M Du, X D Ma, and Z K Zhu. Shape- and size-controlled synthesis of nanometre ZnO from a simple solution route at room temperature. *Nanotechnology*, 17(15):3632–3636, 2006.

[33] Qian Chen, Yingying Sun, Ying Wang, Hongbin Cheng, and Qing Ming Wang. ZnO nanowires-polyimide nanocomposite

piezoresistive strain sensor. *Sensors and Actuators, A: Physical*, 190:161–167, 2013.

[34] Xianping Chen, Cell K Y Wong, Cadmus A Yuan, and Guoqi Zhang. Sensors and Actuators B : Chemical Nanowire-based gas sensors. 177:178–195, 2013.

[35] Bin Cheng and Edward T Samulski. Hydrothermal synthesis of one-dimensional ZnO nanostructures with different aspect ratios. *Chemical communications (Cambridge, England)*, (8):986–987, 2004.

[36] Wen-Ting Chiou, Wan-Yu Wu, and Jyh-Ming Ting. Growth of single crystal ZnO nanowires using sputter deposition. *Diamond and Related Materials*, 12(10):1841–1844, 2003.

[37] I. D. Choi, D. K. Matlock, and D. L. Olson. An analysis of diffusion-induced porosity in CuNi laminate composites. *Materials Science and Engineering A*, 124(2), 1990.

[38] Chen Shiun Chou, Yung Chen Wu, and Che Hsin Lin. High performance oxygen sensor utilizing ultraviolet irradiation assisted ZnO nanorods under low operation temperature. *8th Annual IEEE International Conference on Nano/Micro Engineered and Molecular Systems, IEEE NEMS 2013*, 4:72–75, 2013.

[39] Kan Sen Chou and Yueh Sheng Lai. Effect of polyvinyl pyrrolidone molecular weights on the formation of nanosized silver colloids. *Materials Chemistry and Physics*, 83(1):82–88, 2004.

[40] Kevin David Cleaver. The analysis of process gases: A review. *Accreditation and Quality Assurance*, 6(1):8–15, 2001.

[41] S. F. Cogan, S. Kwon, J. D. Klein, and R. M. Rose. Fabrication of Large Diameter External-Diffusion Processed Nb3Sn Composites. *IEEE Transactions on Magnetics*, 19(3):1139–1142, 1983.

[42] Philip G Collins. Extreme Oxygen Sensitivity of Electronic Properties of Carbon Nanotubes. 1801(2000), 2012.

[43] Elisabetta Comini. Metal oxide nano-crystals for gas sensing. *Analytica Chimica Acta*, 568(1-2):28–40, 2006.

[44] James S Cooper, Mathew Myers, Edith Chow, and Lee J Hubble. Performance of graphene , carbon nanotube , and gold nanoparticle chemiresistor sensors for the detection of petroleum hydrocarbons in water. 2014.

[45] Guorui Dai. A study of the sensing properties of thin film sensor to trimethylamine. *Sensors and Actuators B: Chemical*, 53(1):8–12, 1998.

[46] E. De La Rosa, S. Sepúlveda-Guzman, B. Reeja-Jayan, a. Torres, P. Salas, N. Elizondo, and M. Jose Yacaman. Controlling the growth and luminescence properties of well-faceted ZnO nanorods. *Journal of Physical Chemistry C*, 111(24):8489–8495, 2007.

[47] L. N. Demianets, D. V. Kostomarov, I. P. Kuz'mina, and S. V. Pushko. Mechanism of growth of ZnO single crystals from hydrothermal alkali solutions. *Crystallography Reports*, 47(S1):S86–S98, 2002.

[48] L. N. Dem'yanets, D. V. Kostomarov, and I. P. Kuz'mina. Chemistry and kinetics of ZnO growth from alkaline hydrothermal solutions. *Inorganic Materials*, 38(2):124–131, 2002.

[49] Serge Desgreniers. High-density phases of ZnO:âStructural and compressive parameters. *Physical Review B*, 58(21):14102–14105, 1998.

[50] A. B. Djuriić, A. M C Ng, and X. Y. Chen. ZnO nanostructures for optoelectronics: Material properties and device applications. *Progress in Quantum Electronics*, 34(4):191–259, 2010.

[51] a Dong, F Wang, T L Daulton, and W E Buhro. Solution- Liquid-Solid (SLS) Growth of ZnSe- ZnTe Quantum Wires having Axial Heterojunctions. *Nano Lett*, 7(5):1308–1313, 2007.

[52] P. R. Emtage. The physics of zinc oxide varistors. *Journal of Applied Physics*, 48(10):4372–4384, 1977.

[53] Jens Eriksson, Volodymyr Khranovskyy, Fredrik Söderlind, Per-Olov Käll, Rositza Yakimova, and Anita Lloyd Spetz. ZnO nanoparticles or ZnO films: A comparison of the gas sensing capabilities. *Sensors and Actuators B: Chemical*, 137(1):94–102, mar 2009.

[54] Åakir Erkoç and Hatice Kökten. Structural and electronic properties of single-wall ZnO nanotubes. *Physica E: Low-dimensional Systems and Nanostructures*, 28(2):162–170, 2005.

[55] Stephen D Evans, Simon R Johnson, Yaling L Cheng, and Tiehan Shen. Vapour sensing using hybrid organic-inorganic nanostructured materials {. 10:183–188, 2000.

[56] Jiandong Fan, Reza Zamani, Cristian Fábrega, Alexey Shavel, Cristina Flox, Maria Ibáñez, Teresa Andreu, Antonio M López, Jordi Arbiol, Joan Ramón Morante, and Andreu Cabot. Solution-growth and optoelectronic performance of ZnO : Cl/TiO 2 and ZnO : Cl/Zn x TiO y /TiO 2 coreâshell nanowires with tunable shell thickness. *Journal of Physics D: Applied Physics*, 45(41):415301, 2012.

[57] Zhiyong Fan, Dawei Wang, Pai-Chun Chang, Wei-Yu Tseng, and Jia G. Lu. ZnO nanowire field-effect transistor and oxygen sensing property[J]. *Appl. Phys. Lett.*, 85(24):5923–5925, 2004.

[58] George F. Fine, Leon M. Cavanagh, Ayo Afonja, and Russell Binions. Metal oxide semi-conductor gas sensors in environmental monitoring. *Sensors*, 10(6):5469–5502, 2010.

[59] Marion E Franke, Tobias J Koplin, and Ulrich Simon. reviews Metal and Metal Oxide Nanoparticles in Chemiresistors : Does the Nanoscale Matter ? (1):36–50.

[60] Shinobu Fujihara, Yusuke Ogawa, and Asayo Kasai. Tunable visible photoluminescence from ZnO thin films through Mg-doping and annealing. *Chemistry of Materials*, 16(14):2965–2968, 2004.

[61] Elena Gálvez. Swiss Federal Institute of Technology Zurich ETHZ CO 2 splitting via a solar thermochemical cycle based on Zn / ZnO redox reactions : Thermodynamic and kinetic analysis Illias Hischier Master Thesis Prof . Aldo Steinfeld Professorship in Renewable Energy . (January), 2008.

[62] Pu Xian Gao and Zhong L. Wang. Nanopropeller arrays of zinc oxide. *Applied Physics Letters*, 84(15):2883–2885, 2004.

[63] L Gerward and J S Olsen. The high-pressure phase of zincite. *Journal of synchrotron radiation*, 2:233–235, 1995.

[64] Mohammad Ghasdi and Houshang Alamdari. CO sensitive nanocrystalline LaCoO3 perovskite sensor prepared by high energy ball milling. *Sensors and Actuators, B: Chemical*, 148(2):478–485, 2010.

[65] Mahdieh Ghobadifard, Qasem Maleki, Mostafa Khelghati, Ehsan Zamani, Saeid Farhadi, and Alireza Aslani. Zinc oxide nanocrystals assisted for carbon dioxide gas sensing prepared by solvothermal and sonochemical methods. *Iranian Chemical Communication*, 3(916):32–49, 2015.

[66] M. Gillet, K. Aguir, M. Bendahan, and P. Mennini. Grain size effect in sputtered tungsten trioxide thin films on the sensitivity to ozone. *Thin Solid Films*, 484(1):358–363, 2005.

[67] K. Govender, D. S. Boyle, P. O'Brien, D. Binks, D. West, and D. Coleman. Room-temperature lasing observed from ZnO nanocolumns grown by aqueous solution deposition. *Advanced Materials*, 14(17):1221–1224, 2002.

[68] Kuveshni Govender, David S. Boyle, Peter B. Kenway, and Paul O'Brien. Understanding the factors that govern the deposition and morphology of thin films of ZnO from aqueous solution. *Journal of Materials Chemistry*, 14(16):2575–2591, 2004.

[69] Lori E. Greene, Matt Law, Dawud H. Tan, Max Montano, Josh Goldberger, Gabor Somorjai, and Peidong Yang. General route

to vertical ZnO nanowire arrays using textured ZnO seeds. *Nano Letters*, 5(7):1231–1236, 2005.

[70] Lori E. Greene, Benjamin D. Yuhas, Matt Law, David Zitoun, and Peidong Yang. Solution-grown zinc oxide nanowires. *Inorganic Chemistry*, 45(19):7535–7543, 2006.

[71] a Gurlo, M Ivanovskaya, N Bârsan, M Schweizer-Berberich, U Weimar, W Göpel, and a Diéguez. Grain size control in nanocrystalline In2O3 semiconductor gas sensors. *Sensors and Actuators B: Chemical*, 44(1-3):327–333, 1997.

[72] Alexander Gurlo. Interplay between O2 and SnO2: Oxygen ionosorption and spectroscopic evidence for adsorbed oxygen. *ChemPhysChem*, 7(10):2041–2052, 2006.

[73] K. I. Hagemark. Defect structure of Zn-doped ZnO. *Journal of Solid State Chemistry*, 16(3-4):293–299, 1976.

[74] Barr Halevi, Sen Lin, Aaron Roy, He Zhang, Ese Jeroro, John Vohs, Yong Wang, Hua Guo, and Abhaya K Datye. High CO 2 Selectivity of ZnO Powder Catalysts for Methanol Steam Reforming. 2013.

[75] A. Helwig, G. Müller, G. Sberveglieri, and M. Eickhoff. On the low-temperature response of semiconductor gas sensors. *Journal of Sensors*, 2009, 2009.

[76] Y. W. Heo, L. C. Tien, Y. Kwon, D. P. Norton, S. J. Pearton, B. S. Kang, and F. Ren. Depletion-mode ZnO nanowire field-effect transistor. *Applied Physics Letters*, 85(12):2274, 2004.

[77] Mokhtar Hjiri, Lassaad El Mir, Salvatore Leonardi, Nicola Donato, and Giovanni Neri. CO and NO2 Selective Monitoring by ZnO-Based Sensors. *Nanomaterials*, 3(3):357–369, 2013.

[78] Jung-Il Hong, Joonho Bae, Zhong Lin Wang, and Robert L Snyder. Room-temperature, texture-controlled growth of ZnO thin films and their application for growing aligned ZnO nanowire arrays. *Nanotechnology*, 20(8):085609, 2009.

[79] Hanmei Hu, Xianhuai Huang, Chonghai Deng, Xiangying Chen, and Yitai Qian. Hydrothermal synthesis of ZnO nanowires and nanobelts on a large scale. *Materials Chemistry and Physics*, 106(1):58–62, 2007.

[80] Jiyong Huang, Zhixiang Wei, and Jinchun Chen. Sensors and Actuators B : Chemical Molecular imprinted polypyrrole nanowires for chiral amino acid recognition. 134:573–578, 2008.

[81] Michael H. Huang, Yiying Wu, Henning Feick, Ngan Tran, Eicke Weber, and Peidong Yang. Catalytic growth of zinc oxide nanowires by vapor transport. *Advanced Materials*, 13(2):113–116, 2001.

[82] Francisco J Ibañez and Francis P Zamborini. Chemiresistive Sensing with Chemically Modified Metal and Alloy Nanoparticles. (2):174–202, 2012.

[83] S.-H. Jung, E. Oh, K.-H. Lee, W. Park, and S.-H. Jeong. A Sonochemical Method for Fabricating Aligned ZnO Nanorods. *Advanced Materials*, 19(5):749–753, 2007.

[84] Keisen Kanda and Toru Maekawa. Development of a WO3 thick-film-based sensor for the detection of VOC. *Sensors and Actuators B: Chemical*, 108(1):97–101, 2005.

[85] H. Karzel, W. Potzel, M. Köfferlein, W. Schiessl, M. Steiner, U. Hiller, G. Kalvius, D. Mitchell, T. Das, P. Blaha, K. Schwarz, and M. Pasternak. Lattice dynamics and hyperfine interactions in ZnO and ZnSe at high external pressures. *Physical Review B*, 53(17):11425–11438, 1996.

[86] Zuraida Khusaimi, Mohamad Hafiz Mamat, Mohamad Zainizan Sahdan, Norbani Abdullah, and Mohamad Rusop. The Effect of Stabiliser's Molarity to the Growth of ZnO Nanorods. *Defect and Diffusion Forum*, 312-315:99–103, 2011.

[87] Hye-young Kim, Kangho Lee, Niall Mcevoy, Chanyoung Yim, and Georg S Duesberg. Chemically Modulated Graphene Diodes. 2013.

[88] Jinwoong Kim, Huiseong Jeong, and Ji-Yong Park. Patterned horizontal growth of ZnO nanowires on SiO2 surface. *Current Applied Physics*, 13(2):425–429, 2013.

[89] C. Klingshirn, R. Hauschild, H. Priller, M. Decker, J. Zeller, and H. Kalt. ZnO rediscovered - Once again!? *Superlattices and Microstructures*, 38(4-6):209–222, 2005.

[90] Seung Hwan Ko, Daeho Lee, Hyun Wook Kang, Koo Hyun Nam, Joon Yeob Yeo, Suk Joon Hong, Costas P. Grigoropoulos, and Hyung Jin Sung. Nanoforest of hydrothermally grown hierarchical ZnO nanowires for a high efficiency dye-sensitized solar cell. *Nano Letters*, 11(2):666–671, 2011.

[91] D. Kohl. Surface processes in the detection of reducing gases with SnO2-based devices. *Sensors and Actuators*, 18(1):71–113, jun 1989.

[92] Agnieszka Kołodziejczak-Radzimska and Teofil Jesionowski. Zinc OxideâFrom Synthesis to Application: A Review. *Materials*, 7(4):2833–2881, 2014.

[93] Jing Kong, Nathan R Franklin, and Chongwu Zhou. Nanotube Molecular Wires as Chemical Sensors. 287(January):622–625, 2000.

[94] Y. C. Kong, D. P. Yu, B. Zhang, W. Fang, and S. Q. Feng. Ultraviolet-emitting ZnO nanowires synthesized by a physical vapor deposition approach. *Applied Physics Letters*, 78(4):407–409, 2001.

[95] G. Korotcenkov. Metal oxides for solid-state gas sensors: What determines our choice? *Materials Science and Engineering B: Solid-State Materials for Advanced Technology*, 139(1):1–23, 2007.

[96] G. Korotcenkov. The role of morphology and crystallographic structure of metal oxides in response of conductometric-type gas sensors. *Materials Science and Engineering R: Reports*, 61(1-6):1–39, 2008.

[97] G. Korotcenkov, V. Brinzari, A. Cerneavschi, M. Ivanov, A. Cornet, J. Morante, A. Cabot, and J. Arbiol. In2O3 films deposited by spray pyrolysis: Gas response to reducing (CO, H2) gases. *Sensors and Actuators, B: Chemical*, 98(2-3):122–129, 2004.

[98] G. Korotcenkov, V. Brinzari, A. Cerneavschi, M. Ivanov, V. Golovanov, A. Cornet, J. Morante, A. Cabot, and J. Arbiol. The influence of film structure on In2O3 gas response. *Thin Solid Films*, 460(1-2):315–323, 2004.

[99] G. Korotcenkov, S. D. Han, B. K. Cho, and V. Brinzari. Grain Size Effects in Sensor Response of Nanostructured SnO2- and In2O3-Based Conductometric Thin Film Gas Sensor. *Critical Reviews in Solid State and Materials Sciences*, 34(1):1–17, 2009.

[100] Ghenadii Korotcenkov. *Handbook of Gas Sensor Materials*, volume 2. 2014.

[101] F. A. Kröger and Norman H. Nachtrieb. *The Chemistry of Imperfect Crystals*, volume 17. 1964.

[102] Qin Kuang, Zhi Yuan Jiang, Zhao Xiong Xie, Shui Chao Lin, Zhi Wei Lin, Su Yuan Xie, Rong Bin Huang, and Lan Sun Zheng. Tailoring the optical property by a three-dimensional epitaxial heterostructure: A case of ZnO/SnO2. *Journal of the American Chemical Society*, 127(33):11777–11784, 2005.

[103] Bin Lai, Xinghua Tang, Haoran Li, Zhuwei Du, Xinwei Liu, and Qian Zhang. Biosensors and Bioelectronics Power production enhancement with a polyaniline modified anode in microbial fuel cells. *Biosensors and Bioelectronics*, 28(1):373–377, 2011.

[104] C Lai, H Z Zhang, G R Li, and X P Gao. Mesoporous polyaniline / TiO 2 microspheres with core â shell structure as anode materials for lithium ion battery. 196:4735–4740, 2011.

[105] Rawiwan Laocharoensuk, Kumaranand Palaniappan, Nickolaus a Smith, Robert M Dickerson, Donald J Werder, Jon K Baldwin,

and Jennifer a Hollingsworth. Flow-based solution-liquid-solid nanowire synthesis. *Nature nanotechnology*, 8(9):660–6, 2013.

[106] R A Laudise and A A Ballman. Hydrothermal Synthesis of Zinc Oxide and Zinc Sulfide. *Journal of Physical Chemistry*, 64(5):688–691, 1960.

[107] Matt Law, Lori E. Greene, Justin C. Johnson, Richard Saykally, and Peidong Yang. Nanowire dye-sensitized solar cells. *Nature Materials*, 4(6):455–459, 2005.

[108] Lionel M. Levinson and H. R. Philipp. The physics of metal oxide varistors. *Journal of Applied Physics*, 46(3):1332–1341, 1975.

[109] Lionel M. Levinson and H. R. Philipp. Low-temperature ac properties of metal-oxide varistors. *Journal of Applied Physics*, 49(12):6142–6146, 1978.

[110] Claude Lévy-Clément, Ramon Tena-Zaera, Margaret A. Ryan, Abou Katty, and Gary Hodes. CdSe-sensitized p-CuSCN/nanowire n-ZnO heterojunctions. *Advanced Materials*, 17(12):1512–1515, 2005.

[111] Q. H. Li, Y. X. Liang, Q. Wan, and T. H. Wang. Oxygen sensing characteristics of individual ZnO nanowire transistors. *Applied Physics Letters*, 85(26):6389–6391, 2004.

[112] Wen-Jun Li, Er-Wei Shi, Wei-Zhuo Zhong, and Zhi-Wen Yin. Growth mechanism and growth habit of oxide crystals. *Journal of Crystal Growth*, 203(1-2):186–196, 1999.

[113] Noncommercial-noderivatives International License, Y Liu, J Yu, W M Tang, and P T Lai. On the voltage dependence of sensitivity for Schottky-type gas sensor. (223503):1–5, 2015.

[114] Bixia Lin, Zhuxi Fu, and Yunbo Jia. Green luminescent center in undoped zinc oxide films deposited on silicon substrates. *Applied Physics Letters*, 79(7):943–945, 2001.

[115] Dandan Lin, Wei Pan, and Hui Wu. Morphological control of centimeter long aluminum-doped zinc oxide nanofibers prepared by electrospinning. *Journal of the American Ceramic Society*, 90(1):71–76, 2007.

[116] Dandan Lin, Hui Wu, and Wei Pan. Photoswitches and memories assembled by electrospinning aluminum-doped zinc oxide single nanowires. *Advanced Materials*, 19(22):3968–3972, 2007.

[117] Bin Liu, Hua Chun Zeng, Bin Liu, and Hua Chun Zeng. Hydrothermal Synthesis of ZnO Nanorods in the Diameter Regime of 50 nm Hydrothermal Synthesis of ZnO Nanorods in the Diameter Regime of 50 nm. 125(March):4430–4431, 2003.

[118] Xiang Liu, Xiaohua Wu, Hui Cao, and R. P H Chang. Growth mechanism and properties of ZnO nanorods synthesized by plasma-enhanced chemical vapor deposition. *Journal of Applied Physics*, 95(6):3141–3147, 2004.

[119] Harald Lorenz, Matthias Friedrich, Marc Armbrüster, Bernhard Klötzer, and Simon Penner. ZnO is a CO 2 -selective steam reforming catalyst. *Journal of Catalysis*, 297:151–154, 2013.

[120] G. D. Mahan. Intrinsic defects in ZnO varistors. *Journal of Applied Physics*, 54(7):3825–3832, 1983.

[121] G. D. Mahan, Lionel M. Levinson, and H. R. Philipp. Theory of conduction in ZnO varistors. *Journal of Applied Physics*, 50(4):2799–2812, 1979.

[122] S M Mahpeykar, J Koohsorkhi, and H Ghafoori-fard. Ultrafast microwave-assisted hydrothermal synthesis of long vertically aligned ZnO nanowires for dye-sensitized solar cell application. *Nanotechnology*, 23(16):165602, 2012.

[123] Soumen Maiti, Shreyasi Pal, and Kalyan Kumar Chattopadhyay. Recent advances in low temperature, solution processed morphology tailored ZnO nanoarchitectures for electron emission and photocatalysis applications. *CrystEngComm*, 17(48):9264–9295, 2015.

[124] A. Mang, K. Reimann, and St Rübenacke. Band gaps, crystal-field splitting, spin-orbit coupling, and exciton binding energies in ZnO under hydrostatic pressure. *Solid State Communications*, 94(4):251–254, 1995.

[125] Rex B. McLellan. The thermodynamics of interstitial-vacancy interactions in solid solutions. *Journal of Physics and Chemistry of Solids*, 49(10):1213–1217, 1988.

[126] X.Q. Meng, D.X. Zhao, J.Y. Zhang, D.Z. Shen, Y.M. Lu, L. Dong, Z.Y. Xiao, Y.C. Liu, and X.W. Fan. Wettability conversion on ZnO nanowire arrays surface modified by oxygen plasma treatment and annealing. *Chemical Physics Letters*, 413(4-6):450–453, 2005.

[127] Daniel Moore, Yong Ding, and Lin Wang Zhong. Hierarchical structured nanohelices of ZnS. *Angewandte Chemie - International Edition*, 45(31):5150–5154, 2006.

[128] W. Mtangi, F. D. Auret, W. E. Meyer, M. J. Legodi, P. J. Janse van Rensburg, S. M. M. Coelho, M. Diale, and J. M. Nel. Effects of hydrogen, oxygen, and argon annealing on the electrical properties of ZnO and ZnO devices studied by current-voltage, deep level transient spectroscopy, and Laplace DLTS. *Journal of Applied Physics*, 111(9):094504, 2012.

[129] Shinji Nakagomi, Anita Lloyd Spetz, Ingemar Lundström, and Peter Tobias. Electrical Characterization of Carbon Monoxide Sensitive High Temperature Sensor Diode Based on Catalytic Metal Gate â Insulator â Silicon Carbide Structure. 2(5):379–386, 2002.

[130] Markus Niederberger. *Metal Oxides: Chemistry and Applications. Edited by J. L. G. Fierro.*, volume 8. mar 2007.

[131] Lian Ouyang, Kristin N Maher, Chun Liang Yu, Justin Mccarty, and Hongkun Park. Catalyst-Assisted Solution - Liquid - Solid Synthesis of CdS / CdSe Nanorod Heterostructures. (34):133–138, 2007.

[132] Z W Pan, Z R Dai, and Z L Wang. Nanobelts of semiconducting oxides. *Science*, 291(5510):1947–1949, 2001.

[133] Bharati Panigrahy, M. Aslam, D. S. Misra, and D. Bahadur. Polymer-mediated shape-selective synthesis of ZnO nanostructures using a single-step aqueous approach. *CrystEngComm*, 11(9):1920, 2009.

[134] W. I. Park, D. H. Kim, S. W. Jung, and Gyu Chul Yi. Metalorganic vapor-phase epitaxial growth of vertically well-aligned ZnO nanorods. *Applied Physics Letters*, 80(22):4232–4234, 2002.

[135] W. I. Park, J. S. Kim, Gc Yi, and Hj Lee. ZnO Nanorod Logic Circuits. *Advanced Materials*, 17(11):1393–1397, 2005.

[136] Won Il Park and Gyu Chul Yi. Electroluminescence in n-ZnO Nanorod Arrays Vertically Grown on p-GaN. *Advanced Materials*, 16(1):87–90, 2004.

[137] Won Il Park, Gyu Chul Yi, Miyoung Kim, and Stephen J. Pennycook. ZnO nanoneedles grown vertically on Si substrates by noncatalytic vapor-phase epitaxy. *Advanced Materials*, 14(24):1841–1843, 2002.

[138] G. S. Parks and C. E. Hablutzel. The Heat of Formation of Zinc Oxide. *Journal of the American Chemical Society*, 49(11):2792–2795, 1927.

[139] Arun Patil, Chandrakant Dighavkar, and Ratan Borse. Al doped ZnO thick films as CO 2 gas sensors. 13(10):1331–1337, 2011.

[140] Hans Pink, Ludwig Treitinger, and Lutz Vité. Preparation of fast detecting SnO2 gas sensors. *Japanese Journal of Applied Physics*, 19(3):513–517, 1980.

[141] Ahsanulhaq Qurashi, N. Tabet, M. Faiz, and Toshinari Yamzaki. Ultra-fast microwave synthesis of ZnO nanowires and their dynamic response toward hydrogen gas. *Nanoscale Research Letters*, 4(8):948–954, 2009.

[142] Niranjan Ramgir, Niyanta Datta, Manmeet Kaur, S. Kailasaganapathi, Anil K. Debnath, D. K. Aswal, and S. K. Gupta. Metal oxide nanowires for chemiresistive gas sensors: Issues, challenges and prospects. *Colloids and Surfaces A: Physicochemical and Engineering Aspects*, 439:101–116, 2013.

[143] Frank Rettig and Ralf Moos. Morphology dependence of thermopower and conductance in semiconducting oxides with space charge regions. *Solid State Ionics*, 179(39):2299–2307, 2008.

[144] D.C. Reynolds, D. C. Look, B. Jogai, C. Litton, G. Cantwell, and W. Harsch. Valence-band ordering in ZnO. *Physical Review B*, 60(4):2340–2344, 1999.

[145] D.C. Reynolds, D.C. Look, and B. Jogai. Optically pumped ultraviolet lasing from ZnO. *Solid State Communications*, 99(12):873–875, 1996.

[146] Krishnendu Saha, Sarit S Agasti, Chaekyu Kim, Xiaoning Li, and Vincent M Rotello. Gold Nanoparticles in Chemical and Biological Sensing. 2012.

[147] P. Samarasekara, N. U S Yapa, N. T R N Kumara, and M. V K Perera. CO2 gas sensitivity of sputtered zinc oxide thin films. *Bulletin of Materials Science*, 30(2):113–116, 2007.

[148] G SBERVEGLIERI, C BARATTO, E COMINI, G FAGLIA, M FERRONI, A PONZONI, and A VOMIERO. Synthesis and characterization of semiconducting nanowires for gas sensing. *Sensors and Actuators B: Chemical*, 121(1):208–213, jan 2007.

[149] Giorgio Sberveglieri. Classical and novel techniques for the preparation of SnO2 thin-film gas sensors. *Sensors and Actuators B: Chemical*, 6(1):239–247, 1992.

[150] F Schedin, A K Geim, S V Morozov, E W Hill, P Blake, M I Katsnelson, and K S Novoselov. Detection of individual gas molecules adsorbed on graphene. 6(2):6–9, 2007.

[151] W M Sears, K Colbow, and F Consadori. General characteristics of thermally cycled tin oxide gas sensors. *Semiconductor Science and Technology*, 4(5):351–359, may 1989.

[152] A. Sedky, M. Abu-Abdeen, and Abdalaziz A. Almulhem. Non-linear I-V characteristics in doped ZnO based-ceramic varistor. *Physica B: Condensed Matter*, 388(1-2):266–273, 2007.

[153] A. Sedky, T. A. El-Brolossy, and S. B. Mohamed. Correlation between sintering temperature and properties of ZnO ceramic varistors. *Journal of Physics and Chemistry of Solids*, 73(3):505–510, 2012.

[154] F. Seitz. On the porosity observed in the Kirkendall effect. *Acta Metallurgica*, 1(3):355–369, 1953.

[155] Liang Shi, Keyan Bao, Jie Cao, and Yitai Qian. Sunlight-assisted fabrication of a hierarchical ZnO nanorod array structure. *CrystEngComm*, 11(9):2009, 2009.

[156] Parasharam M. Shirage, Amit Kumar Rana, Yogendra Kumar, Somaditya Sen, S. G. Leonardi, and G. Neri. Sr- and Ni-doping in ZnO nanorods synthesized by a simple wet chemical method as excellent materials for CO and CO ₂ gas sensing. *RSC Adv.*, 6(86):82733–82742, 2016.

[157] Amna Sirelkhatim, Shahrom Mahmud, Azman Seeni, Noor Haida Mohamad Kaus, Ling Chuo Ann, Siti Khadijah Mohd Bakhori, Habsah Hasan, and Dasmawati Mohamad. Review on zinc oxide nanoparticles: Antibacterial activity and toxicity mechanism. *Nano-Micro Letters*, 7(3):219–242, 2015.

[158] X. M. Sui, C. L. Shao, and Y. C. Liu. White-light emission of polyvinyl alcohol/ZnO hybrid nanofibers prepared by electrospinning. *Applied Physics Letters*, 87(11), 2005.

[159] Ye Sun, Gareth M. Fuge, and Michael N R Ashfold. Growth of aligned ZnO nanorod arrays by catalyst-free pulsed laser deposition methods. *Chemical Physics Letters*, 396(1-3):21–26, 2004.

[160] Ye Sun, N. George Ndifor-Angwafor, D. Jason Riley, and Michael N.R. Ashfold. Synthesis and photoluminescence of ultra-thin ZnO nanowire/nanotube arrays formed by hydrothermal growth. *Chemical Physics Letters*, 431(4-6):352–357, 2006.

[161] V. V. Sysoev, T. Schneider, J. Goschnick, I. Kiselev, W. Habicht, H. Hahn, E. Strelcov, and A. Kolmakov. Percolating SnO2 nanowire network as a stable gas sensor: Direct comparison of long-term performance versus SnO2 nanoparticle films. *Sensors and Actuators, B: Chemical*, 139(2):699–703, 2009.

[162] Publisher Taylor, M S Dresselhaus, and G Dresselhaus. Advances in Physics Intercalation compounds of graphite. (June 2012):37–41, 2010.

[163] Zhengrong R. Tian, James A. Voigt, Jun Liu, Bonnie Mckenzie, Matthew J. Mcdermott, Mark A. Rodriguez, Hiromi Konishi, and Huifang Xu. Complex and oriented ZnO nanostructures. *Nature Materials*, 2(12):821–826, 2003.

[164] Alexey a. Tomchenko, Gregory P. Harmer, Brent T. Marquis, and John W. Allen. Semiconducting metal oxide sensor array for the selective detection of combustion gases. *Sensors and Actuators, B: Chemical*, 93(1-3):126–134, 2003.

[165] F Udrea, J W Gardner, D Setiadi, and J A Covington. Design and simulations of SOI CMOS micro-hotplate gas sensors. 78:180–190, 2001.

[166] J. Ulrich, T. Stelzer, John W. Mullin, and J.W. Mullin. *Crystallization*. 2001.

[167] Husnu Emrah Unalan, Pritesh Hiralal, Nalin Rupesinghe, Sharvari Dalal, William I Milne, and Gehan A J Amaratunga. Rapid synthesis of aligned zinc oxide nanowires. *Nanotechnology*, 19(25):255608, 2008.

[168] L Valentini, I Armentano, J M Kenny, C Cantalini, L Lozzi, L Valentini, I Armentano, and J M Kenny. Sensors for sub-ppm

NO2 gas detection based on carbon nanotube thin films Sensors for sub-ppm NO 2 gas detection based on carbon nanotube thin films. 961:10–13, 2003.

[169] Nguyen Van Hieu, Nguyen Duc Khoang, Do Dang Trung, Le Duc Toan, Nguyen Van Duy, and Nguyen Duc Hoa. Comparative study on CO2 and CO sensing performance of LaOCl-coated ZnO nanowires. *Journal of Hazardous Materials*, 244-245(2):209–216, 2013.

[170] A. Varpula, S. Novikov, J. Sinkkonen, and M. Utriainen. Bias dependent sensitivity in metal-oxide gas sensors. *Sensors and Actuators, B: Chemical*, 131(1):134–142, 2008.

[171] Aapo Varpula. Modeling of transient electrical characteristics for granular semiconductors. *Journal of Applied Physics*, 108(3), 2010.

[172] Aapo Varpula. Modeling of transient electrical characteristics for granular semiconductors. *Journal of Applied Physics*, 108(3):1–14, 2010.

[173] Aapo Varpula, Sergey Novikov, Antti Haarahiltunen, and Pekka Kuivalainen. Transient characterization techniques for resistive metal-oxide gas sensors. *Sensors and Actuators, B: Chemical*, 159(1):12–26, 2011.

[174] Lionel Vayssieres. Growth of arrayed nanorods and nanowires of ZnO from aqueous solutions. *Advanced Materials*, 15(5):464–466, 2003.

[175] M. Andres Verges, A. Mifsud, and C. J. Serna. Formation of rod-like zinc oxide microcrystals in homogeneous solutions. *Journal of the Chemical Society, Faraday Transactions*, 86(6):959, 1990.

[176] Tobias Vossmeyer. Gold-nanoparticle / organic linker films : self-assembly , electronic and structural characterisation , composition and vapour sensitivity. pages 77–97, 2004.

[177] Junpeng Wang, Zeyan Wang, Baibiao Huang, Yandong Ma, Yuanyuan Liu, Xiaoyan Qin, Xiaoyang Zhang, and Ying Dai. Oxygen vacancy induced band-gap narrowing and enhanced visible light photocatalytic activity of ZnO. *ACS Applied Materials and Interfaces*, 4:4024–4030, 2012.

[178] X. Wang, J. Song, J. Liu, and Z. L. Wang. Direct-Current Nanogenerator Driven by Ultrasonic Waves. *Science*, 316(5821):102–105, 2007.

[179] Xiaohua Wang, Jian Zhang, and Ziqiang Zhu. Ammonia sensing characteristics of ZnO nanowires studied by quartz crystal microbalance. *Applied Surface Science*, 252(6):2404–2411, jan 2006.

[180] Zhong Lin Wang. Nanopiezotronics. *Advanced Materials*, 19(6):889–892, 2007.

[181] Zhong Lin Wang. The new field of nanopiezotronics Semiconducting and piezoelectric nanowires and nanobelts have exciting. *Materials today*, 10(5):20–28, 2007.

[182] Zhong Lin Wang. Towards self-powered nanosystems: From nanogenerators to nanopiezotronics. *Advanced Functional Materials*, 18(22):3553–3567, 2008.

[183] Zhong Lin Wang. Ten years' venturing in ZnO nanostructures: From discovery to scientific understanding and to technology applications. *Chinese Science Bulletin*, 54(22):4021–4034, 2009.

[184] Zhong Lin Wang. ZnO nanowire and nanobelt platform for nanotechnology. *Materials Science and Engineering R: Reports*, 64(3-4):33–71, 2009.

[185] Zhong Lin Wang and Jinhui Song. Piezoelectric Nanogenerators Based on Zinc Oxide Nanowire Arrays. *Science*, 312(5771):242–246, 2006.

[186] S. F. Wei, J. S. Lian, and Q. Jiang. Controlling growth of ZnO rods by polyvinylpyrrolidone (PVP) and their optical properties. *Applied Surface Science*, 255(15):6978–6984, 2009.

[187] Yaguang Wei, Chen Xu, Sheng Xu, Cheng Li, Wenzhuo Wu, and Zhong Lin Wang. Planar waveguide-nanowire integrated three-dimensional dye-sensitized solar cells. *Nano Letters*, 10(6):2092–2096, 2010.

[188] Benjamin Weintraub, Yaguang Wei, Zhong Lin Wang, B. Weintraub, Y. Wei, and Z. L. Wang. Optical fiber/nanowire hybrid structures for efficient three-dimensional dye-sensitized solar cells. *Angewandte Chemie - International Edition*, 48(47):8981–8985, 2009.

[189] Benjamin a Weintraub. One-dimensional zinc oxide nanomaterials synthesis and photovoltaic applications. (August), 2010.

[190] Hank Wohltjen and Arthur W. Snow. Colloidal MetalâInsulatorâMetal Ensemble Chemiresistor Sensor. *Analytical Chemistry*, 70(14):2856–2859, 1998.

[191] C. Wongchoosuk, S. Choopun, A. Tuantranont, and T. Kerdcharoen. Au-doped zinc oxide nanostructure sensors for detection and discrimination of volatile organic compounds. *Materials Research Innovations*, 13(3):185–188, 2009.

[192] Z Y Wu, F R Chen, J J Kai, W B Jian, and J J Lin. Fabrication, characterization and studies of annealing effects on ferromagnetism in Zn 1â x Co x O nanowires. *Nanotechnology*, 17(21):5511–5518, 2006.

[193] C. H. Xu, H. F. Lui, and C. Surya. Optical and sensor properties of ZnO nanostructure grown by thermal oxidation in dry or wet nitrogen. *Journal of Electroceramics*, 28(1):27–33, 2012.

[194] Congkang Xu, Guoding Xu, Yingkai Liu, and Guanghou Wang. A simple and novel route for the preparation of ZnO nanorods. *Solid State Communications*, 122(3):175–179, 2002.

[195] Sheng Xu, Yong Ding, Yaguang Wei, Hao Fang, Yue Shen, Ashok K. Sood, Dennis L. Polla, and Lin Wang Zhong. Patterned

growth of horizontal ZnO nanowire arrays. *Journal of the American Chemical Society*, 131(19):6670–6671, 2009.

[196] Sheng Xu, Yue Shen, Yong Ding, and Zhong Lin Wang. Growth and transfer of monolithic horizontal ZnO nanowire superstructures onto flexible substrates. *Advanced Functional Materials*, 20(9):1493–1497, 2010.

[197] Sheng Xu and Zhong Lin Wang. One-dimensional ZnO nanostructures: Solution growth and functional properties. *Nano Research*, 4(11):1013–1098, 2011.

[198] Kavita Yadav, Shashank K. Gahlaut, B. R. Mehta, and J. P. Singh. Photoluminescence based H2 and O2 gas sensing by ZnO nanowires. *Applied Physics Letters*, 108(7):1–6, 2016.

[199] Hiroki Yamagiwa, Seiko Sato, Tadashi Fukawa, Tsuyoshi Ikehara, Ryutaro Maeda, Takashi Mihara, and Mutsumi Kimura. Detection of Volatile Organic Compounds by Weight-Detectable Sensors coated with Metal-Organic Frameworks. *Scientific Reports*, 4(1):6247, 2015.

[200] N. Yamazoe, Y. Kurokawa, and T. Seiyama. Effects of additives on semiconductor gas sensors. In *Sensors and Actuators*, volume 4, pages 283–289. 1983.

[201] K Yanagi, H Udoguchi, S Sagitani, Y Oshima, T Takenobu, H Kataura, T Ishida, K Matsuda, and Y Maniwa. Transport mechanisms in metallic and semiconducting single-wall carbon nanotube networks. *ACS Nano*, 4(7):4027–4032, 2010.

[202] By Peidong Yang, Haoquan Yan, Samuel Mao, Richard Russo, Justin Johnson, Richard Saykally, Nathan Morris, Johnny Pham, Rongrui He, and Heon-jin Choi. Controlled Growth of ZnO Nanowires and Their Optical Properties **. (5):323–331, 2002.

[203] Rusen Yang, Yong Qin, Liming Dai, and Zhong Lin Wang. Power generation with laterally packaged piezoelectric fine wires. *Nature nanotechnology*, 4(1):34–39, 2009.

[204] B. D. Yao, Y. F. Chan, and N. Wang. Formation of ZnO nanostructures by a simple way of thermal evaporation. *Applied Physics Letters*, 81(4):757–759, 2002.

[205] Ping Hung Yeh, Zhou Li, and Zhong Lin Wang. Schottky-gated probe-free ZnO nanowire biosensor. *Advanced Materials*, 21(48):4975–4978, 2009.

[206] Hongtao Yuan and Yao Zhang. Preparation of well-aligned ZnO whiskers on glass substrate by atmospheric MOCVD. *Journal of Crystal Growth*, 263(1):119–124, 2004.

[207] Jun Zhang, Lingdong Sun, Jialu Yin, Huilan Su, and Chunsheng Liao. Control of ZnO Morphology via a Simple Solution Route Control of ZnO Morphology via a Simple Solution Route. 14(10):4172–4177, 2002.

[208] Peishuo Zhang, Guofeng Pan, Bingqiang Zhang, Jiali Zhen, and Yicai Sun. High Sensitivity Ethanol Gas Sensor Based on Sn-doped ZnO Under Visible Light Irradiation at Low Temperature. 17(4):817–822, 2014.

[209] Zhao Qiang Zheng, Lian Feng Zhu, and Bing Wang. In2O3 Nanotower Hydrogen Gas Sensors Based on Both Schottky Junction and Thermoelectronic Emission. *Nanoscale Research Letters*, 10:1–14, 2015.

[210] Xi Zhou, Zhao-Xiong Xie, Zhi-Yuan Jiang, Qin Kuang, Shu-Hong Zhang, Tao Xu, Rong-Bin Huang, and Lan-Sun Zheng. Formation of ZnO hexagonal micro-pyramids: a successful control of the exposed polar surfaces with the assistance of an ionic liquid. *Chemical communications (Cambridge, England)*, 1(44):5572–5574, 2005.

[211] Y. W. Zhu, H. Z. Zhang, X. C. Sun, S. Q. Feng, J. Xu, Q. Zhao, B. Xiang, R. M. Wang, and D. P. Yu. Efficient field emission from ZnO nanoneedle arrays. *Applied Physics Letters*, 83(1):144–146, 2003.